Declaration

Honorable Commissioner of Patents:

I, Xu Youhao, hereby declare that:

1. I'm living in Beijing, People's Republic of China.

2. I'm a citizen of People's Republic of China.

3. From September 1981 to July 1985, I studied in the Department of Petroleum Refining in East China University of Science and Technology and obtained my Bachelor's degree; from September 1985 to July 1987, I studied in the Department of Chemical Engineering in East China University of Science and Technology and obtained my Master's degree; from September 2001 to December 2006, I studied in the Research Institute of Petroleum Processing and obtained my Doctor's degree.

4. Since August 1987, I've been devoting myself to the development of catalytic cracking technology in the Research Institute of Petroleum Processing, and have twenty years' experience. I took part in the development of Deep Catalytic Cracking (DCC) technology, and I'm currently in charge of the development and application of a newly series of FCC processes for producing maximum isoparaffins in cracked naphtha or clean gasoline and propylene (MIP and MIP-CGP). I have written more than forty papers on this subject, six of which were published in internationally significant periodicals and international academic conferences, and applied for, altogether, more than seventy patents domestically and abroad.

5. In US Patent Application 09/553,990, I propose a novel riser reactor, wherein the ratio of the diameter of a second reaction zone to the diameter of a first reaction zone ranges from 1.5: 1 to 5: 1. However, in catalytic cracking of the prior art, the ratio of the diameter of a second reaction zone to the diameter of a first reaction zone in a riser reactor should be less than 1.5: 1.

6. On the basis of the European patent EP0171460, Kmecak et al., the Examiner in charge of this application drew the conclusion, after manually making a measurement in Figure 8 of EP0171460, that "DR_2: DR_1 is equal to approximately 3: 1". In my point of view, this is impossible because of the following reasons:

6.1. In catalytic cracking of the prior art, the ratio of the diameter of a so-called second reaction zone to the diameter of a so-called first reaction zone in a riser reactor should be less than 1.5: 1.

6.2. Figure 8 in EP0171460 is merely a schematic drawing without the specific dimensions available. Thus, the value obtained by manual measurement on the basis of the schematic drawing is inaccurate. One skilled in the art would never do this.

6.3. If "DR_2: DR_1 is equal to approximately 3: 1", it will be obtained upon scientific calculation (see Item 8 for details) that the ratio of the velocity at the outlet of the first reaction zone to the velocity at the inlet of the first reaction zone, i.e. u_1/u_0, is 18.7, which is far greater than the generally recognized ratio of less than 3 in the art. Thus, the Examiner's conclusion cannot be fulfilled.

7. In my point of view, the present invention achieves unexpected technical effects, which can be seen clearly from Example 1 and the corresponding Comparative Example 1, and Example 2 and the corresponding Comparative Example 2, as given hereinbelow.

Comparative Example 2 is a complementary test, and Example 1, Comparative Example 1 and Example 2 are recited in the original application document. The properties of feedstock used in the Examples and Comparative Examples and the properties of the catalyst are respectively listed in Tables 1 and 2.

Example 1

This Example showed the use of catalyst A in a novel pilot plant riser reactor according to the present invention for the production of

isobutane and isoparaffin enriched gasoline.

The total height of the prelift zone, the first reaction zone, the second reaction zone, the outlet zone of the riser reactor was 15 meters, in which the height of the prelift zone with the diameter of 0.025 meter was 1.5 meters, the height of the first reaction zone with a diameter of 0.025 meter was 4 meters, the height of the second reaction zone with a diameter of 0.1 meter was 6.5 meters, the height of the outlet zone with a diameter of 0.025 meter was 3 meters. The isotrapezia vertex angle of the vertical section of the conjunct section between the first reaction zone and the second reaction zone was 45°. The isotrapezia base angle of the vertical section of the conjunct section between the second reaction zone and the outlet zone was 60°.

The reactor and operating conditions were different from those used in conventional catalytic cracking, while the regenerating and fractionating systems were the same as those used in conventional catalytic cracking. The operating conditions and product slate are listed in Table 3, and the gasoline properties are listed in Table 4.

Comparative Example 1

Compared with example 1, this comparative example was practiced in a conventional pilot plant iso-diameter riser reactor.

The operating conditions and product slate are listed in Table 3, and the gasoline properties are listed in Table 4.

It can be seen clearly from Tables 3 and 4 that:

1) in Example 1, 35.07 wt% of LPG was isobutane, while in Comparative Example 1, 15.74 wt% of LPG was isobutane (see Table 3);

2) in Example 1, the gasoline had an isoparaffin content of 36.0 wt% and an olefin content of 28.11 wt%, while in Comparative Example 1, the gasoline had an isoparaffin content of 11.83wt % and an olefin content of 56.49 wt% (see Table 4).

Example 2

This Example showed the use of gasoline with high olefin content as a quenching medium in a novel riser reactor for the production of isoparaffin enriched gasoline by means of catalytic conversion in the riser reactor.

The total height of the prelift zone, the first reaction zone, the second reaction zone, the outlet zone of the riser reactor was 15 meters, in which the height of the prelift zone with the diameter of 0.025 meter was 1.5 meters, the height of the first reaction zone with a diameter of 0.025 meter was 4 meters, the height of the second reaction zone with a diameter of 0.05 meter was 6.5 meters, the height of the outlet zone with a diameter of 0.025 meter was 3 meters. The isotrapezia vertex angle of the vertical section of the conjunct section between the first reaction zone and the second reaction zone was 45°. The isotrapezia base angle of the vertical section of the conjunct section between the second reaction zone and the outlet zone was 60°.

The catalyst and gasoline feedstock used in this Example were the same as those used in Example 1. The gasoline produced in comparative example 1 as a quenching medium was charged into the conjunct section between the first reaction zone and the second reaction zone. The other steps were basically the same as those in Example 1.

The operating conditions and product slate are listed in table 5, and the gasoline properties are listed in table 6.

Comparative Example 2

Compared with example 2, this comparative example was practiced in a conventional pilot plant iso-diameter riser reactor.

The operating conditions and product slate are listed in Table 5, and the gasoline properties are listed in Table 6.

It can be seen clearly from Tables 5 and 6 that, when the ratio of the diameter of the second reaction zone to the diameter of the first reaction zone was 1 in Comparative Example 2, LPG had an isobutane content of

only 14.63 wt% and the gasoline had an isoparaffin content of only 9.51 wt%; when the ratio of the diameter of the second reaction zone to the diameter of the first reaction zone was 2 in Example 2, LPG had an isobutane content of up to 34.15 wt% and the gasoline had an isoparaffin content of up to 43.86 wt%, which are respectively 19.52 percentages and 34.35 percentages higher than those in Comparative Example 2.

In other words, when the ratio of the diameter of the second reaction zone to the diameter of the first reaction zone is 2 or 4, the present invention has a significant advantage in respect of effects over the prior art in which the diameter ratio is 1: 1.

Table 1

Density (20 °C), kg/m^3	890.5
Kinematic Viscosity (100 °C), mm^2/s	5.08
Carbon Residue, wt%	0.7
Pour Point, °C	40
Total Nitrogen, wt%	0.16
Sulfur, wt%	0.53
Carbon, wt%	85.00
Hydrogen, wt%	12.62
Heavy Metal Content, ppm	
Ni	0.16
V	0.15
Fe	—
Cu	—
Na	0.45
Distillation, °C	
IBP	278
10%	385
30%	442
50%	499
70%	—
90%	—
EP	—

Table 2

Catalyst Name	A	B
Trade Mark	ZCM-7	CRP-1
Chemical Composition, wt%		
Aluminum Oxide	46.4	54.2
Sodium Oxide	0.22	0.03
Ferric Oxide	0.32	
Apparent Bulk Density, kg/m^3	690	860
Pore Volume, ml/g	0.38	0.26
Surface Area, m^2/g	164	160
Attrition Index, wt% hr^{-1}	—	1.2
Particle Size Distribution, wt%		
0~40 microns	4.8	26.0
40~80 microns	47.9	60.8
>80 microns	47.3	13.2

Table 3

	Example 1	Comparative Example 1
Reactor	Novel Riser of the Present Invention	Conventional Riser
Reaction Temperature, °C		495
The First Reaction Zone	545	—
The Second Reaction Zone	495	—
Reaction Time, sec	5.0	2.89
The First Reaction Zone	1.0	—
The Second Reaction Zone	3.5	—
The Outlet Zone	0.5	—
C/O Ratio	4.5	4.5
S/O Ratio	0.05	0.05
Product Slate, wt%		
Dry Gas	1.83	1.62
LPG	16.11	11.88
In which Isobutane	5.65	1.87
Gasoline	46.86	41.59
LCO	23.44	22.81
HCO	7.77	18.76
Coke	3.88	2.86
Loss	0.11	0.48

Table 4

	Example 1	Comparative Example 1
Reactor	Novel Riser of the Present Invention	Conventional Riser
Density (20 °C), kg/m^3	743.6	749.8
Octane Number		
RON	90.0	91.0
MON	79.0	79.8
Induction Period, min	>1000	>485
Existent Gum, mg/100ml	2.0	2.0
Sulfur, wt%	0.0095	0.0120
Nitrogen, wt%	0.0028	0.0033
Carbon, wt%	86.14	86.81
Hydrogen, wt%	13.72	13.12
Distillation, °C		
IBP	46	50
10 %	73	77
30 %	95	99
50 %	114	122
70 %	143	145
90 %	171	175
EP	202	205
Gasoline composition, wt%		
Paraffins	41.01	15.81
In which Iso-paraffins	36.00	11.83
Naphthenes	7.20	6.50
Olefins	28.11	56.49
Aromatics	23.68	21.20

Table 5

	Example 2	Comparative Example 2
Reactor	Novel Riser of the Present Invention	Conventional Riser
Operating Conditions		
Reaction Temperature, °C		495
The first reaction zone	545	
The second reaction zone	495	
Reaction Time, sec	5.3	2.8
The first reaction zone	0.8	
The second reaction zone	3.9	
The outlet zone	0.6	
C/O ratio	5.0	5.0
S/O ratio	0.05	0.05
Product Slate, wt%		
Dry Gas	1.78	1.65
LPG	17.51	11.07
In which Iso-butane	5.98	1.62
Gasoline	47.98	41.39
LCO	22.30	22.81
HCO	6.22	19.76
Coke	4.00	3.00
Loss	0.21	0.32

Table 6

	Example 2	Comparative Example 2
Reactor	Novel Riser of the Present Invention	Conventional Riser
Density(20 °C), kg/m^3	745.3	743.2
Octane Number		
RON	90.1	89.8
MON	80.9	79.8
Induction Period, min	800.0	>485
Existent Gum, mg/100ml	2.0	2.0
Sulfur, wt%	0.01	0.02
Nitrogen, wt%	0.003	0.004
Carbon, wt%	86.51	86.81
Hydrogen, wt%	13.42	13.52
Distillation, °C		
IBP	48	45
10%	75	72
30%	97	99
50%	118	120
70%	144	145
90%	173	174
EP	203	202
Gasoline Composition, wt%		
Paraffins	47.87	14.41
In which Iso-Paraffins	43.86	9.51
Naphthenes	7.45	9.50
Olefins	20.51	56.89
Aromatics	24.17	19.20

8. I have found out, upon scientific calculation, that if "DR_2: DR_1 is equal to approximately 3: 1", the ratio of the velocity at the outlet of the first reaction zone to the velocity at the inlet of the second reaction zone, i.e. u_1/u_0, will be 18.7. However, it is generally accepted in the art that the ratio of the velocity at the outlet of an iso-diameter riser(i.e. the so-called first reaction zone) to the velocity at the inlet of the iso-diameter riser(i.e. the so-called first reaction zone) is less than 3, and absolutely no more than 10. Thus, the Examiner's conclusion cannot be fulfilled.

The technical background, prerequisites for deduction and detailed deduction procedure are described hereinbelow.

Technical Background of the Patent Application

The fluidized catalytic cracking process was developed to meet the high reactivity of a zeolite molecular sieve, and namely, the reaction time in the reactor is not supposed to be too long to produce undesirable products, such as excess coke and dry gas, and is generally controlled within 2 to 3 seconds. In order to meet the requirement of a short reaction time, isodiametric riser reactors disposed vertically are used for industrial purposes. According to the principles of fluidization, the effluent velocity at the inlet of the riser reactor is supposed to be 4 to 5 m/s under normal operating conditions; otherwise, the device will not work. Cracking is a reaction resulting in an increased number of molecules. Such molecular expansion directly results in that the effluent velocity in the riser reactor increases sharply, and the effluent velocity at the outlet of the riser reaches as high as 15 to 18 m/s. Moreover, judging from the industrial design and application in the prior art, the diameter of the riser is not allowed to be too big. The diameter ratio of the upper and lower reaction zones in a riser is generally less than 1.5: 1 in the art.

During examination of this application, the Examiner in charge of this application drew the conclusion on the basis of the European patent EP0171460, after manually making a measurement in Figure 8 of EP0171460, that "DR_2: DR_1 is equal to approximately 3: 1". In my point of view, this is impossible because of the following reasons:

Since reactions basically including cracking occur at the bottom of the riser (the so-called first reaction zone) after a hydrocarbon feedstock contacts with a hot regenerated catalyst, the conversion of the feedstock in said zone increases rapidly, and a large amount of small-molecular products are produced, which is the manifestation of molecular expansion. The reactions at the top of the riser (the so-called second reaction zone) basically include conversion reactions, such as hydrogen transfer and alkylation, and cracking does not occur there in a large scale. Consequently, the increase of the conversion of the feedstock slows down in said zone. These are all general knowledge in the field of catalytic cracking, as seen from, for example, Figure 1 which illustrates the distribution of conversion along the axial direction of the height of the riser (In-Su Han, Chang-Bock Chung, *Chemical Engineering Science 56*, 2001, page 1954, see Annex I).

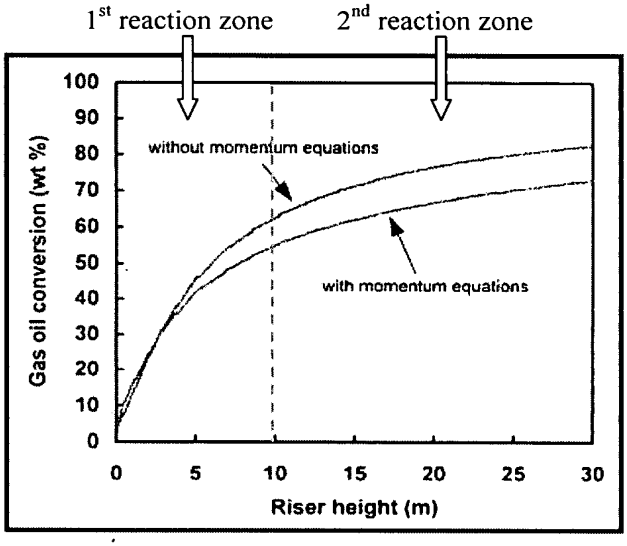

Fig 1: Distribution of conversion along the axial direction of the height of the riser

It is generally accepted in the art that the ratio of the velocity at the outlet of an iso-diameter riser(i.e. the so-called first reaction zone) to the velocity at the inlet of the iso-diameter riser(i.e. the so-called first reaction zone) is less than 3, and absolutely no more than 10. This is exemplified by the following two examples:

(1) Figure 2 illustrates the distribution of velocity along the axial direction of the height of the riser (In-Su Han, Chang-Bock Chung, *Chemical Engineering Science 56*, 2001, page 1978, see Annex II). It can

be seen that the ratio of the velocity at the outlet of the first reaction zone to the velocity at the inlet of the first reaction zone (i.e. u_1/u_0 in Figure 2) is less than 2.

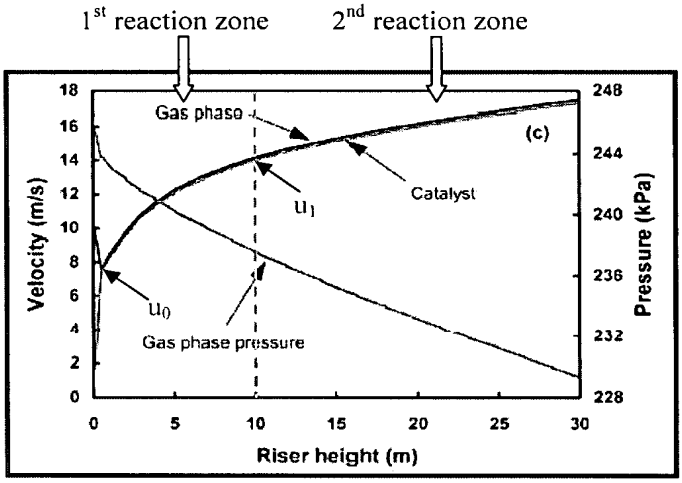

Fig. 2 Distribution of velocity along the height of the riser

(2) It can be readily seen from the reference *Process Calculation and Technical Analysis of Catalytic Cracking* (written by Cao Hanchang, Hao Xiren and Zhang Han, see Annex III, and the translation thereof, Annex IV) attached to this Declaration that, for example, the calculation results on page 242 (see also pages 5 and 6 of Annex IV) show a velocity of 11.45 m/s at the outlet of the riser, a velocity of 5.78 m/s at the inlet of the riser and a ratio of the former to the latter of 1.98.

In the Office Action issued by the Examiner ("DATE MAILED: 01/23/2006"), the Examiner makes the following comments:

Looking only to the data provided on page 49, lines 8-24, of Kmecak, et al (in the "specific embodiment" for FIG. VIII), the following can be said of the riser reactor:

-riser reactor height=about 49 meters

-average linear velocity of the suspension in the riser reactor=about 24m/s.

-total time required to traverse the riser reactor=about 2 seconds

-total time within the prelift zone of the riser reactor(i.e., the dry gas-steam-catalyst suspension residence time before contact with the atomized oil feed)= a fraction of a second up to 0.5 seconds

-total time within the first reaction zone, second reaction zone, and first conjunct section, combined (i.e. a hydrocarbon residence contact time with catalyst particles)=up to about 1 or 1.5 seconds

In the case that the total residence time within the riser reactor is set at 2 seconds, we can properly assume a residence time of roughly 0.5 seconds within the prelift zone and a residence time of roughly 1.5 seconds within the first reaction zone, second reaction zone, and first conjunct section.

Looking now to Figure VIII, we can further assume from the proportions given in the drawing the riser reactor is roughly configured as follows:

*-Pre-lift zone height (0.1*H)=4.9 m*

*-First reaction zone height (0.3*H)=14.7 m*

*-second reaction zone height (0.5*H)=24.5 m*

*-First conjunct section height (0.1*H)=4.9 m*

-the average linear velocity of the suspension in the prelift zone =9.8 m/s

My deduction is based on the Examiner's analysis mentioned above and Figure 3 as shown hereinbelow:

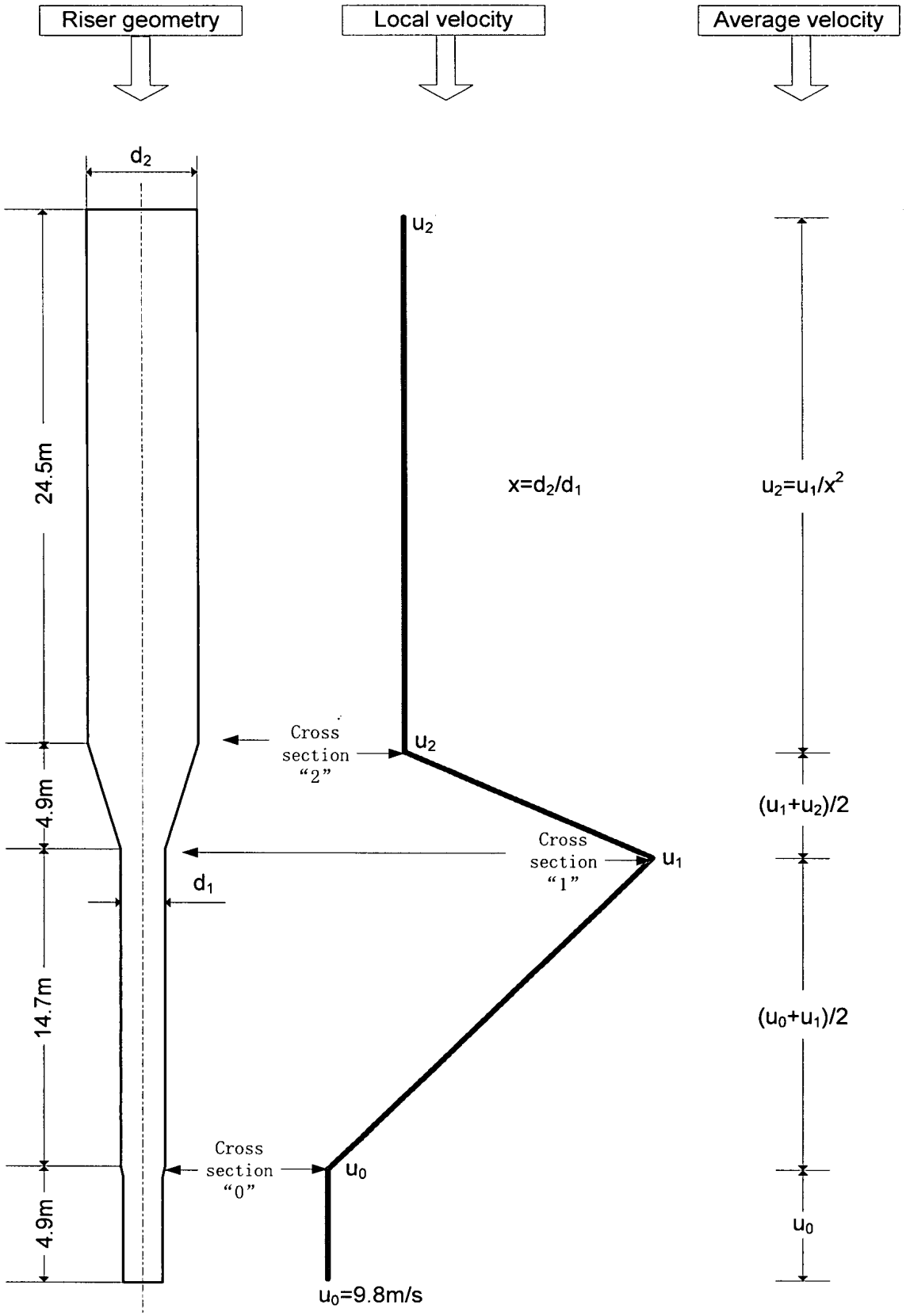
Riser geometry
Local velocity
Average velocity
d2
24.5m
4.9m
14.7m
4.9m
d1
u2
Cross section "2"
u2
x=d2/d1
u2=u1/x2
(u1+u2)/2
Cross section "1"
u1
(u0+u1)/2
Cross section "0"
u0
u0
u0=9.8m/s

Fig. 3

The symbols are defined as follows:
u—velocity, m/s;
h—height of the riser, m
t—residence time, s
V—volume flow rate, m^3/s;
A—cross-sectional area of the riser, m^2;
d—diameter of the riser, m;
x—ratio of the diameter of the second reaction zone to the diameter of the first reaction zone, dimensionless;
p—pressure, Pa;
M—molar mass, g/mol;
R—gas constant, 8.314 J/mol•K;
T—temperature, K
ρ—density, kg/m^3.

Symbols t, ρ and V are defined by the following equations:

$$t = \frac{h}{u} \quad (1)$$

$$\rho = \frac{P \times M}{R \times T} \quad (2)$$

$$V = u \times A = u \times \pi \times \left(\frac{d}{2}\right)^2 \quad (3)$$

Prerequisites or Assumptions for said Deduction

(1) No chemical reaction occurs in the prelift zone, the fluid is in a uniform motion state, and the average velocity is represented by u_0.

(2) The velocity in the first reaction zone exhibits a logarithmic increase tendency along the axial direction of the riser, and the average velocity in the first reaction zone is represented by the logarithmic mean value of the velocity at the inlet (u_0) and the velocity at the outlet (u_1), which is calculated as described hereinbelow:

$$\frac{u_1 - u_0}{\ln u_1 - \ln u_0}$$

(3) The basic reactions in the second reaction zone are conversion reactions, and molecular expansion may be neglected. The state of the fluid may approximately be regarded as uniform motion state. The average velocity is presented by u_2.

(4) The velocity in the conjunct section between the first and second reaction zones exhibits a linear decrease tendency along the axial height of the riser, and the average velocity is presented by the mean value of the velocity at the inlet (u_1) and the velocity at the outlet (u_2), which is calculated as described hereinbelow:

$$\frac{u_1 + u_2}{2}$$

Detailed Deduction Procedure:

Based on the above-mentioned prerequisites or assumptions for deduction and the data disclosed in EP0171460 (the height of the prelift zone is 4.9 m, the height of the first reaction zone is 14.7 m, the height of the conjunct section between the first and second reaction zone is 4.9 m, the height of the second reaction zone is 24.5 m, the total height of the riser is 49 m and the average velocity in the whole riser is 24.5 m/s), the residence time in the whole riser is calculated as described hereinbelow:

$$\frac{4.9\text{m}}{u_0} + \frac{14.7\text{m}}{\frac{u_1 - u_0}{\ln u_1 - \ln u_0}} + \frac{4.9\text{m}}{\frac{u_1 + u_2}{2}} + \frac{24.5\text{m}}{u_2} = \frac{49\text{m}}{24.5\text{m/s}} \qquad (4)$$

It can be seen from the data provided by the Examiner that u_0=9.8 m/s, and thus Equation (4) may be written as:

$$\frac{4.9\text{m}}{9.8\text{m/s}} + \frac{14.7\text{m}}{\frac{u_1 - 9.8\text{m/s}}{\ln u_1 - \ln 9.8\text{m/s}}} + \frac{4.9\text{m}}{\frac{u_1 + u_2}{2}} + \frac{24.5\text{m}}{u_2} = 2\text{s} \qquad (5)$$

According to the law of conservation of mass, the mass flowrates at all cross-sections of the riser are equal, and, in terms of Figure 3, the mass flowrate at the inlet of the conjunct section between the first and second

reaction zones (shown by the subscript "1") and the mass flowrate at the outlet of the conjunct section between the first and second reaction zones (shown by the subscript "2") are equal, as shown by the following equation:

$$\rho_2 \times V_2 = \rho_1 \times V_1 \qquad (6)$$

The general knowledge of the principles of catalytic cracking teaches us that the reactions occurring at cross-section "1" and cross-section "2" are basically conversion reactions and cracking does not occur in a large scale. Accordingly, it may be concluded that the number of molecules at said two cross-sections remains unchanged. Since the pressures and temperatures at said two cross-sections do not change much, it may be concluded, on the basis of the density definition, i.e. equation (2), that the densities at said two cross-sections are equal:

$$\rho_2 = \rho_1 \qquad (7)$$

Equation (6) can thus be written as:

$$V_2 = V_1 \qquad (8)$$

Upon substitution of the mass flowrate definition, i.e. Equation (3), into Equation (8), a new equation is obtained, which is as follows:

$$u_2 \times \pi \times \left(\frac{d_2}{2}\right)^2 = u_1 \times \pi \times \left(\frac{d_1}{2}\right)^2 \qquad (9)$$

Equation (9) is transformed to obtain the following equation:

$$u_2 = \frac{u_1}{\left(\frac{d_2}{d_1}\right)^2} = \frac{u_1}{(x)^2} \qquad (10)$$

The following monadic nonlinear equation about u_1 is thus obtained by substituting Equation (10) into Equation (5):

$$0.5s + \frac{14.7m}{\frac{u_1 - 9.8m/s}{\ln u_1 - \ln 9.8m/s}} + \frac{4.9m}{\frac{u_1 + \frac{u_1}{x^2}}{2}} + \frac{24.5m}{\frac{u_1}{x^2}} = 2s \qquad (11)$$

The Examiner believes that the ratio of the diameter of the second reaction zone to the diameter of the first reaction zone is 3, which means that x=3 in Equation (11). The following result is then obtained by solving Equation (11):

$$u_1 = 183.3\text{m/s} \quad (13)$$

Obviously,

$$\frac{u_1}{u_0} = \frac{183.3\text{m/s}}{9.8\text{m/s}} = 18.7 \quad (14)$$

The ratio of 18.7 is far greater than the generally recognizable ratio of less than 3 in the art, and is even greater than 10. This is highly contrary to the fact pointed out in Item 8 herein that "it is generally accepted in the art that the ratio of the velocity at the outlet of an iso-diameter riser(i.e. the so-called first reaction zone) to the velocity at the inlet of the iso-diameter riser(i.e. the so-called first reaction zone) is less than 3, and absolutely no more than 10".

Thus, the Examiner's opinion that "DR_2: DR_1 is equal to approximately 3: 1" is incorrect and impossible.

9. I further declare that all statements made herein on personal knowledge are true and that all statements made on information and belief are believed to be true; and that these statements are made with the knowledge that willfully or intentionally false statements made by declaration to the United States Patent and Trademark Office are punishable by fine or imprisonment, or both, under 18 U.S.C. §1001; and that such willfully or intentionally false statements may jeopardize the validity and/or enforceability of the patent application with Appl. No. 09/553,990 and any United States Patent issuing therefrom.

Signed at Beijing this 11th day of June, 2007.

Xu Youhao

Dr. Xu Youhao

ANNEX I

PERGAMON

Chemical Engineering Science 56 (2001) 1951–1971

Chemical Engineering Science

www.elsevier.nl/locate/ces

Dynamic modeling and simulation of a fluidized catalytic cracking process. Part I: Process modeling

In-Su Han, Chang-Bock Chung*

Faculty of Applied Chemistry, Chonnam National University, Kwangju 500-757, South Korea

Received 16 December 1999; received in revised form 18 August 2000; accepted 5 September 2000

Abstract

The purpose of this study is to develop a detailed dynamic model of a typical FCC unit that consists of the reactor, regenerator, and catalyst transfer lines. A distributed parameter model is presented for the reactor riser to predict the distributions of the catalyst and gas-phase velocities, the molar concentrations of 4-lump species, and the temperatures. The regenerator is also modeled in such detail that the two-regime, two-phase behavior of typical fluidized beds can be accounted for. An efficient model solver was constructed on the basis of a modular approach in which the model equations are grouped into 12 modules each corresponding to a specific part of the unit and type of equations. The dynamic model is implemented in Part II of this paper for extensive simulation study on FCC processes. © 2001 Published by Elsevier Science Ltd.

Keywords: Dynamic simulation; Modeling; Fluidized catalytic cracking; Fluidized bed; Modular approach

1. Introduction

A fluidized catalytic cracking (FCC) process is a unit that converts heavy distillates like gas oils or residues to gasolines and middle distillates using cracking catalyst. Various types of FCC units are being operated over the world, including the Flexicracker and MODEL IV unit of Exxon, the Orthoflow unit of M.W. Kellogg, the FCC resid cracker of Stone & Webster. Since a typical FCC unit can process a large amount of the feedstock into more valuable products, the overall economic benefits of a refinery could be considerably increased if proper control and optimization strategies are implemented. The first step toward the goal will be to develop an accurate model that represents the dynamics of the process.

FCC processes are known to be very difficult to model because of the large process scale, complicated hydrodynamics, and complex kinetics of both cracking and coke burning reactions. Accordingly, numerous papers on FCC modeling have had widely varying scopes and levels of modeling rigor. Some papers are focused on specific parts of the unit while others are only concerned with reaction kinetics or steady-state behavior. Several studies on dynamic modeling of the whole FCC unit also have limited applicability due to the outdated process type or the oversimplified assumptions introduced in the modeling.

Early papers on FCC modeling are mainly concerned with the reaction kinetics or steady-state process behavior. Weekman and coworkers (Jacob, Gross, Voltz, & Weekman, 1976; Voltz, Nace, & Weekman, 1971; Weekman & Nace, 1970) proposed the three-lump and 10-lump cracking reaction models. Several variations of these models are also available in the literature. Weisz and Goodwin (1963, 1966a) and Weisz (1966b) carried out extensive studies on the kinetics of coke burning reactions in the regenerator. Hano, Nakashio, and Kusunoki (1975) and Morley and de Lasa (1987, 1988) also estimated the kinetic parameters of the coke burning reactions for zeolite catalyst. De Lasa and Grace (1979), De Lasa, Errazu, Barreiro, and Solioz (1981) and Errazu, de Lasa, and Sarti (1979) performed steady-state analyses of the regenerator using their models based on the two-phase theory. Elshishini and Elnashaie (1990a,b), Elshishini, Elnashaie, and Alzahrani (1992), Arbel, Huang, Rinard, Shinnar, and Sapre (1995a) and Arbel, Rinard, Shinnar, and Sapre (1995b) reported the multiple steady states of an FCC unit found in their steady-state simulations.

Dynamic models have been developed in several studies for certain parts of the FCC process. Faltsi-Saravelou

* Corresponding author. Tel.: + 82-62-530-1884; fax: + 82-62-530-1899.

E-mail address: chungcb@chonnam.ac.kr (C.-B. Chung).

0009-2509/01/$ - see front matter © 2001 Published by Elsevier Science Ltd.
PII: S0009-2509(00)00493-0

and Vasalos (1991a) and Faltsi-Saravelou, Vasalos, and Dimogiorgas (1991b) developed a fluidized-bed model for a regenerator comprising the dense bed and the freeboard. The model is based on the two-phase theory (Kunii & Levenspiel, 1991) and contains some empirical equations obtained from fluidization experiments. Theologos and Markatos (1993) and Theologos, Nikou, Lygeros, and Markatos (1997) presented a quite detailed dynamic model of a reactor riser. Their model consists of a set of three-dimensional partial differential equations that describe the distributions of catalyst and gas velocities, pressure, component concentrations, and temperature. The model appears to represent the maximum conceivable rigor for the riser dynamics, but it would be a formidable task to extend the rigor to other parts of an FCC unit as well.

Dynamic models for the whole FCC unit have been presented in recent papers. Elnashaie and coworkers (Elnashaie & Elshishini, 1993; Elnashaie, Abasaeed, & Elshishini, 1995) extended their steady-state model to a simple dynamic model, and investigated the sensitivity and stability of a bed-cracking type FCC unit. Lopez-Isunza (1992) presented a distributed parameter dynamic model for mass and energy balance, but their model neglects the hydrodynamic aspects of the FCC unit. Moreover, their model did not take into account the mixing characteristics of catalysts in the regenerator. Mcfarlane, Reineman, Bartee, and Georgakis (1993) presented quite a comprehensive model that covers most parts of a Model IV type FCC unit, including the reactor, regenerator, bowers, U-bends, compressors, furnace, and valves. But their models seem to be so oversimplified that the distributed characteristics of the reactor riser or the regenerator are not properly accounted for. Furthermore, the numerous empirical equations in the model are tailored to the Model IV FCC unit, making it difficult to extend to other FCC units of different type. Arbel et al. (1995a,b) developed a model that can describe both the steady-state and dynamic behavior of an FCC unit being operated in both partial and full combustion modes. The model seems to be very successful to predict the steady-state behavior of an FCC unit such as steady-state and input multiplicities. Ali and Rohani (1997) presented a dynamic model that consists of several ordinary differential equations. They presented analytic solutions of the differential equations after adopting pseudo steady-state assumptions. However, it is impossible to predict the after burning reaction because they do not take into consideration the freeboard region of the regenerator in their model.

The purpose of this study is to develop a detailed dynamic model of a modern riser-type FCC unit that consists of the reactor, regenerator, and catalyst transport lines with slide valves. Once the dynamic model and a simulator implementing the model are available, they can be used as a tool (i.e., as a hypothetical plant) for carrying our various process system studies like control and optimization. The dynamic model is developed to complement the previous models presented in the literature and is expected to serve as a tool for various process system studies on an FCC process. Hydrodynamic descriptions for the crucial parts of the unit are incorporated into the model. Special attention has been paid to the reactor riser to predict the velocity distributions of the catalyst and gas phases, the molar concentrations of 4-lump species, and the temperatures. The regenerator is also modeled in such detail that the two-regime (dense bed and freeboard), two-phase (emulsion and bubble) behavior of typical fluidized beds can be described. The cyclones in both the reactor and the regenerator are modeled to take into account their effect on overall dynamics of an FCC process. Pressure and valve equations are included in the modeling of the catalyst transport lines to describe of the interaction between the reactor and the regenerator. The model solver was constructed on the basis of a modular approach. The model equations are grouped into 12 modules each of which corresponds to a specific part of the unit and type of equations, and then an efficient iterative scheme is employed for convergence of all the modules. The results of steady-state and dynamic simulations using the developed model are presented in Part II of this paper. Since the most important model fidelity consideration for FCC modeling is how well the model reproduces the steady-state behavior (Arbel et al., 1995a), we compared in Part II the steady-state behavior predicted by our model with those in the literature.

2. Process modeling

The FCC units can be grouped into a side-by-side type and a stacked type according to the configuration of the reactor and the regenerator. Fig. 1 shows a typical side-by-side type FCC unit that comprises a reactor and a regenerator joined by two catalyst transport lines. It accounts for large part of the modern-type FCC units being operated over the world. In the stacked type FCC unit the reactor is placed directly above the regenerator to straighten the catalyst transport line. Because the major physicochemical phenomena taking place in both the side-by-side type and the stacked type units are very similar to each other, we describe the modeling procedure only for the side-by-side type unit.

Before presenting the detailed model of each process unit, we describe the major physicochemical phenomena taking place in the FCC unit. The cracking reaction of hydrocarbon feeds takes place in the riser, while the regeneration of deactivated catalyst by coke deposition takes place in the regenerator. The hydrocarbon feed like vacuum gas oil is injected into the bottom of the riser along with a small amount of steam (0.5–3 wt% of feed),

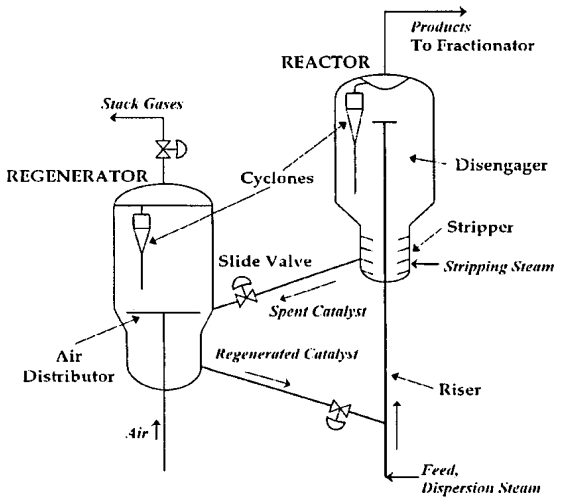

Fig. 1. Schematic diagram of a side-by-side type FCC unit.

which leads to good atomization and reduces coke formation. The feed is subsequently vaporized upon contacting the hot catalyst flowing from the regenerator. The hydrocarbon vapors go through endothermic catalytic cracking reactions on their way up through the riser. Lighter hydrocarbons are produced as main cracking products along with by-product coke, which deposits on the catalyst surface and lowers the catalyst activity. The residence time of the catalyst and hydrocarbon vapors in the riser is typically in the range of 2–5 s. The riser top temperature is typically between 750 and 820 K and is usually controlled by regulating the flow of hot regenerated catalyst to the riser. The disengaging section of a modern riser-type reactor only serves to separate catalyst particles from vapors. The product vapor from the disengaging section enters a main-fractionator where vapor products are separated into various boiling point fractions. The spent catalyst is separated from the vapor in the reactor cyclone and falls into the stripping section where the hydrocarbons remaining on the surface are removed by stripping steam. The stripped spent catalyst is recycled through a catalyst transport line to the regenerator.

In the regenerator which is operated in the fluidization regime, the coke is burnt off the catalyst surface by the air blown into the bed. This combustion reaction serves to reactivate the catalyst and to maintain the bed temperature (950–980 K for a gas oil cracker, 980–1080 K for a resid cracker) high enough to supply the heat required for the vaporization and cracking reaction of the feed in the reactor. The regenerated catalyst flows continuously into the riser bottom through another catalyst transport line. The catalyst circulation rate between the reactor and the regenerator is controlled by the two slide valves attached on the catalyst transport lines.

In this paper, the modeling is concentrated on the reactor, regenerator, and catalyst transport lines. The catalytic cracking unit has several auxiliary units: the air blower, expander, wet gas compressor, feed pre-heater, air heater, catalyst cooler, CO boiler, and so on. Because different catalytic cracking units have different designs for these auxiliary units, the modeling of these auxiliary units is not included in this paper. In the subsequent sections, we describe the structures and features of our model and modeling assumptions. The entire model equations are presented in detail in the Appendix.

2.1. Reactor

Fig. 2 shows a schematic of the reactor which is dissected into several sections (the feed vaporization section, the riser, the disengaging-stripping section, and the reactor cyclones) for modeling purpose. The rectangles in the figure denote the control domains on which the model equations are derived, and the arrows denote flow directions between sections. In our study the riser was modeled as a tubular reactor consisting of the catalyst and gas phases and the feed vaporization section as a junction of two streams. The disengaging-stripping section and cyclones are modeled as a continuous stirred tank (CST). Quasi-steady-state models are applied to the feed vaporization section, the riser, and the reactor cyclones because these sections or units (with the time constant in the range of a few seconds) show much faster

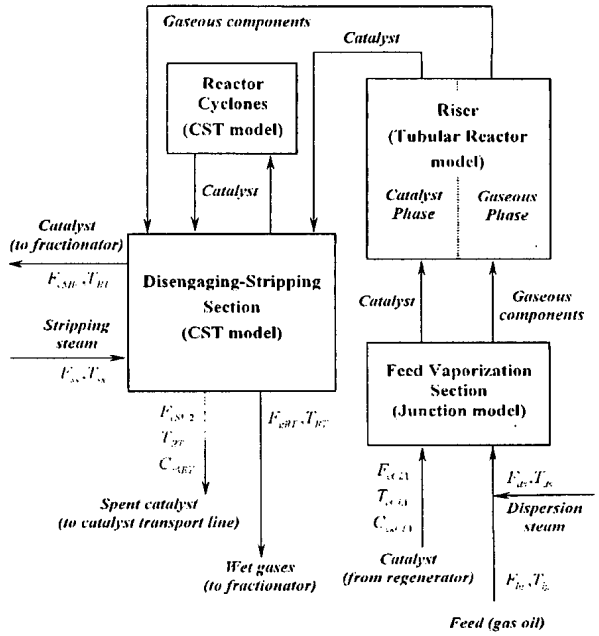

Fig. 2. Schematic diagram of the reactor model.

dynamics than other units like the disengaging-stripping section (with the time constant in the order of a few minutes) or the regenerator (with the time constant in the range of several minutes to an hour). Thus, the overall dynamics of the reactor can be reasonably taken to be dominated by the dynamics of the disengaging-stripping section. In fact, the quasi-steady state assumptions for the riser are common in the modeling of the modern-type FCC units (Elnashaie & Elshishini, 1993, 1995; Arbel et al., 1995a; Ali & Rohani, 1997; Ali, Rohani, & Corriou, 1997).

2.1.1. Feed vaporization section

The feed vaporizes when it is mixed with the regenerated catalyst in the feed vaporization section located at the bottom of the riser. The feed vaporization section is modeled as a pseudo-heat transfer system in which two streams (catalyst and feed) join. The temperature, pressure, and velocity of the vapor and the catalyst coming out of the vaporization section are calculated. These variables depend on the process variables such as feed temperature, feed characteristics, feed droplet size, catalyst temperature, and pressure. The volume expansion and temperature variation caused by the vaporization of liquid feed are considered in the modeling of the feed vaporization section.

Because modern FCC units have a number of feed nozzles designed to help rapid vaporizations of the feed, it is possible to assume that the feed vaporizes instantly upon contacting the hot catalyst. This assumption is supported by the paper of Ali et al. (1997) in which it takes about 0.1 s (corresponding to about 3% of the residence time of the gas–catalyst mixture in the riser) to fully vaporize the feed. Based on the characteristics stated above, a quasi-steady-state model is postulated for the feed vaporization section. It is further assumed that the vapor feed is at the saturated state after vaporization and that the riser is operated under adiabatic condition.

2.1.2. Reactor riser

The riser is modeled as a one-dimensional tubular reactor without radial and axial dispersion. Momentum, mass, and energy balance equations are derived for both the catalyst phase and the gas phase under the following assumptions: (1) the cracking reactions only take place in the riser; (2) the riser wall is adiabatic; (3) dispersion and adsorption inside the catalyst particles are negligible; (4) the coke deposited on the catalyst does not affect the fluid flow; (5) the coke has the same properties as the catalyst; (6) the riser dynamics is fast enough to justify a quasi-steady-state model.

The momentum equations are included in the riser modeling to describe the significant variation of the linear velocities of the catalyst and gas phases along the riser. There is significant molar expansion with increasing conversion of the feed and consequent acceleration of

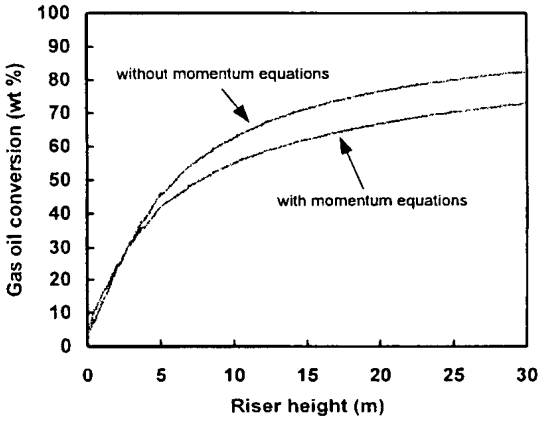

Fig. 3. Profiles of gas oil conversion calculated with and without momentum equations.

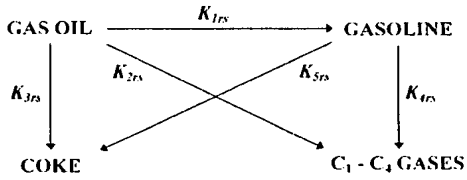

Fig. 4. Four-lump model for gas oil cracking reactions.

both the catalyst and gas phases (Theologos & Markatos, 1993; Theologos et al., 1997). But, most studies on the riser modeling in the literature assumed the linear velocity to be constant throughout the riser, probably to keep the momentum equations from making the entire model stiff and complex. To investigate the degree of error arising from assuming constant velocity, we compared the gas oil conversions obtained by including and excluding the momentum equations in the riser model, respectively. Fig. 3 shows that the conversions at the riser exit can deviate from each other by as large as 9.6%. It becomes clear that the momentum equations can explain the molar expansion and catalyst slip in the riser and can considerably reduce the error arising from assuming constant values for such properties of the catalyst and gas phases as velocities, volume fractions, density, and pressure. Furthermore, the momentum equations enable one to predict the pressure drop across the riser and consequently the pressure in the feed vaporization section.

The mass balance equations are used for predicting the component weight fractions of the four lumps: gas oil, gasoline, light gases (C_1–C_4), and coke. Fig. 4 shows the four-lump model of Lee, Chen, and Huang (1989) that expresses the kinetics of cracking reactions in the riser. This model which is a revised version of the three-lump model of Weekman and Nace (1970) takes the coke

yield into account. The more detailed 5-lump model (Ancheyta-Juarez, Lopez-Isunza, Aguilar-Rodriguez, & Moreno-Mayorga, 1997) or 10-lump model (Jacob et al., 1976) may be used if one wants to predict the yields of subdivided fractions. It is assumed that cracking of gas oil is a second-order reaction but that of gasoline is a first-order reaction, and that the reactions take place only in the gas phase. Since the overall cracking rate is affected by the catalyst activity, its effect should be incorporated into the kinetic expressions. However, the catalyst activity is very hard to model with certainty since the intrinsic catalyst activity and the coking rate depend upon feed composition, the addition of catalyst activity modifiers, and the rate at which the catalyst is replaced with fresh catalyst. In this study it is assumed that coke deposition on catalyst is the major cause of catalyst deactivation, and that its effect can be described by a catalyst deactivation function of the following form:

$$\phi_c = \exp(-\alpha_c C_{ckRS}). \tag{1}$$

where the catalyst deactivation coefficient α_c is related to the temperature and the feedstock composition by the following equation:

$$\alpha_c = \alpha_{c0} \exp\left(\frac{-E_c}{RT_{gRS}}\right)(R_{AN})^{\alpha_c^*}. \tag{2}$$

Heavier gas oil feeds generally contain large amount of Conradson carbon and may affect the catalytic cracking rate. It is assumed that the Conradson carbon in the virgin feedstock is directly converted to coke at the entrance of the riser and deactivates the catalyst.

The catalyst temperature is higher than the gas temperature throughout the riser and the consequent heat transfer provides the heat required for the vaporization and endothermic reaction of the feedstock. The heat transfer between the two phases and the heat of cracking reaction are considered in the energy balance for the riser to predict the temperature of each phase.

2.1.3. Disengaging-stripping section

The disengager and the stripper of the reactor are combined into a single section called the "disengaging-stripping section" in our model. The section is modeled as a perfectly mixed continuous tank with no reaction taking place. Because the catalyst is immediately separated from the product vapor via the cyclones, further cracking reaction seldom occurs in the disengaging-stripping section. The disengaging-stripping model comprising the coke, catalyst, gas component, energy, and pressure balances is used to calculate several major state variables: the coke on catalyst after stripping, the catalyst and gas holdups, the concentrations of the gaseous component into the main-fractionator, and the reactor temperature and pressures.

A portion of hydrocarbons is trapped in the pores of the catalyst in the riser. The unremoved hydrocarbons are converted in the regenerator to coke (called *catalyst-to-oil coke* or *occluded coke*) and thus cause the loss of product yield and an increase in the air required for catalyst generation. Some of the hydrocarbons can be removed in the stripper by steam stripping the rate of which depends on the catalyst-to-oil ratio and steam injection rate. In this study, the following exponential type stripping function is developed to account for the catalyst-to-oil coke:

$$C_{ckST} = C_{ckST0} + k_{ss0} \exp\left[-\frac{E_{ss}F_{cRS}F_{ss}}{F_{lg}}\right]. \tag{3}$$

In the modeling of an FCC unit, pressure should be treated as one of the most important process variables because the pressure difference between the reactor and the regenerator determines the catalyst circulation rate and thus the degree of interaction between the two vessels. The pressure in the disengaging-stripping section is calculated from the ideal gas law and the pressure at the bottom of the reactor is estimated using the static head exerted by the stacked catalyst particles.

2.1.4. Reactor cyclones

Both the reactor and the regenerator of an FCC unit are usually equipped with several multi-stage cyclones to separate catalyst particles from entraining vapors. All the cyclones in the reactor are lumped into one modeling unit, which is then described as a continuous stirred tank (CST). It is assumed that all the reactor cyclones have the same dimensions and that the catalyst holdup in each cyclone is equal to each other. It is further assumed that the flow rate of the catalyst exiting the cyclone dip-legs is only determined by the catalyst holdup in the cyclones. Because no cracking reaction takes place in the reactor cyclones, the cyclones are in thermal equilibrium with the disengaging-stripping section. Therefore, only the mass balances are required to calculate the following state variables: the reactor cyclone inlet velocity, the catalyst holdup in the reactor cyclones, and the mass flow rate of the fluids exiting the reactor.

2.2. Regenerator

The regenerators of most FCC units are operated as a fluidized bed which consists of two sections commonly called a *dense bed* and a *freeboard*. The dense bed contains the majority of the catalyst in the regenerator and thus accounts for the generation of spent catalyst by coke burning reactions. The well-known two-phase theory of fluidization (Kunii & Levenspiel, 1991) describes the dense bed as comprising a particle-lean bubble phase and a particle-rich emulsion phase surrounding the bubbles.

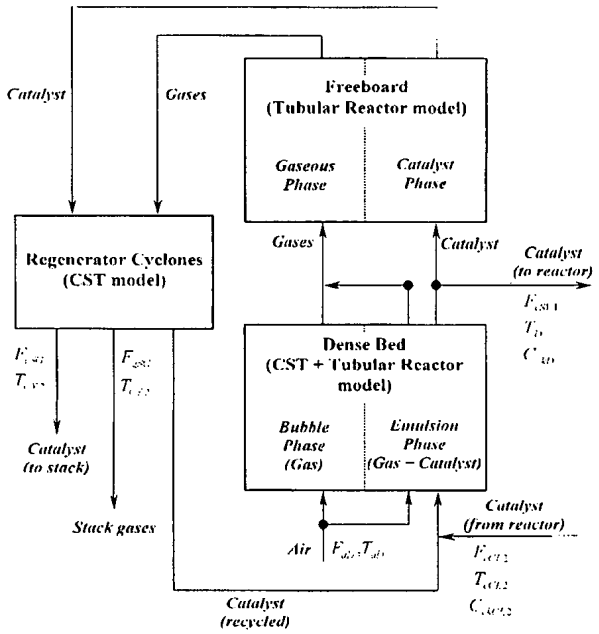

Fig. 5. Schematic diagram of the regenerator model.

The gas bubbles erupt at the surface of the dense bed and eject the catalyst particles into the freeboard. Since the catalyst bulk density is very low in the freeboard, the coke burning reaction is slower than in the dense bed, but there take place the after-burning reactions that oxidize carbon monoxide to carbon dioxide. The catalyst particles entrained in the stack gas are separated in the cyclone and then are recycled to the dense bed. The physical situations described here are illustrated in a schematic diagram of the regenerator shown in Fig. 5. The dense bed is modeled as a hybrid reactor that employs a mixed-tank model for energy and coke balances but a tubular reactor model for gas component balances. The freeboard is modeled as a two-phase tubular reactor, and the cyclone as a mixed-tank.

Because the regenerator contains much larger amount of catalyst than the reactor, the residence time of catalyst in the former (usually falling within the range of several minutes to an hour depending on the type of FCC units) is much longer than in the latter. Thus, the overall dynamics of an FCC process is largely dominated by the dynamics of the regenerator, which necessitates quite a detailed description of the regenerator for reliable predicting of the entire process behavior. In this study, dynamic balances are set up for the coke, catalyst, gas component, and energy in every dissected region.

We begin with the reaction kinetics and the overall hydraulics of the regenerator.

2.2.1. Coke burning kinetics

The typical coke consists of various chemical compounds including hydrocarbons, sulfuric and nitrogenous compounds. Since the hydrocarbons are dominant, however, in this study the coke is assumed to have the formula CH_q and to burn according to the following reaction schemes (Weisz & Goodwin, 1963, 1966a; Weisz, 1966b; Hano et al., 1975):

$$CH_q + (0.5 + 0.25q)O_2 \rightarrow CO + 0.5qH_2O$$

$$r_{1i} = k^*_{1RG} C_{cki} C_{O_2 i},$$

$$CH_q + (1 + 0.25q)O_2 \rightarrow CO_2 + 0.5qH_2O$$

$$r_{2i} = k^*_{2RG} C_{cki} C_{O_2 i}, \quad i = E, F\}, \tag{4}$$

where the rate constants can be represented by

$$k^*_{1RG} = \frac{k_{1RG}}{1+\sigma}, \quad \text{and} \quad k^*_{2RG} = \frac{k_{1RG}\sigma}{1+\sigma}. \tag{5}$$

Besides the coke burning reaction, there takes place the oxidization reaction of the carbon monoxide. It may take the form of either homogeneous oxidation on the gas phase with the kinetics proposed by Howard, Williams, and Fine (1973)

$$2CO + O_2 \rightarrow 2CO_2 \quad r_{3i} = k_{3RG} C_{COi} C^{0.5}_{O_2 i} C^{0.5}_{H_2 Oi},$$

$$i = B, E, F \tag{6}$$

or heterogeneous oxidation in the presence of the catalyst which contains small amounts of oxidation promoters like vanadium, nickel, or copper. Krishna and Parkin (1985), and Ali and Rohani (1997) reported the following kinetics of heterogeneous oxidation:

$$2CO + O_2 \xrightarrow{\text{catalyst}} 2CO_2 \quad r_{4i} = k_{4RG} C_{COi} C^{0.5}_{O_2 i},$$

$$i = E, F \tag{7}$$

2.2.2. Overall regenerator

The total catalyst and gas holdups, superficial gas velocity, average gas density, and pressures are calculated from the balances around the regenerator as a whole. These values are then used in the model equations for each section. The dynamics of the total catalyst and gas holdups are important in describing the interactions between the reactor and the regenerator because these variables strongly affect the catalyst flow rates between the two vessels. The superficial gas velocity varies along the regenerator due to the volume change. Since the mass influent to the gas phase increases in proportion to the coke burned off the catalyst, the superficial gas velocity can be correlated to the average gas density in the regenerator:

$$u_{gRG} = \frac{F_{aD}(1 - \delta_{gRG}) + F_{gSG}\delta_{gRG}}{\rho_{gRG}\Omega_{RG}}. \tag{8}$$

In the above equation, δ_{gRG} denotes the relative extent to which the gas phase mass flow rate increases by the coke burning reaction. It is defined to vary from 0 at the bottom to 1 at the top of the regenerator, and can be calculated by the following expression:

$$\delta_{gRG} = \left[\frac{0.5q\rho_{gRG} - C_{H_2OF}^{(h_{RG})}M_{wck}}{0.5q\rho_{gRG} - C_{H_2Oi}^{(z)}M_{wck}}\right]\left[\frac{C_{H_2Oi}^{(z)} - C_{H_2OD}^{(0)}}{C_{H_2OF}^{(h_{RG})} - C_{H_2OD}^{(0)}}\right],$$
$$i = D, F. \quad (9)$$

The pressures at the dense bed outlet and the bottom of the regenerator are calculated by applying average gas density and are then used to compute the flow rates through the catalyst transport lines.

2.2.3. Dense bed

In this study, the dense bed is modeled to consist of the emulsion and bubble phases on the basis of the two-phase theory. This contrasts with the approaches of Arandes and de Lasa (1992) and Arbel et al. (1995a) who modeled the bed to consist of gas and catalyst phases. The two-phase model can describe the whole range of fluidization regimes that cover the operating conditions of various types of regenerators. Our dynamic balances for the dense bed are based on the hybrid reactor model combining a mixed-tank reactor for coke and energy balances and a tubular reactor for gas component balances. This also contrasts with Faltsi-Saravelou and Vasalos (1991), Ali and Rohani (1997), and Ali et al. (1997) who used mixed-tank reactors for gas component balances in the emulsion phase.

The following assumptions are introduced to facilitate the modeling of the dense bed: (1) the bubbles do not contain any catalyst particles; (2) all the catalyst particles ejected into the freeboard are returned to the dense bed via cyclones; (3) the catalyst particles in the dense bed are perfectly mixed due to the recycle from the cyclone as well as their own circulation in the bed; (4) the catalyst in the dense bed is in thermal equilibrium with the gases; (5) the gas densities of both the bubble and emulsion phases are the same as each other; (6) the gases in both the bubble and emulsion phases are in tubular flow and (7) the gas in the regenerator consists of oxygen, carbon monoxide, carbon dioxide, water vapor, and nitrogen.

The hydraulic properties like the bed heights, phase volume fractions and velocities represent the major modeling elements for the regenerator because they are closely connected to the mass and energy balances in the bed. But the detailed description of the hydraulics is quite involved due to the inherent complexity of the fluidization phenomena. In this study, an empirical correlation between the volume fraction and the average superficial gas velocity was developed by a nonlinear regression of the experimental data of Schnitzlein (1987).

$$\varepsilon_{cD} = 0.3418\exp[-0.9751\tilde{u}_{gRG}] + 0.1592. \quad (10)$$

Then, the bed height can be calculated on the basis of the above equation. The volume fraction of the bubble gas is predicted by the following expression proposed for fast bubbles and Geldart A type particles (corresponding to most FCC catalysts) (Davidson & Harrison, 1963; Kunii & Levenspiel, 1991):

$$\varepsilon_{gB} = \frac{u_{gRG} - v_{gm}}{v_{gB} - v_{gm}}, \quad (11)$$

where the minimum fluidization velocity (v_{gm}) and bubble rising velocity (v_{gB}) can be estimated by empirical expressions in the literature (Kunii & Levenspiel, 1991).

From the gas component, coke, and energy balances, the following state variables are computed: the molar concentrations of gaseous substances along the axial position of the dense bed, the coke on catalyst, and the dense bed temperature. In addition, the volume fractions and the dense bed height are calculated from other mass balances and empirical expressions.

2.2.4. Freeboard

The freeboard is modeled as a tubular reactor. Employing a freeboard model is important in predicting the after-burning reactions in the freeboard. It is assumed that the catalyst in the freeboard is in thermal equilibrium with the gaseous phase and is in plug flow. In most models for the freeboard in the literature, the hydraulic properties like the volume fraction of catalyst is usually assumed to be constant along the freeboard. But, the concentration of the catalyst tends to decay exponentially with increasing height in the freeboard (Kunii & Levenspiel, 1991). In this study, the catalyst volume fraction in the freeboard is estimated with the following empirical equations (Li & Kwauk, 1980):

$$\varepsilon_{cF} = \varepsilon_{cF}^{*} + (\varepsilon_{cD} - \varepsilon_{cF}^{*})\exp[-\beta_c(z - H_D)], \quad (12)$$

where ε_{cF}^{*} denotes the saturated carrying capacity of gas. We carried out nonlinear regression using the experimental data of Zenz and Weil (1958) to obtain the following correlation equation for ε_{cF}^{*}:

$$\varepsilon_{cF}^{*} = \frac{\rho_{gRG}}{\rho_c}10^{[-0.725-2.517\log\chi-0.627(\log\chi)^2]}, \quad (13)$$

The freeboard model comprising the gas component, energy, and coke balances is used to calculate several state variables: the molar concentrations of gaseous substances, coke on catalyst, and the temperature along the axial position of the freeboard.

2.2.5. Regenerator cyclones

Since the catalyst particles collected by the cyclones are recycled to the dense bed, there is significant interaction between the dynamics of the two sections. The

regenerator cyclone is also modeled as a continuous stirred tank like the reactor cyclone. A pseudo-steady state is postulated because the catalyst residence time in the regenerator cyclone is much shorter than in other regenerator sections. The after-burning of CO to CO_2 in the regenerator cyclones (including a plenum chamber) is likely to occur when there is an excess of both oxygen and carbon monoxide. In this study, the temperature rise across the regenerator cyclones is estimated using the following simple correlation (Kurihara, 1967; Hovd & Skogestad, 1993):

$$T_{CY2} = T_F^{(h_{RG})} + c_T f_{O_2 F}^{(h_{RG})}. \quad (14)$$

The regenerator cyclone model yields the mass flow rate of the catalyst into the regenerator cyclones, the catalyst holdup in the regenerator cyclones, and the regenerator cyclone temperature.

2.3. Catalyst transport lines

The catalyst circulation rate between the reactor and the regenerator is controlled by the two slide valves attached on the catalyst transport lines. The catalyst circulation rate through each catalyst transport line is determined by the pressure drop across a slide valve and can be calculated using the following simple valve equation:

$$F_{cSV} = k_u f_v(x_v) \Delta P_{CL}^{0.5}. \quad (15)$$

Because the catalyst residence time in the catalyst transport lines is in the order of a few seconds for stacked type FCC units and ten seconds for the side-by-side type FCC units, it is possible to ignore the transport lag throughout the catalyst transport lines in their model. The following variables are calculated using the catalyst transport line equations: the mass flow rates through the spent and regenerated catalyst transport lines, the coke on catalyst, and the catalyst temperatures.

Table 1
Types of the model equations derived for each section

Process units	PDEs	ODEs	AEs	No. of Eqs.
Feed vaporization section	0	0	7	7
Riser	0	9	27	36
Disengaging-stripping section	0	7	14	21
Reactor cyclone	0	0	5	5
Overall regenerator	0	2	17	19
Dense bed	12	2	44	58
Freeboard	7	0	23	30
Regenerator cyclone	0	0	5	5
Catalyst transport lines	0	0	8	8
Total No. of Eqs.	19	20	150	189

3. Numerical algorithms

The entire dynamic model equations for the FCC process represent a mixed system of differential (ordinary and partial) and algebraic equations. The total of 189 equations comprising the model are arranged in the Appendix and classified in Table 1. The remainder of this paper describes our numerical algorithms for solving the model equations. The estimation methods for the parameters in the model and the results of simulation runs are presented in Part II of this paper.

3.1. Degree of freedom analysis

A degree of freedom analysis should be the first step in the development of a dynamic simulator, especially for a large and complex system like an FCC process. The FCC model presented in this study contains 202 unknown variables as summarized in Table 2 when excluding such determinable parameters as equipment dimensions, physical properties, feedstock characteristics. Hence, the dynamic model is found to have 13 degrees of freedom (=202 variables − 189 equations), which

Table 2
Unknown variables in the model equations for the FCC unit

Variable type	Symbols	No. of unknown variables
Temperature	T	14
Pressure	P	8
Holdup	w, V, H	12
Density & concentration	C, C_{ck}, f, Y, y, ρ	51
Volume fraction	ε	8
Flow rate & velocity	F, v, u	30
Heat rate	H, Q	18
Reaction coefficient	k, R, r, α_c, ΔH, ϕ_c	43
Valve stem position	x_v	3
Others	C_d, c_f, d_b, f, G, M_w, Re, S, δ, χ	15
Total No. of unknown variables		202

means that we have to provide 13 additional relations among the variables before trying to obtain a unique solution. Typically, these relations are provided by the control laws which connect the manipulated variables to the controlled variables under a given control configuration for the process. Since this paper is focused at present on the dynamic behavior of the FCC process in an open-loop mode, however, the 13 degrees of freedom are fixed by specifying the same number of variables appropriately. The variables chosen for this purpose are presented in Part II of this paper where our process simulation results are presented.

3.2. Model equation solvers

The model solver was developed on the basis of a modular approach (Ponton, 1983; Hillestad & Hertzberg, 1986) in which the equations were grouped into the modules and then all the modules were sequentially solved at the same time step. In this study the model equations are classified into modules, each of which corresponds to a specific physical section of the reactor or regenerator. Then some modules are further divided according to the type of equations or the domain of analysis. Fig. 6 shows the overall structure of the model comprising twelve modules and the flows of information between them. As evident from the figure, the modules are severely coupled to each other due to the recycles and interactions between the sections.

Each individual module was solved using a solver specifically chosen for the type of equations in the module. There are four types of equations, and each type was solved by the following numerical methods:

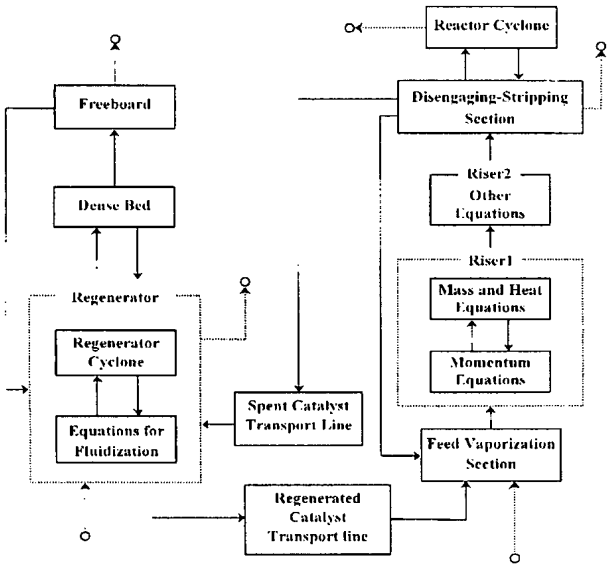

Fig. 6. Information flow between the modules.

(1) *Nonlinear algebraic equations*: The HYBRD1 routine of MINPACK (Garbow, Hillstrom, & More, 1980) was used. It adopts the Powell's hybrid algorithm based on a Newton's method.

(2) *Partial differential equations*: The method of lines (MOL) was employed that converts the partial differential equation into a set of ordinary differential equations using finite difference approximation of the spatial derivatives and then integrates the set of equations with respect to time. First-order backward difference was used to approximate the convection terms and second-order central difference to approximate the diffusion terms. A non-uniform grid scheme was also adopted to enhance the flexibility of meshing.

(3) *Coupled differential and algebraic equations*: The Pezold-Gear's BDF algorithm (Petzold, 1982) was used to solve the momentum equation of the reactor riser that belongs to this class of equations. The algorithm

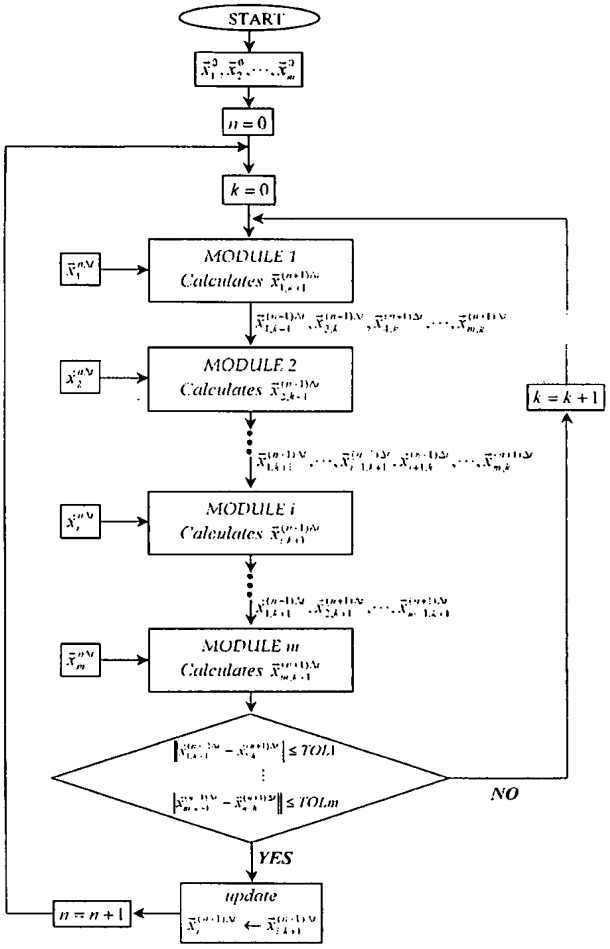

Fig. 7. Modular iteration scheme for convergence.

uses backward difference formulas and shows powerful performance for highly stiff problems.

(4) *Ordinary differential equations*: An LSODE routine (Hindmarsh, 1983) based on the GEAR's algorithm was used. It implements a predictor-corrector method for non-stiff problems and a backward difference formula method for stiff problems. The routine was modified in this study to allow the concurrent integration of multiple modules. It also employs banded matrix algorithms to save storage and computation time.

Fig. 7 shows the iterative procedure employed in this study to obtain convergent solutions for all the modules at every simulation time step. In the figure, n denotes the time step counter, and k the iteration counter at each time step, and $\mathbf{x}_{i,k}^{n\Delta t}$ the vector of the dependent variables of the ith module at the kth iteration step and time $n\Delta t$. Each module is solved in turn at every iteration using an appropriate equation solver discussed previously. An implicit solution in time is sought for in the manner analogous to the Gauss–Seidel algorithm for solving linear algebraic equations. More specifically, in calculating the time-implicit vector $\mathbf{x}_{i,k+1}^{(n+1)\Delta t}$, the updated iteration vectors $\mathbf{x}_{1,k+1}^{(n+1)\Delta t}, \ldots, \mathbf{x}_{i-1,k+1}^{(n+1)\Delta t}$ of the preceding modules and the current iteration vectors $\mathbf{x}_{i+1,k}^{(n+1)\Delta t}, \ldots, \mathbf{x}_{m,k}^{(n+1)\Delta t}$ of the subsequent modules are treated as fixed parameters. On the other hand, when the ith module includes differential equations, the vector $\mathbf{x}_i^{n\Delta t}$ obtained at the previous time step is always used as the initial conditions for time integration. This cycle of computation is repeated until all the modules satisfy their respective specified tolerance, and then the simulation proceeds to the next time step.

4. Conclusions

A detailed dynamic model of a modern riser-type FCC unit that consists of the reactor, regenerator, and catalyst transport lines with slide valves was developed on the basis of the conservation principles. For modeling purposes the reactor was divided into the feed vaporization section, riser, disengaging-stripping section, and reactor cyclones, while the regenerator into the dense bed, freeboard, and regenerator cyclones. Distributed parameter models were presented for the reactor riser, the dense bed, and freeboard of the regenerator, while lumped parameter models were postulated for the other parts of the unit. An efficient model solver was constructed on the basis of a modular approach in which the model equations are grouped into 12 modules each corresponding to a specific part of the unit and type of equations. The dynamic model is implemented by a Fortran code and the simulation results are presented in Part II of this paper.

Notation

All notations should be interpreted according to the following rules. The general form of a symbol is N_{iJk}, where N denotes the property of interest and consists of a letter with or without subscripts. The subscript i in lower-case represents substance or species and may have one or more letters. The subscript J in upper-case designates the part or section of the FCC unit in which the substance i exists and also have one or more letters. The subscript k is optionally used to provide additional information when necessary. Hence, for example, C_{pgRS} denotes the heat capacity of the gas in the riser. It should be noted that subscripts are often omitted for commonly used symbols with obvious meaning, e.g., ρ_c which denotes the catalyst density in all the sections of the FCC unit.

A	surface area, m^2
A_{De}	effective heat transfer area between the dense bed and the surroundings, m^2
A_{lg}, B_{lg}, C_{lg}	coefficients of the Antoine equation for gas oil feedstock
A_{pRSe}	effective interface heat transfer area per unit volume between the catalyst and gas phases in the riser, m^2/m^3
A_{RTe}	effective heat transfer area between the reactor and the surroundings, m^2
c_T	temperature rising factor in the regenerator cyclone equation, K
C	mole concentration, kg mole/m^3
C_{ck}	coke on catalyst, kg coke/kg catalyst
C_{ckSTO}	minimum coke content attainable by stripping, kg coke/kg catalyst
C_d	drag coefficient
C_f	catalyst-gas friction coefficient, kg/m^3 s
C_p	heat capacity, kJ/kg K
$\bar{C}_p$	mean heat capacity, kJ/kg K
d	average diameter, m
d_{cm}	minimum particle diameter that should be completely separated by a cyclone, m
D	diameter, m
E	activation energy, kJ/kg mole
E_{ss}	exponent in the stripping function, s/kg
F	mass flow rate, kg/s
f	mole fraction or friction coefficient
$f^{(0)}$	mole fraction at the bed inlet
$f_v(x_v)$	valve flow characteristic function: $x_v/[\alpha_v + (1-\alpha_v)x_v^2]^{0.5}$ for a linear valve, and $x_v^2/[\alpha_v + (1-\alpha_v)x_v^4]^{0.5}$ for an increasing sensitivity valve
F_a	mass flow rate of the air entering the dense bed, kg/s
F_{ds}	mass flow rate of the dispersion steam entering the feed injection section, kg/s

F_{lg} mass flow rate of the liquid feed entering the feed injection section, kg/s
F_{ss} mass flow rate of the stripping steam entering the disengaging-stripping section, kg/s
g acceleration due to gravity, 9.8 m/s^2
G stress modulus, kg/m s^2
h_{CY1i} inlet height of each cyclone in the reactor, m
h_{CY2i} inlet height of each cyclone in the regenerator, m
h_p interface heat transfer coefficient between the catalyst and gas phases in the riser, kJ/m^2 s K
h_{RG} height of regenerator, m
h_{RS} height of riser, m
h_{RT} height of disengaging section, m
h_{ST} height of stripping section, m
H specific enthalpy, kJ/kg
H, h heights, m
k rate coefficient of a reaction
k_{1RG} rate coefficient of the coke burning reaction, m^3/kg mole s
k_{10RG} frequency factor in the Arrhenius expression for the coke burning reaction, m^3/kg mole s
k_{3RG} rate coefficient of the homogeneous CO oxidation, m^3/kg mole s
k_{30RG} frequency factor in the Arrhenius expression for the homogeneous CO oxidation, m^3/kg mole s
k_{4RG} rate coefficient of the catalytic CO oxidation, m$^{4.5}$/kg catalyst kg mole$^{0.5}$ s
k_{40RG} frequency factor in the Arrhenius expression for the catalytic CO oxidation, m$^{4.5}$/kg catalyst kg mole$^{0.5}$ s
k_{iRS} rate coefficient of the four-lump cracking reaction, 1/s
k_{i0RS} frequency factor in the Arrhenius expression for the four-lump cracking reaction, 1/s
k_{ss0} frequency factor in the stripping function, kg coke/kg catalyst
k_v valve flow rating factor, kg/s kPa$^{0.5}$
k_{vCY1}, k_{vCY2} flow rating factors of the cyclone dip-legs, kg/s m$^{2.5}$
K_I interchange coefficient between the bubble and emulsion phases, 1/s
l length, m
l_{CL1}, l_{CL2} lengths of the catalyst transport lines, m
M_w molecular weight
N_{CY1}, N_{CY2} numbers of cyclones in the reactor and regenerator, respectively
N_t number of turns of 360° made spirally downward in a cyclone
P pressure, kPa
P_{MF} pressure at the main fractionator, kPa
q hydrocarbon to carbon atomic ratio in coke
Q_{react} rate of heat generation or heat removal by reaction, kJ/s
Q_{loss} rate of heat loss to the surroundings, kJ/s
r reaction rate
R ideal gas constant, 8.3143 kPa m^3/kg mole K or kJ/kg mole K)
R_{AN} aromatics-to-naphthenes ratio in liquid feedstock
Re Reynolds number
s_c average sphericity of catalyst particles
S_g total mass interchange rate between the emulsion and bubble phases, 1/s
T temperature, K
T_a temperature of the air entering the dense bed, K
T_{ds} temperature of the dispersion steam entering the feed vaporization section, K
T_e temperature of the surroundings, K
T_{lg} temperature of the liquid feedstock entering the feed vaporization section, K
T_{ref} reference temperature, 298 K
T_{ss} temperature of the stripping steam entering the disengaging-stripping section, K
u superficial velocity, m/s
$\bar{u}$ average superficial velocity, m/s
U overall heat transfer coefficient between a process unit and the surroundings, kJ/m^2 s K
v interstitial velocity, m/s
v_{gm} superficial gas velocity at minimum fluidizing condition, m/s
V volume, m^3
w holdup, kg
x axial coordinate in the riser, m
x_1 axial coordinate in the spent catalyst transport line, m
x_2 axial coordinate in the regenerated catalyst transport line, m
x_v valve stem position, [0 − 1]
y weight fraction, [0 − 1]
Y_{cc} weight fraction of Conradson carbon residue in a feedstock
Y_{conv} gas oil conversion, [0 − 1]
z axial coordinate in the regenerator, m
Z_g gas compressibility factor

Greek letters

α_c catalyst deactivation coefficient
α_{c0} preexponential factor of α_c
α_c^* exponent for representing α_c
α_g gas-phase heat diffusion coefficient, m^2/s

α_v	valve head differential at maximum flow/valve head differential at zero flow, [0 − 1]
β_c	catalyst decay constant, 1/s
δ_g	relative extent to which the gas phase mass flow rate increase by the coke burning reaction
ΔH_f	heat of formation, kJ/kg mole
ΔH_{iRS}	heat of reaction for the four-lump cracking reaction model, kJ/kg
ΔH_{strip}	heat of stripping, kJ/kg
ΔH_{vlg}	heat of vaporization of liquid feedstock in the feed vaporization section, kJ/kg
ε	volume fraction, [0 − 1]
ε_{gm}	void fraction in the dense bed at minimum fluidizing condition, [0 − 1]
η_{CY1}, η_{CY2}	collection efficiencies of cyclones, [0 − 1]
θ_{CL1}, θ_{CL2}	angles of inclination of the catalyst transport lines, degrees
μ	viscosity, kg/m s
ν	stoichiometry coefficient for the coke burning reaction
π	circular constant, 3.141592
ρ	density, kg/m^3
σ	intrinsic CO_2/CO molar ratio in coke
ϕ_c	catalyst deactivation function
χ	$=(u_g^{(h_{RG})})^2/(gd_c\rho_c^2)$
Ω	cross sectional area, m^2
Ω_{CY1d}	cross sectional area of each reactor cyclone dip-leg, m^2
Ω_{CY1i}	cross sectional area of each reactor cyclone inlet, m^2
Ω_{CY2d}	cross sectional area of each regenerator cyclone dip-leg, m^2
Ω_{CY2i}	cross sectional area of each regenerator cyclone inlet, m^2
Ω_{RG}	cross sectional area of regenerator, m^2
Ω_{RS}	cross sectional area of riser, m^2

Subscripts

a	air
B	bubble phase
b	bottom
b	single bubble or catalyst bulk
c	catalyst
cc	Conradson carbon
ck	coke
CL1	regenerated catalyst transport line (to reactor)
CL2	spent catalyst transport line (to regenerator)
CO	carbon monoxide
CO_2	carbon dioxide
CY1	reactor cyclones
CY2	regenerator cyclones
D	dense bed
d	cyclone dip-leg
ds	dispersion steam
E	emulsion phase
e	effective
F	freeboard (dilute phase) region
FS	feed vaporization section
g	gas
gl	gasoline
go	gas oil
gs	light (C1–C4) gases
H_2O	water
hg	hydrocarbon gases
i	inlet
lg	liquid feedstock (gas oil)
m	maximum or minimum
MF	main-fractionator
N_2	nitrogen
O_2	oxygen
RG	regenerator
RS	riser
RT	disengaging-stripping section (or reactor)
s	solid
ss	stripping steam
SG	stack gas valve
ST	stripping section
SV1	slide valve of the regenerated catalyst transport line
SV2	slide valve of the spent catalyst transport line
wv	water vapor
wg	wet gases

Superscripts

in	incoming flow
out	outgoing flow
(*v*)	a variable evaluated at v
(0)	a variable evaluated at the entrance of unit
(H_D)	evaluated at the dense bed exit
(h_{RG})	evaluated at the top of the regenerator
(h_{RS})	evaluated at the riser exit
(*t*)	evaluated at time t
(T_D)	evaluated at the temperature of the dense bed
(T_F)	evaluated at the temperature of the freeboard
(*x*)	evaluated through the axial position of the riser
(*z*)	evaluated through the axial position of the regenerator

Acknowledgements

The study was financially supported by Korea Science and Engineering Foundation under Grant No. 981-1104-013-2.

Appendix A. Process model equations

A.1. Feed vaporization section

The feed vaporization section is modeled as pseudo-heat transfer system in which two streams (catalyst and feed) join. The catalyst temperature after feed vaporization is calculated by the following energy balance assuming adiabatic operation, and the vapor temperature is calculated by the Antoine equation.

$$T_{cFS} = T_{cCL1} - \frac{F_{lg}}{F_{cCL1}\bar{C}_{pc}}\left[\bar{C}_{plg}(T_{gFS} - T_{lg}) + \frac{F_{ds}\bar{C}_{pds}}{F_{lg}}(T_{gFS} - T_{ds}) + \Delta H_{vlg}\right], \tag{A.1}$$

$$T_{gFS} = \frac{B_{lg}}{A_{lg} - \log(P_{FS}y_{goFS})} - C_{lg}, \tag{A.2}$$

where

$$P_{FS} = P_{RT} + \Delta P_{RS} = P_{RT} + [P_{RS}^{(0)} - P_{RS}^{(h_{RS})}], \tag{A.3}$$

$$y_{goFS} = F_{lg}/(F_{ds} + F_{lg}). \tag{A.4}$$

The velocities of the vapor and the entrained catalyst entering the riser are calculated by the continuity equations:

$$v_{gFS} = \frac{F_{lg} + F_{ds}}{\rho_{gFS}(1 - \varepsilon_{cCL1})\Omega_{RS}}, \tag{A.5}$$

$$v_{cFS} = \frac{F_{cCL1}}{\rho_c\varepsilon_{cCL1}\Omega_{RS}}, \tag{A.6}$$

where

$$\rho_{gFS} = \frac{P_{FS}M_{wgFS}}{RT_{gFS}Z_{gFS}}. \tag{A.7}$$

A.2. Reactor riser

The riser is modeled as a one-dimensional tubular reactor without radial and axial dispersion. The momentum equations of both the catalyst and gas phases in the riser are included in the riser modeling and can be summarized by Eqs. (A.8)–(A.16).

$$\frac{dv_{cRS}}{dx} + G_c\frac{\Omega_{RS}}{F_{cRS}}\frac{d\varepsilon_{cRS}}{dx} - \frac{C_{fRS}(v_{gRS} - v_{cRS})\Omega_{RS}}{F_{cRS}} + \frac{2f_{cRS}v_{cRS}}{D_{RS}} + \frac{g}{v_{cRS}} = 0, \tag{A.8}$$

$$\frac{dv_{gRS}}{dx} + \frac{\Omega_{RS}}{F_{gRS}}\frac{dP_{RS}}{dx} - \frac{C_{fRS}(v_{cRS} - v_{gRS})\Omega_{RS}}{F_{gRS}} + \frac{2f_{gRS}v_{gRS}}{D_{RS}} + \frac{g}{v_{gRS}} = 0, \tag{A.9}$$

$$\varepsilon_{cRS} = \frac{F_{cRS}}{v_{cRS}\rho_c\Omega_{RS}}, \tag{A.10}$$

$$\varepsilon_{gRS} = 1 - \varepsilon_{cRS}, \tag{A.11}$$

$$\rho_{gRS} = \frac{F_{gRS}}{\varepsilon_{gRS}v_{gRS}\Omega_{RS}}, \tag{A.12}$$

$$P_{RS} = \rho_{gRS}\frac{RT_{gRS}}{M_{wgRS}}Z_{gRS}, \tag{A.13}$$

where

$$F_{cRS} = F_{cCL1}, \tag{A.14}$$

$$F_{gRS} = F_{lg} + F_{ds}, \tag{A.15}$$

B.C.:

$$v_{cRS}^{(0)} = v_{cFS},$$

$$v_{gRS}^{(0)} = v_{gFS}. \tag{A.16}$$

In the above, the interfacial friction coefficients are based on the following Ergun equation (Tsuo & Gidaspow, 1990):

$$C_{fRS} = 150\frac{\varepsilon_{cRS}^2\mu_{gRS}\rho_c}{(\varepsilon_{gRS}d_cs_c)^2(\rho_c - \rho_{gRS})} + 1.75\frac{\rho_{gRS}\rho_c|v_{gRS} - v_{cRS}|\varepsilon_{cRS}}{\varepsilon_{gRS}d_cs_c(\rho_c - \rho_{gRS})} \quad \text{for } \varepsilon_{gRS} \leqslant 0.8,$$

$$C_{fRS} = \frac{3}{4}C_{dRS}\frac{|v_{gRS} - v_{cRS}|\rho_c\rho_{gRS}\varepsilon_{cRS}}{d_cs_c(\rho_c - \rho_{gRS})}\varepsilon_{gRS}^{-2.65} \quad \text{for } \varepsilon_{gRS} > 0.8, \tag{A.17}$$

where

$$C_{dRS} = \frac{24}{Re_c}(1 + 0.15Re_c^{0.687}) \quad \text{for } Re_c \leqslant 1000,$$

$$C_{dRS} = 0.44 \quad \text{for } Re_c > 1000, \tag{A.18}$$

$$Re_c = \frac{|v_{gRS} - v_{cRS}|d_cF_{gRS}}{\mu_{gRS}v_{gRS}\Omega_{RS}}. \tag{A.19}$$

The stress modulus of the catalyst is calculated by the following equation (Tsuo & Gidaspow, 1990):

$$G_c = 10^{-8.76\varepsilon_{gRS}+5.43}. \quad (A.20)$$

The gas-wall friction factor is calculated using the modified Hagen–Poisuille equations while the catalyst-wall friction factor is calculated using an empirical correlation obtained for a commercial scale riser (Kunii & Levenspiel, 1991).

$$f_{gRS} = \frac{16}{Re_g} \quad \text{for } Re_g \leqslant 2100,$$

$$f_{gRS} = 0.0791 Re_g^{-0.25} \quad \text{for } 2.1\times 10^3 < Re_g \leqslant 10^5,$$

$$f_{gRS} = 0.0008 + 0.0552 Re_g^{-0.237} \quad \text{for } 10^5 < Re_g < 10^8, \quad (A.21)$$

$$f_{cRS} = \frac{0.05}{v_{cRS}}, \quad (A.22)$$

where

$$Re_g = \frac{D_{RS} v_{gRS} \rho_{gRS} \varepsilon_{gRS}}{\mu_{gRS}}. \quad (A.23)$$

The weight fractions of the four lumps comprising the reaction mixture in the riser can be predicted by the following set of component mass balances:

$$\frac{\partial y_{iRS}}{\partial x} = \frac{\rho_c \varepsilon_{cRS} \Omega_{RS} \phi_c}{F_{gRS}} R_{iRS}, \quad i = go, gl, gs, ck, \text{ and } wv, \quad (A.24)$$

where

$$R_{goRS} = -(k_{1RS} + k_{2RS} + k_{3RS}) y_{goRS}^2, \quad (A.25)$$

$$R_{glRS} = (k_{1RS} y_{goRS}^2 - k_{4RS} y_{glRS} - k_{5RS} y_{glRS}), \quad (A.26)$$

$$R_{gsRS} = (k_{2RS} y_{goRS}^2 + k_{4RS} y_{glRS}), \quad (A.27)$$

$$R_{ckRS} = (k_{3RS} y_{goRS}^2 + k_{5RS} y_{glRS}), \quad (A.28)$$

$$R_{wvRS} = 0. \quad (A.29)$$

B.C.:

$$y_{goRS}^{(0)} = 1 - \frac{(F_{lg} Y_{cc} + F_{ds})}{F_{gRS}}, \quad y_{glRS}^{(0)} = 0, \quad y_{gs}^{(0)} = 0,$$

$$y_{ckRS}^{(0)} = \frac{F_{lg} Y_{cc}}{F_{gRS}} \quad \text{and} \quad y_{wvRS}^{(0)} = \frac{F_{ds}}{F_{gRS}}. \quad (A.30)$$

The catalyst deactivation function ϕ_c in Eq. (A.24) is given by Eq. (A.31) where the catalyst deactivation coefficient α_c is related to the temperature and the feedstock composition as in Eq. (A.32):

$$\phi_c = \exp(-\alpha_c C_{ckRS}), \quad (A.31)$$

$$\alpha_c = \alpha_{c0} \exp\left(\frac{-E_c}{RT_{gRS}}\right)(R_{AN})^{\alpha_c^*}. \quad (A.32)$$

The temperature dependency of the five kinetic parameters are represented by the following Arrhenius type relations:

$$k_{iRS} = k_{i0RS} \exp\left(\frac{-E_{iRS}}{RT_{gRS}}\right), \quad i = 1, \ldots, 5. \quad (A.33)$$

The coke on catalyst is calculated as the sum of the residual coke from the regenerator and the coke generated during the cracking reactions:

$$C_{ckRS} = C_{ckCL1} + \frac{F_{gRS} y_{ckRS}}{F_{cRS}}. \quad (A.34)$$

The temperature profiles of the two phases along the riser are governed by the following energy balance equations:

$$\frac{\partial T_{cRS}}{\partial x} = \frac{\Omega_{RS} h_{pRS} A_{pRSe}}{F_{cRS} C_{pc}} (T_{gRS} - T_{cRS}), \quad (A.35)$$

$$\frac{\partial T_{gRS}}{\partial x} = \frac{\Omega_{RS}}{F_{gRS} C_{pgRS}} [h_{pRS} A_{pRSe} (T_{cRS} - T_{gRS}) + \rho_c \varepsilon_{cRS} Q_{reactRS}], \quad (A.36)$$

where

$$Q_{reactRS} = -(\Delta H_{1RS} k_{1RS} y_{goRS}^2 + \Delta H_{2RS} k_{2RS} y_{goRS}^2 + \Delta H_{3RS} k_{3RS} y_{goRS}^2 + \Delta H_{4RS} k_{4RS} y_{glRS} + \Delta H_{5RS} k_{5RS} y_{glRS}) \phi_c. \quad (A.37)$$

B.C.:

$$T_{cRS}^{(0)} = T_{cFS} \quad \text{and} \quad T_{gRS}^{(0)} = T_{gFS}. \quad (A.38)$$

A.3. Disengaging-stripping section

The disengaging-stripping section is modeled as a perfectly mixed continuous tank with no reaction taking place. In this study, the following exponential type stripping function is developed to consider the catalyst-to-oil coke:

$$C_{ckST} = C_{ckST0} + k_{ss0} \exp\left[-\frac{E_{ss} F_{cRS} F_{ss}}{F_{lg}}\right]. \quad (A.39)$$

Then the coke on the catalyst exiting the stripper can be calculated by

$$\frac{dC_{ckRT}}{dt} = \frac{F_{cRS}}{w_{cRT}} (C_{ckRS}^{(hrs)} + C_{ckST} - C_{ckRT}). \quad (A.40)$$

The mass balances are set up for gases and catalysts in the disengaging-stripping section, respectively:

$$\frac{dw_{gRT}}{dt} = F_{gRS}(1 - y_{ckRS}^{(h_{RS})}) + F_{ss} - F_{gRT} - F_{cRS}C_{ckST}. \tag{A.41}$$

$$\frac{dw_{cRT}}{dt} = F_{cRS} - F_{cSV2} - F_{cMF}. \tag{A.42}$$

The weight fractions of the gaseous components exiting to the main fractionator are predicted by the following equations:

$$\frac{dy_{iRT}}{dt} = \frac{1}{w_{gRT}}\left\{y_{iRS}^{(h_{RS})}\left[F_{gRS} - \frac{F_{cRS}C_{ck_{ST}}}{\sum_{j=go,gl,\ and\ gs} y_{jRS}^{(h_{RS})}}\right] - y_{iRT}\left[F_{gRT} + \frac{dw_{gRT}}{dt}\right]\right\},\ i = go, gl\ and\ gs, \tag{A.43}$$

$$y_{wvRT} = 1 - y_{goRT} - y_{glRT} - y_{gsRT}. \tag{A.44}$$

The gas oil conversion based on the fresh feed flowing into the reactor is given by the following equation:

$$Y_{convRT} = 1 - \frac{F_{gRS}y_{goRT}}{F_{lg}}. \tag{A.45}$$

The energy balance is described by the following equation:

$$(w_{cRT}C_{pc} + w_{gRT}C_{pgRT})\frac{dT_{RT}}{dt} = F_{ss}H_{ss} + F_{ds}H_{ds} - (F_{ss} + F_{ds})H_{wvRT}^{out} + F_{cRS}(H_{cRT}^{in} - H_{cRT}^{out}) + (F_{gRS} - F_{ds})(H_{hgRT}^{in} - H_{hgRT}^{out}) - F_{ss}\Delta H_{stripST} + Q_{lossRT}, \tag{A.46}$$

where

$$H_{ss} = \bar{C}_{pwv}(T_{ss} - T_{ref}), \tag{A.47}$$

$$H_{ds} = \bar{C}_{pwv}(T_{gRS}^{(h_{RS})} - T_{ref}), \tag{A.48}$$

$$H_{hgRT}^{in} = \bar{C}_{phg}(T_{gRS}^{(h_{RS})} - T_{ref}), \tag{A.49}$$

$$H_{hgRT}^{out} = \bar{C}_{phg}(T_{RT} - T_{ref}), \tag{A.50}$$

$$H_{cRT}^{in} = \bar{C}_{pc}(T_{cRS}^{(h_{RS})} - T_{ref}), \tag{A.51}$$

$$H_{cRT}^{out} = \bar{C}_{pc}(T_{RT} - T_{ref}), \tag{A.52}$$

$$H_{wvRT}^{out} = \bar{C}_{pwv}(T_{RT} - T_{ref}), \tag{A.53}$$

$$Q_{lossRT} = U_{RT}A_{RTe}(T_e - T_{RT}). \tag{A.54}$$

The gas-phase pressure in the disengaging-stripping section can be calculated by the following equation of state:

$$P_{RT} = \frac{w_{gRT}RT_{RT}}{M_{wgRT}V_{gRT}}Z_{gRT}, \tag{A.55}$$

where

$$V_{gRT} = V_{RT} - \frac{w_{cRT}}{\rho_c}. \tag{A.56}$$

The pressure at the bottom of the disengaging-stripping section is higher than the pressure at the top by the static head exerted by the catalyst:

$$P_{RTb} = P_{RT} + \frac{(w_{cRT} - w_{cCY1})g(h_{RT} + h_{ST})}{1000V_{RT}}. \tag{A.57}$$

A.4. Reactor cyclones

The reactor cyclone is modeled as a continuous stirred tank (CST). After applying a pseudo-steady state assumption to the catalyst balance in the reactor cyclones, the rate of accumulation of catalyst in the cyclones can be expressed by

$$\eta_{CY1}v_{cCY1}\Omega_{CY1i}\frac{w_{cRT}}{V_{RT}} - k_{vCY1}\left[\frac{w_{cCY1}\Omega_{CY1d}/N_{CY1}}{\rho_{bCY1}}\right]^{1/2} = 0. \tag{A.58}$$

Then, rearranging the above equation yields the following equation:

$$w_{cCY1} = \frac{\rho_{bCY1}N_{CY1}}{\Omega_{CY1d}}\left[\frac{\eta_{CY1}v_{cCY1}w_{cRT}\Omega_{CY1i}}{k_{vCY1}V_{RT}}\right]^2, \tag{A.59}$$

where the cyclone inlet velocity is calculated by the equation of Rosin, Rammler, and Intelmann (Schweitzer et al., 1988):

$$v_{cCY1} = \frac{9\mu_{gRT}\Omega_{CY1i}}{d_{cm}^2\pi N_{tCY1}(\rho_c - w_{gRT}/V_{gRT})h_{CY1i}}. \tag{A.60}$$

Then the mass flow rates of catalyst particles and gases to the main fractionator are calculated by the following equations, respectively:

$$F_{cMF} = (1 - \eta_{CY1})v_{cCY1}\Omega_{CY1i}\frac{w_{cRT}}{V_{RT}}N_{CY1}, \tag{A.61}$$

$$F_{gRT} = k_{vMF}\sqrt{P_{RT} - P_{MF}}, \tag{A.62}$$

$$F_{hgRT} = F_{gRT}(1 - y_{wvRT}). \tag{A.63}$$

A.5. Overall regenerator

The equations associated with the total catalyst and gas holdups, superficial velocity, and pressure distribution are derived on the basis of the overall regenerator dynamics. The catalyst and gas holdups in the entire regenerator can be calculated by the following equations:

$$\frac{dw_{cRG}}{dt} = F_{cCL2} - F_{cSV1} - F_{cSG}, \tag{A.64}$$

$$\frac{dw_{gRG}}{dt} = F_{aD} + F_{cCL2}C_{ckCL2} - F_{cSV1}C_{ckD} - F_{cSG}C_{ckF}^{(h_{RG})} - F_{gSG}, \tag{A.65}$$

where

$$F_{gSG} = k_{vSG}f_v(x_{vSG})\sqrt{P_{RG}} - P_{SG}. \tag{A.66}$$

Since the mass influent to the gas phase increases in proportion to the coke burned off the catalyst, the superficial gas velocity can be correlated to the average gas density in the regenerator:

$$u_{gRG} = \frac{F_{aD}(1-\delta_{gRG}) + F_{gSG}\delta_{gRG}}{\rho_{gRG}\Omega_{RG}}, \tag{A.67}$$

where

$$\rho_{gRG} = \frac{w_{gRG}}{V_{RG} - w_{cRG}/\rho_c}, \tag{A.68}$$

$$\delta_{gRG} = \left[\frac{0.5q\rho_{gRG} - C_{H_2Oi}^{(h_{RG})}M_{wck}}{0.5q\rho_{gRG} - C_{H_2Oi}^{(z)}M_{wck}}\right]\left[\frac{C_{H_2Oi}^{(z)} - C_{H_2OD}^{(0)}}{C_{H_2OF}^{(h_{RG})} - C_{H_2OD}^{(0)}}\right],$$

$$i = D, F. \tag{A.69}$$

The average regenerator pressure is assumed to have the pressure value at the dense bed exit and can be calculated by the following equation of state:

$$P_{RG} = \frac{\rho_{gRG}RT_DZ_{gRG}}{M_{wgRG}^{(H_D)}}, \tag{A.70}$$

where

$$M_{wgRG} = \sum_i M_{wi}f_{ij}, \quad i = O_2, CO, CO_2, H_2O, N_2$$

$$\text{and} \quad j = D, F, \tag{A.71}$$

$$f_{ij} = C_{ij}/\sum_i C_{ij}, \quad i = O_2, CO, CO_2, H_2O, N_2$$

$$\text{and} \quad j = D, F. \tag{A.72}$$

The pressure acting on the bottom of the regenerator can be calculated using the static head exerted by the catalyst:

$$P_{RGb} = P_{RG} + \frac{\rho_c g}{1000}\left\{\varepsilon_{cD}H_D + \int_{H_D}^{h_{RG}} \varepsilon_{cF}(z)\,dz\right\}. \tag{A.73}$$

A.6. Dense bed

The dense bed is modeled as a hybrid reactor that employs a mixed-tank model for energy and coke balances but a tubular reactor model for gas component balances. The component balance equations for each gaseous phase are described by the following partial differential equations, respectively:

For the emulsion phase:

$$\frac{\partial C_{iE}}{\partial t} + v_{gE}\frac{\partial C_{iE}}{\partial z} = -\frac{C_{iE}S_{gE}}{\varepsilon_{gE}} + \frac{K_I}{\varepsilon_{gE}}(C_{iB} - C_{iE}) + R_{iE},$$

$$i = O_2, CO, CO_2, H_2O, N_2, \tag{A.74}$$

where

$$R_{O_2E} = -\frac{\rho_c\varepsilon_{cD}}{\varepsilon_{gE}}[(0.5 + 0.25q)r_{1E}/M_{wck} + (1 + 0.25q)r_{2E}/M_{wck} + 0.5r_{4E}] - 0.5r_{3E}, \tag{A.75}$$

$$R_{COE} = \frac{\rho_c\varepsilon_{cD}}{\varepsilon_{gE}}[r_{1E}/M_{wck} - r_{4E}] - r_{3E}, \tag{A.76}$$

$$R_{CO_2E} = \frac{\rho_c\varepsilon_{cD}}{\varepsilon_{gE}}[r_{2E}/M_{wck} + r_{4E}] + r_{3E}, \tag{A.77}$$

$$R_{H_2OE} = \frac{\rho_c\varepsilon_{cD}q}{\varepsilon_{gE}M_{wck}}[0.5r_{1E} + 0.5r_{2E}], \tag{A.78}$$

$$R_{N_2E} = 0, \tag{A.79}$$

$$S_{gE} = \frac{\partial\varepsilon_{gE}}{\partial t} + \frac{\partial(v_{gE}\varepsilon_{gE})}{\partial z}, \tag{A.80}$$

I.C.:

$$C_{iE}^{(0,z)} = C_{iE}^{(z)}, \quad i = O_2, CO, CO_2, H_2O, N_2, \tag{A.81}$$

B.C.:

$$C_{iE}^{(t,0)} = \frac{f_{iE}^{(0)}\rho_{gRG}}{M_{wgRG}^{(0)}}, \quad i = O_2, CO, CO_2, H_2O, N_2, \tag{A.82}$$

For the bubble phase:

$$\frac{\partial C_{iB}}{\partial t} + v_{gB}\frac{\partial C_{iB}}{\partial z} = -\frac{C_{iB}S_{gB}}{\varepsilon_{gB}} + \frac{K_I}{\varepsilon_{gB}}(C_{iE} - C_{iB}) + R_{iB},$$

$$i = O_2, CO, CO_2, H_2O, N_2, \quad (A.83)$$

where

$$R_{O_2B} = -0.5r_{3B}, \quad (A.84)$$

$$R_{COB} = -r_{3B}, \quad (A.85)$$

$$R_{CO_2B} = r_{3B}, \quad (A.86)$$

$$R_{H_2OB} = 0, \quad (A.87)$$

$$R_{N_2B} = 0, \quad (A.88)$$

$$S_{gB} = \frac{\partial \varepsilon_{gB}}{\partial t} + \frac{\partial (v_{gB}\varepsilon_{gB})}{\partial z}, \quad (A.89)$$

I.C.:

$$C_{iB}^{(0,z)} = C_{iB}^{(z)}, \quad i = O_2, CO, CO_2, H_2O, N_2, \quad (A.90)$$

B.C.:

$$C_{iB}^{(t,0)} = \frac{f_{iB}^{(0)}\rho_{gRG}}{M_{wgRG}^{(0)}}, \quad i = O_2, CO, CO_2, H_2O, N_2. \quad (A.91)$$

In the above equations, the kinetic rates are given by the following expressions:

$$r_{1E} = \frac{k_{1RG}C_{ckD}C_{O_2E}}{1+\sigma}, \quad (A.92)$$

$$r_{2E} = r_{1E}\sigma, \quad (A.93)$$

$$r_{3E} = k_{3RG}C_{COE}C_{O_2E}^{0.5}C_{H_2OE}^{0.5}, \quad (A.94)$$

$$r_{3B} = k_{3RG}C_{COB}C_{O_2B}^{0.5}C_{H_2OB}^{0.5}, \quad (A.95)$$

$$r_{4E} = k_{4RG}C_{COE}C_{O_2E}^{0.5}, \quad (A.96)$$

where the temperature dependency of the rate constants are assumed to follow the Arrhenius type relations:

$$k_{iRG} = k_{i0RG}\exp\left(\frac{-E_{iRG}}{RT_j}\right), \quad = 1,3,4 \quad and \quad j = D, F. \quad (A.97)$$

Once the molar composition of each phase is obtained, the mean molar concentration profiles along the dense bed can be calculated by taking a weighted average of each phase values:

$$C_{iD} = \frac{C_{iE}v_{gE}\varepsilon_{gE} + C_{iB}v_{gB}\varepsilon_{gB}}{u_{gRG}},$$

$$i = O_2, CO, CO_2, H_2O, N_2. \quad (A.98)$$

Since the component balance equations presented above include the volume fractions and velocities of the dense bed phases, they have to be correlated to other process variables. First, we explicitly state the requirement that the volume fractions of the catalyst, emulsion gas, and bubble gas sum up to unity at any position:

$$\varepsilon_{cD} + \varepsilon_{gE} + \varepsilon_{gB} = 1 \quad \text{for } 0 \leqslant z \leqslant H_D. \quad (A.99)$$

It is evident from the perfect-mixing assumption for the catalyst that it has a constant volume fraction. An empirical correlation between the volume fraction and the average superficial gas velocity was developed by a nonlinear regression of the experimental data of Schnitzlen (1987).

$$\varepsilon_{cD} = 0.3418\exp[-0.9751\bar{u}_{gRG}] + 0.1592, \quad (A.100)$$

$$\bar{u}_{gRG} = \frac{1}{H_D}\int_0^{H_D} u_{gRG}(z)\,dz. \quad (A.101)$$

Next, the volume fraction of the bubble gas is predicted by the following expression proposed for fast bubbles and Geldart A type particles (Davidson & Harrison, 1963; Kunii & Levenspiel, 1991):

$$\varepsilon_{gB} = \frac{u_{gRG} - v_{gm}}{v_{gB} - v_{gm}}, \quad (A.102)$$

where the minimum fluidization and bubble rising velocities are given by

$$v_{gm} = \frac{d_c^2(\rho_c - \rho_{gRG})g}{150\mu_{gRG}}\frac{\varepsilon_{gm}^3 s_c^2}{1-\varepsilon_{gm}}, \quad (A.103)$$

$$v_{gB} = u_{gRG} - v_{gm} + 0.711\sqrt{gd_b}. \quad (A.104)$$

d_b in Eqs. (A.103) and (A.104) denotes the bubble diameter and is correlated to the axial position in the bed (Kunii & Levenspiel, 1991):

$$d_b = d_{bm} - (d_{bm} - d_{b0})\exp(-0.3z/D_{RGe}), \quad (A.105)$$

where the initial bubble diameter d_{b0} at the bottom and the maximum bubble diameter d_{bm} at the top of the bed are given for a porous plate air distributor as follows (Kunii & Levenspiel, 1991):

$$d_{b0} = \frac{2.78}{g}[u_{gRG}^{(0)} - v_{gm}]^2, \quad (A.106)$$

$$d_{bm} = 0.59[u_{gRG}^{(H_D)} - v_{gm}]^{0.4}D_{RGe}^{0.8}. \quad (A.107)$$

Finally, the interstitial emulsion gas velocity can be easily calculated from the mass balance in the bed:

$$v_{gE} = \frac{u_{gRG} - \varepsilon_{gB}v_{gB}}{\varepsilon_{gE}}. \quad (A.108)$$

The holdups of the catalyst and gas in the dense bed are given by the following expressions

$$w_{cD} = w_{cRG} - w_{cF} - w_{cCY2}, \tag{A.109}$$

$$w_{gD} = H_D \Omega_{RG}(1 - \varepsilon_{cD})\rho_{gRG}, \tag{A.110}$$

from which the height of dense bed can be calculated by

$$H_D = \frac{w_{cD}}{\Omega_{RG}\rho_c \varepsilon_{cD}}. \tag{A.111}$$

The uniformity assumption of the catalyst in the bed leads to the lumped equation for the coke deposited on catalyst as follows:

$$\frac{dC_{ckD}}{dt} = \frac{F_{cCL2}}{w_{cD}}[C_{ckCL2} - C_{ckD}] + \frac{F_{cCY2}}{w_{cD}}[C_{ckF}^{(h_{RG})} - C_{ckD}] + \frac{M_{wck}}{0.5q\rho_{gRG}w_{cD}}[F_{aD}C_{H_2OD}^{(0)} - F_{gD}^{(H_D)}C_{H_2OD}^{(H_D)}], \tag{A.112}$$

where

$$F_{gD} = \rho_{gRG}\Omega_{RG}u_{gRG}. \tag{A.113}$$

Recalling further that all the substances in the bed are in thermal equilibrium, the energy balance also takes the form of the following mixed-tank dynamics:

$$(w_{cD}C_{pc} + w_{gD}C_{pgD})\frac{dT_D}{dt} = F_{cCL2}(H_{cD}^{in} - H_{cD}^{out}) + F_{aD} \times (H_{gD}^{in} - H_{gD}^{out}) + F_{cCY2}(H_{cCY2}^{out} - H_{cD}^{out}) + Q_{lossD} + Q_{reactD}, \tag{A.114}$$

where

$$H_{cD}^{in} = \bar{C}_{pc}(T_{cCL2} - T_{ref}), \tag{A.115}$$

$$H_{cD}^{out} = \bar{C}_{pc}(T_D - T_{ref}), \tag{A.116}$$

$$H_{gD}^{in} = \bar{C}_{pa}(T_{aD} - T_{ref}), \tag{A.117}$$

$$H_{gD}^{out} = \bar{C}_{pgD}(T_D - T_{ref}), \tag{A.118}$$

$$H_{cCY2}^{out} = \bar{C}_{pc}(T_{CY2} - T_{ref}), \tag{A.119}$$

$$Q_{lossD} = U_D A_{De}(T_e - T_D), \tag{A.120}$$

$$Q_{reactD} = \frac{1}{\rho_{gRG}}\sum_i (F_{aD}C_{iD}^{(0)} - F_{gD}^{(H_D)}C_{iD}^{(H_D)})\Delta H_{fi}^{(T_D)} + \frac{1}{0.5q\rho_{gRG}}(F_{aD}C_{H_2OD}^{(0)} - F_{gD}^{(H_D)}C_{H_2OD}^{(H_D)})\Delta H_{fck}^{(T_D)},$$

$$i = O_2, CO, CO_2, H_2O. \tag{A.121}$$

A.7. Freeboard

The molar concentrations of gaseous substances in the freeboard are described by the following component mass balances:

$$\frac{\partial C_{iF}}{\partial t} + \frac{u_{gRG}}{\varepsilon_{gF}}\frac{\partial C_{iF}}{\partial z} = -\frac{\rho_c \varepsilon_{cF}(r_{1F} + r_{2F})}{\rho_{gRG}\varepsilon_{gF}}C_{iF} + R_{iF},$$

$$i = O_2, CO, CO_2, H_2O, N_2, \tag{A.122}$$

where

$$R_{O_2F} = -\frac{\rho_c \varepsilon_{cF}}{\varepsilon_{gF}}[(0.5 + 0.25q)r_{1F}/M_{wck} + (1 + 0.25q)r_{2F}/M_{wck} + 0.5r_{4F}] - 0.5r_{3F}, \tag{A.123}$$

$$R_{COF} = \frac{\rho_c \varepsilon_{cF}}{\varepsilon_{gF}}[r_{1F}/M_{wck} - r_{4F}] - r_{3F}, \tag{A.124}$$

$$R_{CO_2F} = \frac{\rho_c \varepsilon_{cF}}{\varepsilon_{gF}}[r_{2F}/M_{wck} + r_{4F}] + r_{3F}, \tag{A.125}$$

$$R_{H_2OF} = \frac{\rho_c \varepsilon_{cF} q}{\varepsilon_{gF} M_{wck}}[0.5r_{1F} + 0.5r_{2F}], \tag{A.126}$$

$$R_{N_2F} = 0, \tag{A.127}$$

I.C.:

$$C_{iF}^{(0,z)} = C_{iF0}^{(z)}, \quad i = O_2, CO, CO_2, H_2O, N_2, \tag{A.128}$$

B.C.:

$$C_{iF}^{(t,H_D)} = C_{iD}^{(H_D)}, \quad i = O_2, CO, CO_2, H_2O, N_2. \tag{A.129}$$

In the above equations, the kinetic rates are given by the following expressions:

$$r_{1F} = \frac{k_{1RG}C_{ckF}C_{O_2F}}{1 + \sigma}, \tag{A.130}$$

$$r_{2F} = r_{1F}\sigma, \tag{A.131}$$

$$r_{3F} = k_{3RG}C_{COF}C_{O_2F}^{0.5}C_{H_2OF}^{0.5}, \tag{A.132}$$

$$r_{4F} = k_{4RG}C_{COF}C_{O_2F}^{0.5}. \tag{A.133}$$

The vertical distributions of the catalyst and gas volume fractions are estimated as follows. We start again with the requirement that the volume fractions of the catalyst and gas phases sum up to unity at any position:

$$\varepsilon_{cF} + \varepsilon_{gF} = 1 \quad \text{for } H_D < z \leqslant h_{RG}. \tag{A.134}$$

The catalyst volume fraction in the freeboard tends to decay exponentially with increasing height, and can be estimated with the following empirical equation (Li & Kwauk, 1980):

$$\varepsilon_{cF} = \varepsilon^*_{cF} + (\varepsilon_{cD} - \varepsilon^*_{cF})\exp[-\beta_c(z - H_D)], \quad \text{(A.135)}$$

where

$$\varepsilon^*_{cF} = \frac{\rho_{gRG}}{\rho_c} 10^{[-0.725 - 2.517\log\chi - 0.627(\log\chi)^2]}, \quad \text{(A.136)}$$

$$\chi = \frac{(u^{(h_{RG})}_{gRG})^2}{g d_c \rho_c^2}. \quad \text{(A.137)}$$

Then the holdup of the catalysts in the freeboard are given by

$$w_{cF} = \Omega_{RG}\rho_c \int_{H_D}^{h_{RG}} \varepsilon_{cF}(z)\,dz, \quad \text{(A.138)}$$

where

$$h_{RG} = H_D + H_F. \quad \text{(A.139)}$$

The catalyst flow rate in the freeboard is assumed to be constant, leading to the following expressions for the catalyst flow rate and the superficial catalyst velocity:

$$F_{cF} = F_{cCY2}/\eta_{CY2}, \quad \text{(A.140)}$$

$$u_{cF} = \frac{F_{cF}}{\rho_c \Omega_{RG}}. \quad \text{(A.141)}$$

Unlike in the dense bed, the coke on catalyst in the freeboard is expressed by a distributed parameter model as follows:

$$\frac{\partial C_{ckF}}{\partial t} + \frac{u_{cF}}{\varepsilon_{cF}}\frac{\partial C_{ckF}}{\partial z} = -(r_{1F} + r_{2F}), \quad \text{(A.142)}$$

I.C.:

$$C^{(0,z)}_{ckF} = C^{(z)}_{ckF0}, \quad \text{(A.143)}$$

B.C.:

$$C^{(t,H_D)}_{ckF} = C_{ckD}. \quad \text{(A.144)}$$

Neglecting the heat transfer resistance between the catalyst and gas phases, the temperature distribution in the freeboard region can be calculated by the following partial differential equation:

$$(\rho_c \varepsilon_{cF} C_{pc} + \rho_{gRG}\varepsilon_{gF} C_{pgF})\frac{\partial T_F}{\partial t} + (u_{cF}\rho_c C_{pc} + u_{gRG}\rho_{gRG} C_{pgF})\frac{\partial T_F}{\partial z} = Q_{lossF} + Q_{reactF}, \quad \text{(A.145)}$$

where

$$Q_{lossF} = \frac{4U_F}{D_{RG}}(T_e - T_F), \quad \text{(A.146)}$$

$$Q_{reactF} = \frac{\rho_c \varepsilon_{cF}}{M_{wck}}[r_{1F}\Delta H_{r1} + r_{2F}\Delta H_{r2}] + \varepsilon_{gF} r_{3F}\Delta H_{r3} + \rho_c \varepsilon_{cF} r_{4F}\Delta H_{r4}, \quad \text{(A.147)}$$

$$\Delta H_{rl} = -\sum_j \nu_{lj}\Delta H^{(T_r)}_{fj}, i = 1\cdots 4, \quad \text{and}$$

$$j = ck, O_2, CO, CO_2, H_2O, \quad \text{(A.148)}$$

I.C. :

$$T^{(0,z)}_F = T^{(z)}_{F0}, \quad \text{(A.149)}$$

B.C. :

$$T^{(t,H_D)}_F = T_D. \quad \text{(A.150)}$$

A.8. Regenerator cyclones

The regenerator cyclone is modeled as a continuous stirred tank like the reactor cyclone. Similarly to the reactor cyclones, the rate of accumulation of catalyst is given by

$$w_{cCY2} = \frac{\rho_{bCY2} N_{CY2}}{\Omega_{CY2d}}\left[\frac{F_{cCY2}}{k_{vCY2} N_{CY2}}\right]^2, \quad \text{(A.151)}$$

where

$$F_{cCY2} = \eta_{CY2} v_{cCY2}\rho_c \varepsilon^{(h_{RG})}_{cF}\Omega_{CY2i} N_{CY2}, \quad \text{(A.152)}$$

$$v_{cCY2} = \frac{9\mu_{gRG}\Omega_{CY2i}}{d^2_{cm}\pi N_{tCY2}(\rho_c - \rho_{gRG})h_{CY2i}}. \quad \text{(A.153)}$$

The flow rate of the catalyst entering the stack through the cyclone is given by

$$F_{cSG} = (1 - \eta_{CY2})F_{cCY2}/\eta_{CY2}. \quad \text{(A.154)}$$

The temperature rising across the regenerator cyclone is estimated using the following simple correlation (Kurihara, 1967; Hovd & Skogestad, 1993):

$$T_{CY2} = T^{(h_{RG})}_F + c_T f^{(h_{RG})}_{O_2F}. \quad \text{(A.155)}$$

A.9. Catalyst transport lines

The flow rate of catalyst through a catalyst transport line is determined by the pressure drop across a slide

valve. The mass flow rate of the regenerated catalyst through the slide valve can be calculated by

$$F_{cSV1} = k_{vSV1} f_v(x_{vSV1}) \sqrt{P_{RGb} + \rho_c(1 - \varepsilon_{gCL1}) gl_{CL1} \sin\theta_{CL1}/1000 - P_{FS}}. \quad \text{(A.156)}$$

Since the catalyst bulk density is assumed constant in the catalyst transport line, the flow rate through the transport line is just given by

$$F_{cCL1} = F_{cSV1}. \quad \text{(A.157)}$$

Ignoring the transport lag throughout the catalyst transport lines, the temperature and the coke on catalyst at the outlet of the regenerated catalyst transport line are simply given by

$$T_{cCL1} = T_D, \quad \text{(A.158)}$$

$$C_{ckCL1} = C_{ckD}. \quad \text{(A.159)}$$

Similar equations can be derived for the spent catalyst transport line from the reactor to the regenerator as follows:

$$F_{cSV2} = k_{vSV2} f_v(x_{vSV2}) \sqrt{P_{RTb} + \rho_{bCL2} gl_{CL2} \sin\theta_{CL2}/1000 - P_{RG}}, \quad \text{(A.160)}$$

$$F_{cCL2} = F_{cSV2}, \quad \text{(A.161)}$$

$$T_{cCL2} = T_{RT}, \quad \text{(A.162)}$$

$$C_{ckCL2} = C_{ckRT}. \quad \text{(A.163)}$$

References

Ali, H., & Rohani, S. (1997). Dynamic modeling and simulation of a riser-type fluid catalytic cracking unit. *Chemical Engineering Technology, 20*, 118.

Ali, H., Rohani, S., & Corriou, J. P. (1997). Modeling and control of a riser type fluid catalytic cracking (FCC) unit. *Transactions of the Institution of Chemical Engineers Part A, 75*, 401.

Ancheyta-Juarez, J., Lopez-Isunza, F., Aguilar-Rodriguez, E., & Moreno-Mayorga, J. C. (1997). A strategy for kinetic parameter estimation in the fluid catalytic cracking process. *Industrial and Engineering Chemistry Research, 36*, 5170.

Arandes, J. M., & de Lasa, H. I. (1992). Simulation and multiplicity of steady states in fluidized FCCUs. *Chemical Engineering Science, 47*, 2535.

Arbel, A., Huang, Z., Rinard, I. H., Shinnar, R., & Sapre, A. V. (1995a). Dynamics and control of fluidized catalytic crackers-1. Modeling of the current generation of FCC's. *Industrial and Engineering Chemistry Research, 34*, 1228.

Arbel, A., Rinard, I. H., Shinnar, R., & Sapre, A. V. (1995b). Dynamics and control of fluidized catalytic crackers-2. Multiple steady states and instabilities. *Industrial and Engineering Chemistry Research, 34*, 3014.

Davidson, J. F., & Harrison, D. (1963). *Fluidized Particles*. New York: Cambridge University Press.

De Lasa, H. I., & Grace, J. R. (1979). The influence of the freeboard region in a fluidized bed catalytic cracking regenerator. *A.I.Ch.E. Journal, 25*, 984.

De Lasa, H. I., Errazu, A., Barreiro, E., & Solioz, S. (1981). Analysis of fluidized bed catalytic cracking regenerator models in an industrial scale unit. *Canadian Journal of Chemical Engineering, 59*, 549.

Elshishini, S. S., & Elnashaie, S. S. E. H. (1990a). Digital simulation of industrial fluid catalytic cracking units-I. Bifurcation and its implications. *Chemical Engineering Science, 45*, 553.

Elshishini, S. S., & Elnashaie, S. S. E. H. (1990b). Digital simulation of industrial fluid catalytic cracking units-II. Effect of charge stock composition on bifurcation and gasoline yield. *Chemical Engineering Science, 45*, 2959.

Elshishini, S. S., Elnashaie, S. S. E. H., & Alzahrani, S. (1992). Digital simulation of industrial fluid catalytic cracking units-III. Effect of hydrodynamics. *Chemical Engineering Science, 47*, 3152.

Elnashaie, S. S. E. H., & Elshishini, S. S. (1993). Digital simulation of industrial fluid catalytic cracking units-IV. Dynamic behavior. *Chemical Engineering Science, 48*, 567.

Elnashaie, S. S. E. H., Abasaeed, A. E., & Elshishini, S. S. (1995). Digital simulation of industrial fluid catalytic cracking units-V. Static and dynamic bifurcation. *Chemical Engineering Science, 50*, 1635.

Errazu, A. F., de Lasa, H. I., & Sarti, F. (1979). A fluidized bed catalytic cracking regenerator model: Grid effects. *Canadian Journal of Chemical Engineering, 57*, 191.

Faltsi-Saravelou, O., & Vasalos, I. A. (1991a). FBSim: A model for fluidized bed simulation — I. Dynamic modeling of an adiabatic reacting system of small gas fluidized particles. *Computers and Chemical Engineering, 15*, 639.

Faltsi-Saravelou, O., Vasalos, I. A., & Dimogiorgas, G. (1991b). FBSim: A model for fluidized bed simulation — II. Simulation of an industrial fluidized catalytic cracking regenerator. *Computers and Chemical Engineering, 15*, 647.

Garbow, B. S., Hillstrom, K. E., & More, J. J. (1980). *MINPACK Project*. Argonne Nat. Lab.

Hano, T., Nakashio, F., & Kusunoki, K. (1975). The burning rate of coke deposited on zeolite catalyst. *Journal of Chemical Engineering, Japan, 8*, 127.

Hillestad, M., & Hertzberg, T. (1986). Dynamic simulation of chemical engineering systems by the sequential modular approach. *Computers and Chemical Engineering, 10*, 377.

Hindmarsh, A. C. (1983). ODEPACK: A systematized collection of ODE solvers. In R. S. Stepleman (Ed.), *Scientific & computing*. Amsterdam: North-Holland.

Hovd, M., & Skogestad, S. (1993). Procedure for regulatory control structure selection with application to the FCC process. *A.I.Ch.E. Journal, 39*, 1938.

Howard, J. B., Williams, G. C., & Fine, D. H. (1973). Kinetics of carbon monoxide oxidation in post flame gases. *Proceedings of the 14th Symposium on International combustion*, Combustion Institute (p. 975).

Jacob, S. M., Gross, B., Voltz, S. E., & Weekman, V. M. (1976). A lumping and reaction scheme for catalytic cracking. *A.I.Ch.E. Journal, 22*, 701.

Krishna, A. S., & Parkin, E. S. (1985). Modeling the regenerator in commercial fluid catalytic cracking units. *Chemical Engineering Progress, 81*, 57.

Kunii, D., & Levenspiel, O. (1991). *Fluidization engineering* (2nd ed.). Boston: Butterworth-Heinemann.

Lee, L. S., Chen, Y. W., & Huang, T. N. (1989). Four-lumped kinetic model for fluid catalytic cracking process. *Canadian Journal of Chemical Engineering, 67*, 615.

Li, Y., & Kwauk, M. (1980). The dynamics of fast fluidization. In J. R. Grace, & & J. Matsen (Eds.), *Fluidization III*. New York: Plenum.

Lopez-Isunza, F. (1992). Dynamic modeling of an industrial fluid catalytic cracking unit. *Computers and Chemical Engineering, 16*, S139.

Mcfarlane, R. C., Reineman, R. C., Bartee, J. F., & Georgakis, C. (1993). Dynamic simulator for a model IV fluid catalytic cracking unit. *Computers and Chemical Engineering, 17*, 275.

Morley, K., & de Lasa, H. I. (1987). On the determination of kinetic parameters for the regeneration of cracking catalyst. *Canadian Journal of Chemical Engineering, 65*, 773.

Morley, K., & de Lasa, H. I. (1988). Regeneration of cracking catalyst influence of the homogeneous CO postcombustion reaction. *Canadian Journal of Chemical Engineering, 66*, 428.

Petzold, L. R. (1982). A description of DASSL: A differential/algebraic system solver. Sandia Technical Report, 82-8637.

Ponton, J. W. (1983). Dynamic process simulation using flowsheet structure. *Computers and Chemical Engineering, 7*, 13.

Schnitzlein, M. G. (1987). Ph.D. Thesis, City University of New York, New York.

Schweitzer, P. A. et al. (1988). *Handbook of separation techniques for chemical engineers.* New York: McGraw-Hill.

Theologos, K. N., & Markatos, N. C. (1993). Advanced modeling of fluid catalytic cracking riser-type reactors. *A.I.Ch.E. Journal, 39*, 1007.

Theologos, L. N., Nikou, I. D., Lygeros, A. I., & Markatos, N. C. (1997). Simulation and design of fluid catalystic-cracking riser-type reactors. *A.I.Ch.E. Journal, 43*, 486.

Tsuo, Y. P., & Gidaspow, D. (1990). Computation of flow patterns in circulating fluidized beds. *A.I.Ch.E. Journal, 36*, 885.

Voltz, S. E., Nace, D. M., & Weekman Jr., V. W. (1971). Application of a kinetic model for catalytic cracking: Some correlations of rate constant. *Industrial and Engineering Chemistry Process Design and Development, 10*, 538.

Weekman Jr., V. W., & Nace, D. M. (1970). Kinetics of catalytic cracking selectivity in fixed, moving, and fluid bed reactors. *A.I.Ch.E. Journal, 16*, 397.

Weisz, P. B., & Goodwin, R. D. (1963). Combustion of carbonaceous deposits within porous catalyst particles: I. Diffusion controlled kinetics. *Journal of Catalysis, 2*, 397.

Weisz, P. B., & Goodwin, R. D. (1966a). Combustion of carbonaceous deposits within porous catalyst particles: II. Intrinsic burning rate. *Journal of Catalysis, 6*, 227.

Weisz, P. B. (1966b). Combustion of carbonaceous deposits within porous catalyst particles: III. The CO_2/CO product ratio. *Journal of Catalysis, 6*, 425.

Zenz, F. A., & Weil, N. A. (1958). A theoretical-empirical approach to the mechanism of particle entrainment of fluidized beds. *A.I.Ch.E. Journal, 4*, 472.

ANNEX II

PERGAMON

Chemical Engineering Science 56 (2001) 1973–1990

Chemical Engineering Science

www.elsevier.nl/locate/ces

Dynamic modeling and simulation of a fluidized catalytic cracking process. Part II: Property estimation and simulation

In-Su Han, Chang-Bock Chung*

Faculty of Applied Chemistry, Chonnam National University, Kwangju 500-757, South Korea

Received 16 December 1999; received in revised form 18 August 2000; accepted 5 September 2000

Abstract

A dynamic simulator was developed which implements the detailed dynamic model for an FCC process and the model solver presented in Part I of this paper. The simulator incorporates the correlation equations developed in this study for the thermodynamic properties and transport parameters contained in our model. First, the simulator was validated by comparing the overall steady-state behavior of the system with those in the literature. Then, base case steady-state profiles were obtained for major process variables in the reactor riser and regenerator of an industrial scale FCC unit. Next, the issue of multiple steady states in FCC operations was addressed and confirmed by investigating the sensitivity of our model to initial conditions. Finally, the dynamic responses to step changes in three major process inputs were presented and discussed with an emphasis on the interaction between the reactor and regenerator dynamics. © 2001 Published by Elsevier Science Ltd.

Keywords: Fluid catalytic cracking; Dynamic simulator; Property estimation; Multiple steady states; Sensitivity

1. Introduction

Dynamic simulations have been widely used in chemical process engineering to predict and analyze the dynamic behavior of chemical processes. An accurate and efficient dynamic simulator is recognized as a valuable tool for various studies on advanced control, online optimization, hazard analysis, and operator training. Since a typical FCC unit processes a large amount of feedstock into products of additional value, a refinery can achieve enormous economic benefits from such process improvement studies.

A detailed dynamic model of an FCC process was developed in Part I of this paper on the basis of conservation principles. Then an efficient model solver was constructed on the basis of a modular approach where the model equations were grouped into 12 modules each corresponding to a specific part of the process and type of equations. The model and numerical algorithms developed in the previous part are implemented by a dynamic simulator written in Fortran. Since our dynamic simulator for fluid catalytic crackers (called *DSim-FCC*) takes the structure of Fortran 90 module procedures comprising versatile subprogram units (Meissner, 1995), it can be easily modified when one wants to extend the simulator function or to append additional modules. Interested readers can obtain the dynamic simulator by writing to the authors.

This paper presents the simulation and its results obtained using DSim-FCC. First, the estimation technique is presented for the thermodynamic properties and transport parameters contained in our model. The correlation equations for each property estimated on the basis of data in the various literatures are presented in detail in the Appendix A. Next, to show the validity of our simulator, the steady-state behavior of the system is compared with those in the literature. Then, steady-state profiles of major process variables along the axial position of the riser and regenerator are shown and compared with other information in the literature for an industrial scale FCC unit. The issue of multiple steady states in FCC operations is also addressed and confirmed by investigating the sensitivity of our model to initial conditions. Finally, the dynamic responses to step changes in major process inputs are presented and discussed.

* Corresponding author. Tel.: + 82-62-530-1884; fax: + 82-62-530-1899.

E-mail address: chungcb@chonnam.ac.kr (C.-B. Chung).

0009-2509/01/$ - see front matter © 2001 Published by Elsevier Science Ltd.
PII: S0009-2509(00)00494-2

2. Property estimation

The dynamic model upon which our simulator DSim-FCC is based contains numerous property parameters that have to be specified before carrying out simulation runs. The parameters mainly consist of the thermodynamic properties of the substances that are involved either in cracking reactions or in coke burning reactions and the transport parameters between two phases in the reactor riser and the regenerator. Since the cracking reaction mixture comprising numerous hydrocarbon species is represented by the four lumps (gas oil, gasoline, light gases, and coke) in this study, it is necessary to estimate the properties of each lump using an appropriate characterization method for petroleum fractions. It is also necessary to develop correlation equations that express the properties as functions of system temperature and pressure. This section briefly describes the scheme used in this paper to develop such correlation. The correlation equations incorporated in our simulator are presented in detail in the Appendix A.

True boiling point (TBP) or American Society for Testing and Materials D86 (ASTM D86); ASTM Committee D-2, 1991 distillations are two standard methods to characterize crude oil or petroleum fractions that have a wide range of boiling points. Once either distillation curve is obtained experimentally, it can be converted into the other and can be used to calculate average boiling points of various types. The average boiling point thus obtained and the specific gravity measured in the lab together form the basis for estimating other physical properties of the petroleum fraction such as average molecular weight, heat capacity, vapor pressure, and so on. Hence the physical properties of the gas oil and gasoline lumps that are included in our FCC model are correlated with the average boiling points and specific gravity as well as with the process temperature and pressure. It should be noted that the correlation equations presented in Appendix A include several empirical equations that were developed in this study by nonlinear regression of literature data.

The heat capacities and viscosities of the light gases (C_1–C_4) and the products of coke burning reactions are expressed as functions of temperature only. Since the light gases are treated as a single lump in our model, its property is assumed independent of composition. For the purpose of property estimation, however, it is assumed that the light gas lump has typical composition as found in field operations and that its property can be calculated as a weighted sum of component properties.

Our dynamic model postulates two-phase tubular reactor models for the reactor riser and as well as the dense bed and freeboard of the regenerator. The parameters associated with the heat and mass transfer between these two phases are thermal conductivities, heat transfer coefficients, diffusivities, and mass transfer coefficients. As shown in Appendix A, these parameters are estimated using correlation equations either found in the literature (Baird & Rice, 1975; Kunii & Levenspiel, 1991) or obtained by nonlinear regression of literature data (Technical Data Committee, 1988).

3. Simulations and discussions

The simulator DSim-FCC was used to investigate the behavior of a side-by-side type FCC unit shown in Fig. 1. Recall that the dynamic model presented in Part I of this paper was found to have 13 degrees of freedom that has to be specified before carrying out an open-loop simulation. Table 1 lists 13 variables chosen in this study as specifications of the degrees of freedom as well as eight parameters related to feedstock characteristics and six parameters related to ambient air characteristics. From the viewpoint of process control, these 27 variables represent either external disturbances to the process or prospective manipulated variables in a certain control configuration. From the viewpoint of dynamic simulation, they represent process inputs whose values can be altered during the execution of the simulator in order to obtain dynamic responses to such changes. Table 1 also lists the assumed values of the 27 inputs at the base case operating conditions. Table 2 lists the dimensions of an 30,000 BPD FCC unit assumed in this study. Table 3 shows the properties of the catalyst and coke, and Table 4 lists the kinetic parameters of cracking reactions and coke burning reactions. The kinetic parameters of the four-lump cracking reactions in Table 4 were reported by Ancheyta-Juarez, Lopez-Isunza,

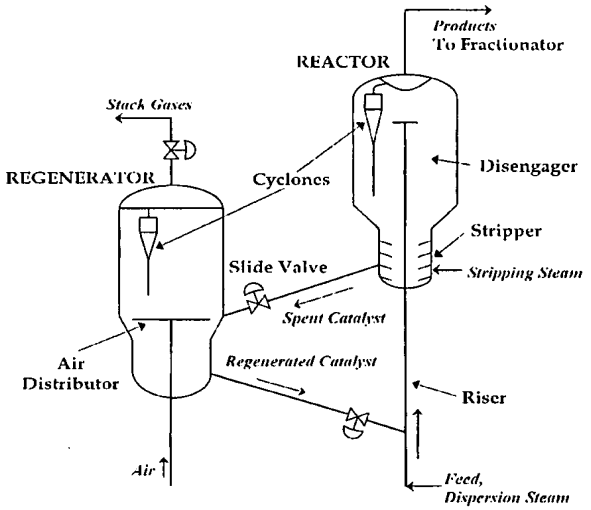

Fig. 1. Schematic diagram of a side-by-side type FCC unit.

Table 1
Process inputs and base case operating conditions

Type	Variable	Description	Base case operating conditions
Degrees of freedom	F_{lg}	Entrance flow rate of liquid feedstock	49.3 kg/s
	T_{lg}	Entrance temperature of liquid feedstock	535 K
	F_a	Flow rate of the air entering the regenerator	34.0 kg/s
	T_a	Temperature of the air entering the regenerator	432 K
	F_{ss}	Flow rate of stripping steam	1.1 kg/s
	T_{ss}	Temperature of stripping steam	430 K
	F_{ds}	Flow rate of dispersion steam	1.6 kg/s
	T_{ds}	Temperature of dispersion steam	430 K
	P_{MF}	Pressure at main-fractionator	185.5 kPa
	P_{SG}	Downstream pressure of the stack gas valve	110.0 kPa
	x_{vSV1}	Stem position of the slide valve on the regenerated catalyst transport line	0.57
	x_{vSV2}	Stem position of the slide valve on the spent catalyst transport line	0.46
	x_{vSG}	Stem position of the regenerator stack gas valve	0.70
Feedstock characteristics	T_{10}, T_{30}, T_{50}, T_{70}, T_{90}	TBP distillation temperatures at distilled vol% equal to 10, 30, 50, 70, and 90, respectively.	554.3,605.4, 647.0, 688.2, and 744.8 K, respectively.
	S_g	Specific gravity of liquid feedstock	0.894 (API: 26.8)
	R_{AN}	Aromatics to naphthenes weight ratio in feedstock	2.1
	Y_{cc}	Weight fraction of Conradson carbon residue in feedstock	0.5 wt%
Ambient air characteristics	$f_{O_2}^{(0)}$, $f_{CO}^{(0)}$, $f_{CO_2}^{(0)}$, $f_{H_2O}^{(0)}$, $f_{N_2}^{(0)}$	Composition of ambient air	0.2097, 0, 0.0003, 0, and 0.79, respectively.
	T_e	Ambient air temperature	300 K

Table 2
Dimensions of the simulated FCC unit

Process unit	Dimension	
	Length (m)	*Diameter (m)*
Riser	30.0	1.1
Disengaging section	8.5	5.1
Stripping section	6.2	3.2
Regenerator	18.0	8.2
Spent catalyst transport line	10.5	0.8
Regenerated catalyst transport line	12.5	0.8
	Total no. of cyclones equipped	*Dimensions of cyclone inlet (m)*
Reactor cyclones	2	0.8 (H)/0.4 (W)
Regenerator cyclones	2	1.0 (H)/0.5 (W)

Table 3
Characteristics of catalyst and coke used in simulations

Catalyst	
Average particle diameter	7×10^{-5} m
Minimum particle diameter	2×10^{-5} m
Sphericity	0.72
Density	1410 kg/m^3
Specific heat	1.15 kJ/(kg K)
Coke	
Density	The same as catalyst
Specific heat	The same as catalyst
Atomic ratio of hydrogen to carbon	1.2

Aguila-Rodriguez, and Moreno-Mayorga (1997). The heats of cracking reactions were roughly estimated by trial-and-error to match the calculated riser outlet temperature with a typical operation temperature reported by Callahan and Ushiba (1988). The kinetic parameters for oxidation of coke, homogeneous and catalytic oxidations of carbon monoxide were adopted from the papers of Morley and de Lasa (1987), Howard, Williams, and Fine (1973), and Ali and Rohani (1997), respectively. The intrinsic CO_2/CO molar ratio was estimated using the empirical equations proposed by Errazu, de Lasa, and Sarti (1979).

Table 4
Kinetic parameters of cracking and coke burning reactions

Four-Lump cracking reaction			
	Frequency factor (s^{-1})	Activation energy (kJ/kg mol)	Heat of reaction (kJ/kg)
Gas oil to gasoline	1457.50	57359	195
Gas oil to C_1–C_4 gases	127.59	52754	670
Gas oil to coke	1.98	31820	745
Gasoline to C_1–C_4 gases	256.81	65733	530
Gasoline to coke	6.29×10^{-4}	66570	690
Catalyst deactivation	$\alpha_{c10}\alpha_{c20} = 1.1 \times 10^{-5}$	$E_{1c} = 49000$ kJ/kg mol	$\alpha^*_{c20} = 0.1177$

Coke burning reaction and oxidation		
	Frequency factor	Activation energy (kJ/(kg mol)
Coke burning reaction	1.4×10^8 m^3/(kg mol s)	125000
CO oxidation (non-catalytic)	3.5×10^9 m^3/(kg mol s)	165000
CO oxidation (catalytic)	247.75 m$^{4.5}$/(kg mol$^{0.5}$ kg s)	70480
Intrinsic CO_2/CO molar ratio	$\sigma = 0.000953\exp(5585/T)$	
Heat of formation	$\Delta H_{fck} = -4800.22 + 16.1T$, kJ/kg mol	
	$\Delta H_{fO_2} = -10364.88 + 34.60T + 0.00055T^2$, kJ/kg mol	
	$\Delta H_{fCO} = -118975.04 + 27.61T + 0.00251T^2$, kJ/kg mol	
	$\Delta H_{fCO_2} = -406909.11 + 43.26T + 0.00575T^2$, kJ/kg mol	
	$\Delta H_{fH_2O} = -252111.38 + 34.39T + 0.000315T^2$, kJ/kg mol	

The simulation results presented in this section cover both the steady state and dynamic responses of the FCC unit described previously. First, steady-state responses were obtained by executing the simulator for a sufficiently long time until all the variables lined out. These steady-state simulations were carried out many times each with altered values of the two major operating variables (the catalyst circulation rate (F_c) and the air flow rate into the regenerator (F_a)). Then, the simulation results were compared with those in the literature. In addition, the predicted profiles of several process variables are plotted along the height of reactor riser or regenerator for the base case operating conditions. Next, the multiple steady states in FCC operations were confirmed by investigating the sensitivity of our model to initial conditions. Finally, the dynamic responses of the process to step changes in several process input variables were predicted and analyzed.

3.1. Comparison of steady-state behavior with the previous models

In this section we show the validity of our simulator by comparing our simulation results with those from the previous FCC models. Although direct and qualitative comparison is not feasible due to different kinetics and unavailability of simulation data, we investigate the overall steady-state behavior of the FCC unit as functions of the catalyst circulation and the air flow rate.

Fig. 2 shows the steady-state behavior of major state variables as functions of the air-flow rate when the catalyst circulation rate is fixed at a specified value of 250 or 300 kg/s. Fig. 2a shows that with decreasing air flow rate the oxygen concentration gradually decreases until almost all the oxygen is exhausted. In this transition the system moves from a so-called *full-combustion* mode to a *partial-combustion* mode (Arbel, Huang, Rinard, Shinnar, & Sapre, 1995a; Arbel, Rinard, Shinnar, & Sapre, 1995b). The point of transition in combustion mode can be easily located at the maximum points of the curves for the regenerator and reactor temperatures in Fig. 2b. Alternatively, this point corresponds to either the maximum points of the gas-oil conversion or the minimum points of the coke on catalyst in Fig. 2c. The results shown in Fig. 2 exhibit good matches with the field observations and simulation results of Arbel et al. (1995a) not only in terms of qualitative trend but also in terms of the slopes of the curves.

Fig. 3 shows the steady-state behavior of major state variables as functions of the catalyst circulation rate when the air flow is fixed at a specified value of 35 or 40 kg/s. As the catalyst circulation rate increases, the CO combustion in the regenerator transits from a full combustion mode to a partial combustion model with accompanying changes in the state variables. Again, these results are in good agreement with Arbel et al. (1995a). The steady-state behavior of the regenerator temperature shown in Fig. 3b is also analogous to that of Kumar, Chadha, Gupta, and Sharma (1995). Ali and Rohani (1997) presented similar results for the regenerator temperature and the coke on catalyst, but opposite trend in the reactor temperature to ours as well as Arbel et al. (1995a).

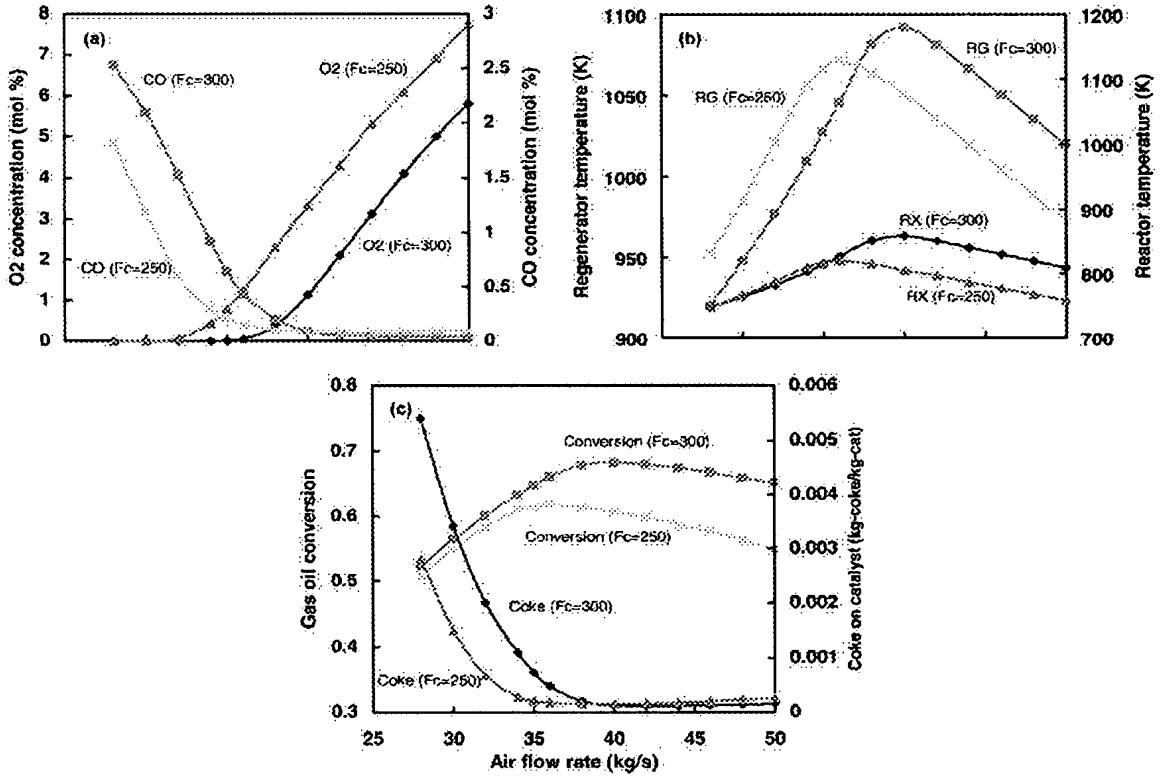

Fig. 2. Steady-state responses to changes in air flow rate.

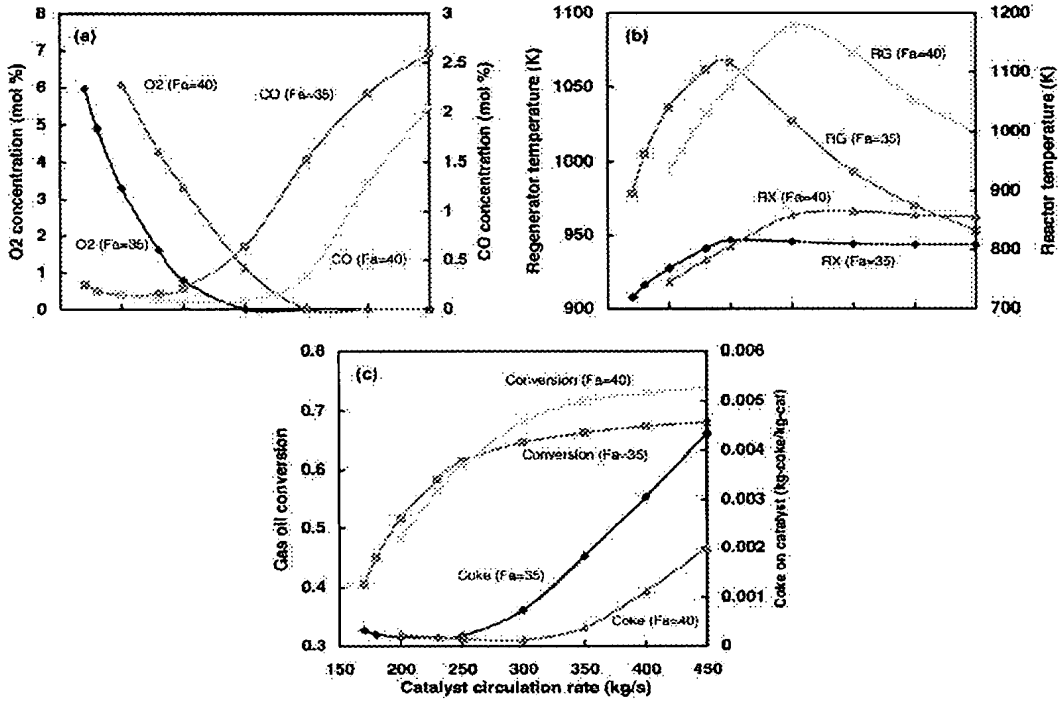

Fig. 3. Steady-state responses to changes in catalyst circulation rate.

3.2. Steady-state profiles along the riser and the regenerator

Fig. 4 depicts the predicted steady-state profiles of several process variables along the reactor riser under the base case operating conditions. The conversion of gas oil reaches 73 wt% at the riser outlet and 90% of the conversion is attained within the first 20 m of the riser (Fig. 4a). Most heat exchange between the catalyst phase and the gas phase takes place within the first 10 m, thus two-phase temperatures approaching each other within 3.0 K at the riser outlet (Fig. 4b). After sufficient heat is transferred from the catalyst to the gas phase, the gas temperature as well as the catalyst temperature drops with increasing riser height because of endothermic cracking reactions. Both the catalyst and gas velocities sharply rise to about 7.5 m/s at the riser bottom due to the volume expansion accompanying feed vaporization (Fig. 4c). There is significant molar expansion of gaseous substance as large molecules crack to smaller molecules, so the interstitial velocities of both phases steadily increase up to 17 m/s at the outlet. The slip velocity between two phases is maintained within 0.25 m/s. It can be inferred from the predicted velocity profiles that assuming constant velocity in the riser would result in significant error in describing cracking reactions. The pressure shows an almost linear decrease along the riser with the total drop of about 16 kPa. This value shows good agreement with a measured value (16.7 kPa) and a predicted value (13.7 kPa) reported by Theologos, Nikou, Lygeros, and Markatos (1997) who developed a very rigorous three-dimensional riser model.

Fig. 5 shows the predicted profiles of several process variables along the regenerator height at the same steady state as in Fig. 4. Since the predicted catalyst bulk density of 448 kg/m^3 in the dense bed is much larger than 31 kg/m^3 in the freeboard, most coke burning reactions take place in the dense bed (Fig. 5a). The molar stack-gas composition was predicted to be 0.2% O_2, 0.6% CO, 14.8% CO_2, and 9.2% H_2O, which also agrees well with the observations obtained for typical promoted coke burning reactions (Faltsi-Saravelou, Vasalos, & Dimogiorgas, 1991; Zheng, 1994). Since catalyst particles are assumed perfectly mixed in the dense bed, they have uniform coke concentration and temperature profiles in the dense bed (Figs. 5b and c). As a result of the after-burning oxidation of CO, CO concentration is lower and temperature is higher in the freeboard than in the dense bed.

3.3. Multiple steady-states and sensitivity to initial conditions

There has been plethora of literature on the subject of multiple steady states and their stability of FCC units in the past three decades. Since Iscol (1970) proposed the

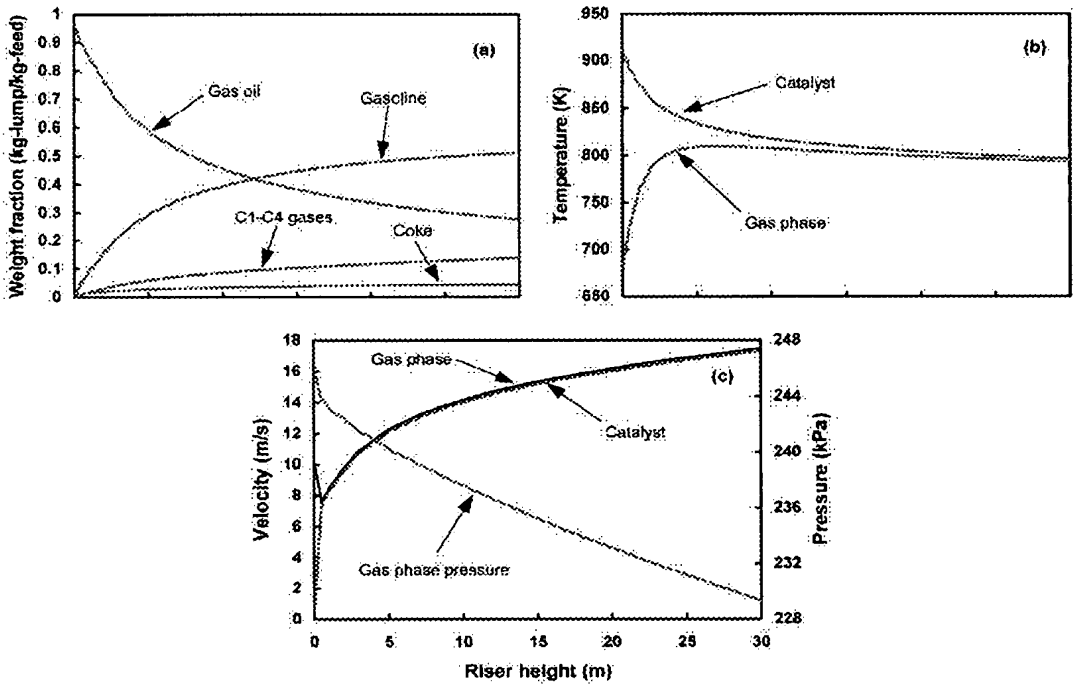

Fig. 4. Base case steady-state profiles along the riser.

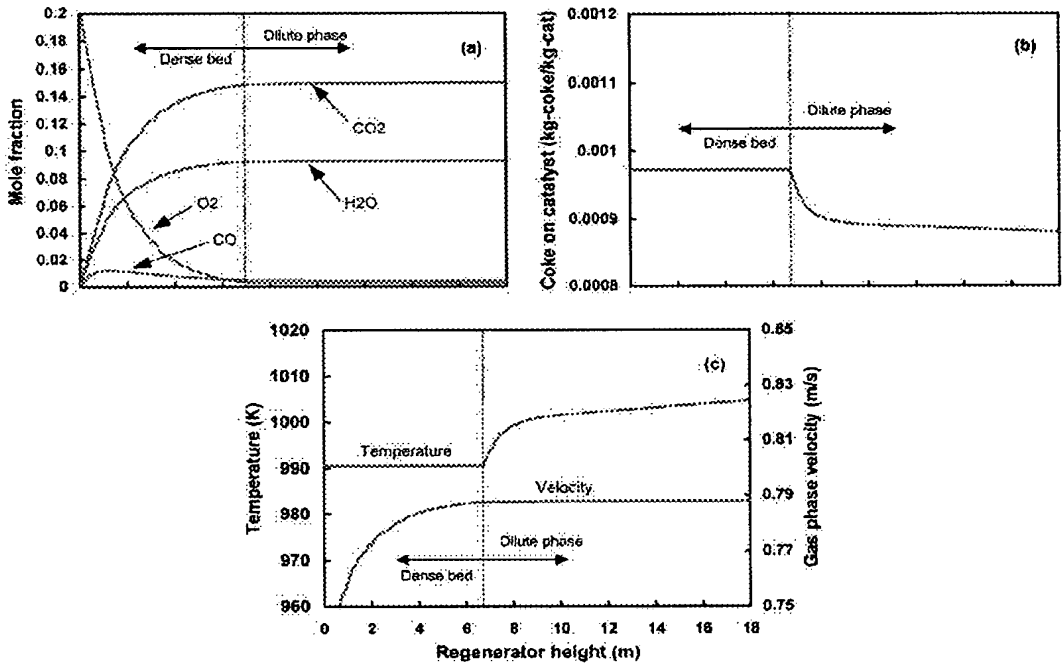

Fig. 5. Base case steady-state profiles along the regenerator.

existence of multiple steady states in the normal ranges of commercial operation, many papers followed arguing pro and con on the possibility of multiplicity and its conditions (Lee & Kugelman, 1973; Edwards & Kim, 1988; Elshishini & Elnashaie, 1990, Arandes & de Lasa, 1992). The dispute and confusion on the issue seems to be clarified by Arbel et al. (1995a,b), who performed a systematic analysis based on a relatively detailed model of modern FCC units. A part of the authors' conclusions can be summarized as follows: (1) there are at least three steady states for fixed inputs to present design units. In case there is only one, it is a trivial quenched state; (2) the upper (ignited) and the lower (quenched) state are always stable whereas the intermediate one is always unstable.

Most analyses on multiple steady states for a process involving exothermic reactions are carried out using a steady-state model to find the operating points at which the rate of heat generation equals that of heat removal. Dynamic models can be also used to confirm the multiple steady states by investigating the trajectories of the system subject to different initial conditions because each stable steady state has a unique domain of attraction on the phase plane. Elnashaie and Elshishini (1993) studied the sensitivity of their dynamic model to initial conditions. The process trajectories starting from several initial conditions were found to drift either to an upper steady state or to a lower steady state. They found that the dynamic behavior of their FCC model is very sensitive to the initial catalyst activity in the reactor.

Dynamic simulations were performed starting from perturbed initial conditions to investigate multiple steady states for our FCC model. First, the initial conditions were set as the values at the base case steady state obtained previously except the dense bed temperature which was perturbed to 1100, 900, and 820 K, respectively. Fig. 6 compares the transient trajectories of reactor temperature, dense-bed temperature, and coke on regenerated catalyst evolving from each initial condition. When starting from 1100 or 900 K, the process shows different transient responses (curves 1 and 2) but ultimately converges to the original base case steady state. When starting from 820 K, however, both the reactor and dense-bed temperatures keep decreasing until it reaches the point where the regenerated catalyst is not capable of vaporizing gas oil feed any more. Since then the riser will be filled with liquid gas oil feed, normal operation of the unit would not be possible any longer. This state of inoperability of an FCC unit is called a quenched state in the literature (Elshishini & Elnashaie, 1990; Arbel et al., 1995b) whereas the normal steady state obtained above is called an ignited state. It is clear that the unstable steady state in the middle cannot be identified in open-loop dynamic simulations.

It may be interesting to check the sensitivity of our FCC model to initial conditions of several key variables. It was found in our simulations that the process is sensitive to dense bed temperature in that an initial temperature below 827 K would cause the process to

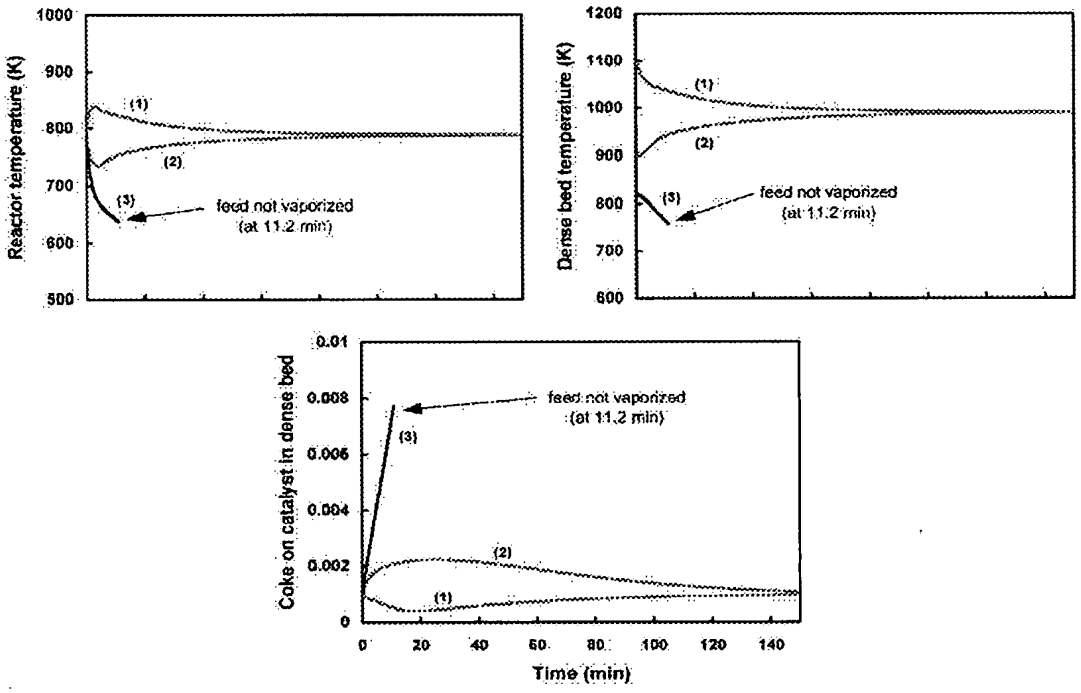

Fig. 6. Transient responses starting from different initial dense bed temperatures: (1) $T_B^{(0)} = 1100$ K, (2) $T_B^{(0)} = 900$ K, (3) $T_B^{(0)} = 820$ K.

drift toward the quenched state. On the other hand, the process always drifts toward the upper steady state whatever temperature the reactor initially may assume between 270 and 920 K. The different sensitivity behavior between the two cases can be attributed to much larger thermal holdup of the regenerator compared to the reactor. The process also drifts to the upper steady states when the initial coke on spent and regenerated catalyst is less than 0.055 and 0.054, respectively.

It is the regenerator with exothermic reactions and back-mixed thermal dynamics that is responsible for the multiple steady states in FCC operation. Since the riser is modeled as a tubular reactor with endothermic reactions and the disengaging-stripping section does not involve any reaction, the reactor does not have dynamic characteristics that may lead to multiple steady states (Maya-Yescas & Lopez-Isunza, 1997). To investigate the steady-state multiplicity inherent in the regenerator dynamics, dynamic simulations were performed with the scope confined to the regenerator. Fig. 7 compares the transient responses evolving from two different initial temperatures (1100 and 500 K) of the dense bed when the conditions of spent catalyst entering the regenerator are fixed. It is clear that the high-initial temperature leads to the upper steady state whereas the low initial temperature leads to the lower steady state. The upper and lower steady states represent two stable modes of

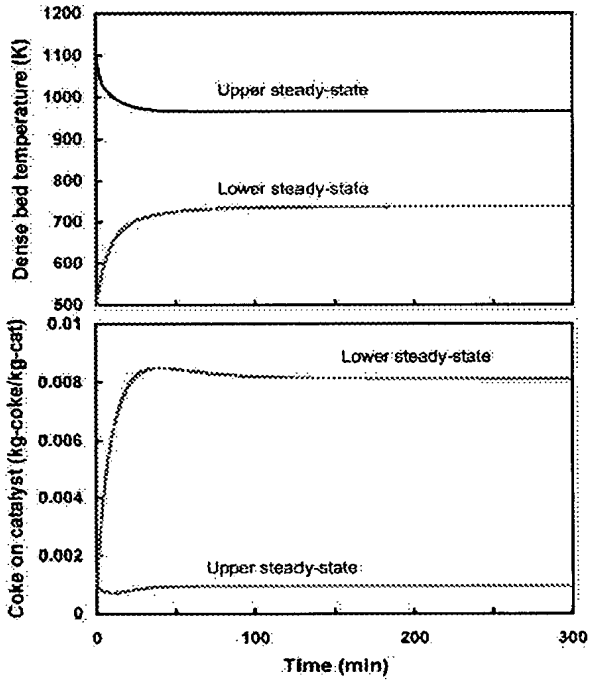

Fig. 7. Multiple steady states in regenerator operation with catalyst inflow conditions fixed.

Table 5
Step change scheme for process inputs in dynamic simulation

Step change scheme

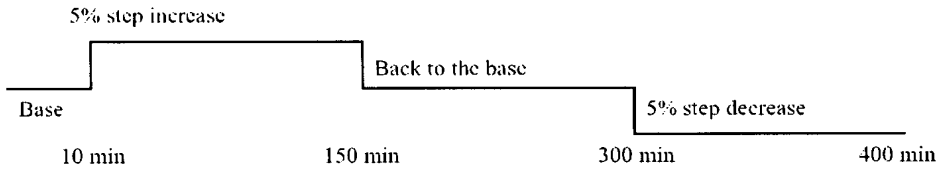

Case 1: Changes in gas oil feed rate.
Case 2: Changes in air flow rate.
Case 3: Changes in stem positions of the slide valves at both catalyst transport lines.

operation as far as the regenerator is concerned. When connected to a reactor with catalyst circulated in-between, however, the lower steady state would result in the quenching of the whole unit because the regenerated catalyst at such low temperature would fail to vaporize gas oil feed.

3.4. Dynamic responses

Dynamic simulation of the FCC process was performed according to the simulation scheme shown in Table 5. Gas oil feed rate, air flow rate, and stem positions of the slide valves at both catalyst transport lines were chosen as simulation variables to whose changes the dynamic responses are demonstrated. Each simulation run started from the steady state corresponding to the base case operating conditions and the subsequent transient response was obtained as each simulation variable went through a series of step changes shown in Table 5.

3.4.1. Changes in gas-oil feed rate

Fig. 8 shows the predicted dynamic responses to the changes in gas oil feed rate. After the gas oil feed rate is increased by 5% at time equal to 10 min, the reactor temperature drops because of an increase in heat consumption to vaporize the gas-oil feed (Fig. 8a). The lowered riser temperature results in a considerable decrease in gas oil conversion by about 6.1 wt% (Fig. 8e) while the increased feed rate leads to a sharp rise in coke on spent catalyst and subsequently on regenerated catalyst (Fig. 8f). Because the increased feed rate also raises the density of hydrocarbon gases in the reactor, there is a jump of gas pressure as well as of the pressure at the reactor bottom (Fig. 8c). This jump will also trigger a jump of spent catalyst flow rate but an opposite effect upon regenerated catalyst flow rate (Fig. 8d). Therefore, the catalyst holdup in the reactor steadily decreases until a new steady state is reached where the two catalyst circulation rates are balanced each other (Fig. 8b). Since decreasing catalyst holdup means decreasing static head acting on the reactor bottom, the pressure at the bottom will descend from the aforementioned initial jump until it settles down to a new steady-state value which is lower than the original steady state (Fig. 8c). This inverse response behavior of the reactor bottom pressure also explains the similar behavior of the spent catalyst flow rate which is directly influenced by the reactor bottom pressure (Fig. 8d). Regenerator temperatures start to decrease in both the dense bed and freeboard regions since the increased spent catalyst inflow from the reactor cooler than before implies an enhanced heat removal rate in energy balance (Fig. 8a). Since the fixed air flow does not supply enough oxygen to burn off the increased coke in the dense bed nor to sustain after-burning reactions in the freeboard, CO concentration in the stack gas steadily rises (Fig. 8e). The oxygen deficiency in the regenerator also leads to no more rise in the freeboard temperature above the dense bed temperature at the new steady state (Fig. 8a).

When the gas oil feed rate is decreased to its previous value at time equal to 150 min, the system completely recovers its original steady state. The transient responses over the second time interval in Fig. 8 show in what an orderly and coordinated fashion the process variables are returning to the old steady state.

A 5% step decrease in the gas oil feed rate at 300 min causes the system to move in the opposite direction to the case of the 5% step increase but the detailed responses show quite different aspects due to process nonlinearity. The gas oil conversion increases by about 3.9 wt% due to increased catalyst-to-oil ratio in the riser as well as better regeneration of catalyst in the regenerator (Figs. 8d–f). The reactor bottom pressure and the spent catalyst flow rate again show inverse responses which, on this occasion, are characterized by initial drop followed by eventual rise (Figs. 8c and d). Accordingly, catalyst holdup shows a steady increase in the reactor whereas a steady decrease in the regenerator (Fig. 8b). Contrary to the oxygen deficiency encountered before, oxygen surplus prevails throughout the regenerator because of

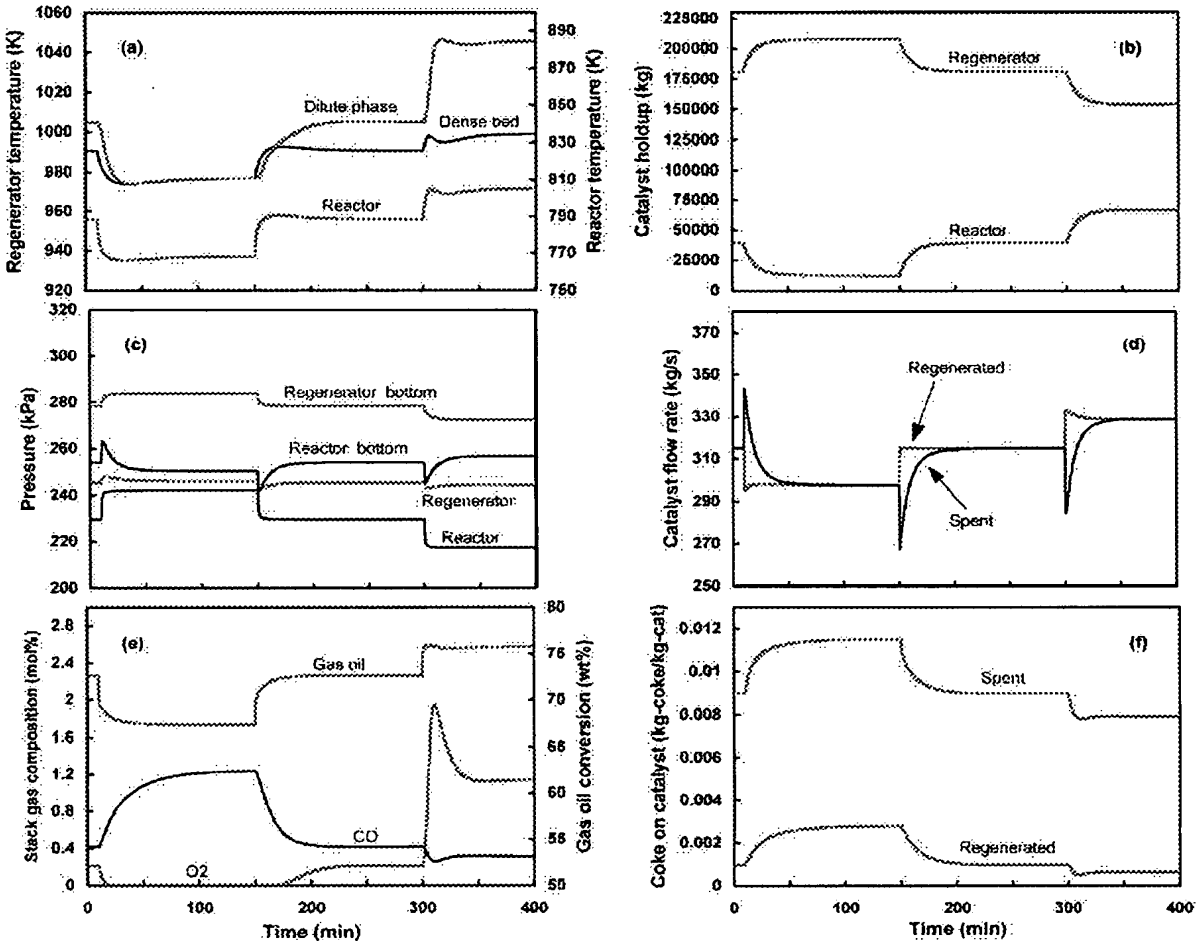

Fig. 8. Dynamic responses to step changes in gas oil feed rate (case 1).

the decreased spent catalyst inflow from the reactor. This causes a rise in the dense bed temperature, a much higher rise in the freeboard temperature due to after-burn of CO, and a consequent drop in the CO concentration of stack gas (Figs. 8a and 8e).

It was found in the simulations described above that the step changes in gas oil feed rate immediately alter the reactor pressure which subsequently triggers a series of changes upon the process dynamics. Since the stem positions of the slide valves on catalyst transport lines are held fixed in our open-loop simulation, catalyst circulation rates are solely determined by pressure differences across the valves. Accordingly, the pressure variation leads to serious unbalance between the flow rates of spent and regenerated catalyst and consequently to significant changes in the catalyst holdups in two vessels. In our simulations, the process was found to keep on stable operation in the face of step changes in feed rate of magnitude of about $\pm$ 7%. However, a large change exceeding this range caused the process to drift to a quenched state where normal operation of the unit is impossible.

3.4.2. *Changes in air flow rate*

Fig. 9 shows the predicted dynamic responses to the changes in the air flow rate to the regenerator. A 5% step increase in air flow causes a sharp increase in the regenerator pressure as well as in the regenerated catalyst flow rate to the riser bottom (Figs. 9c and d). On the other hand, the spent catalyst flow rate shows an inverse response behavior of initial decrease followed by ultimate increase (Fig. 9d). This behavior can be explained by a steady increase in the reactor bottom pressure (Fig. 9c) due to increasing static pressure exerted by the rising catalyst holdup in the reactor (Fig. 9b). The increased air flow rate also accelerates coke burning and thus raises temperature in every part of the unit (Fig. 9a) and reduces

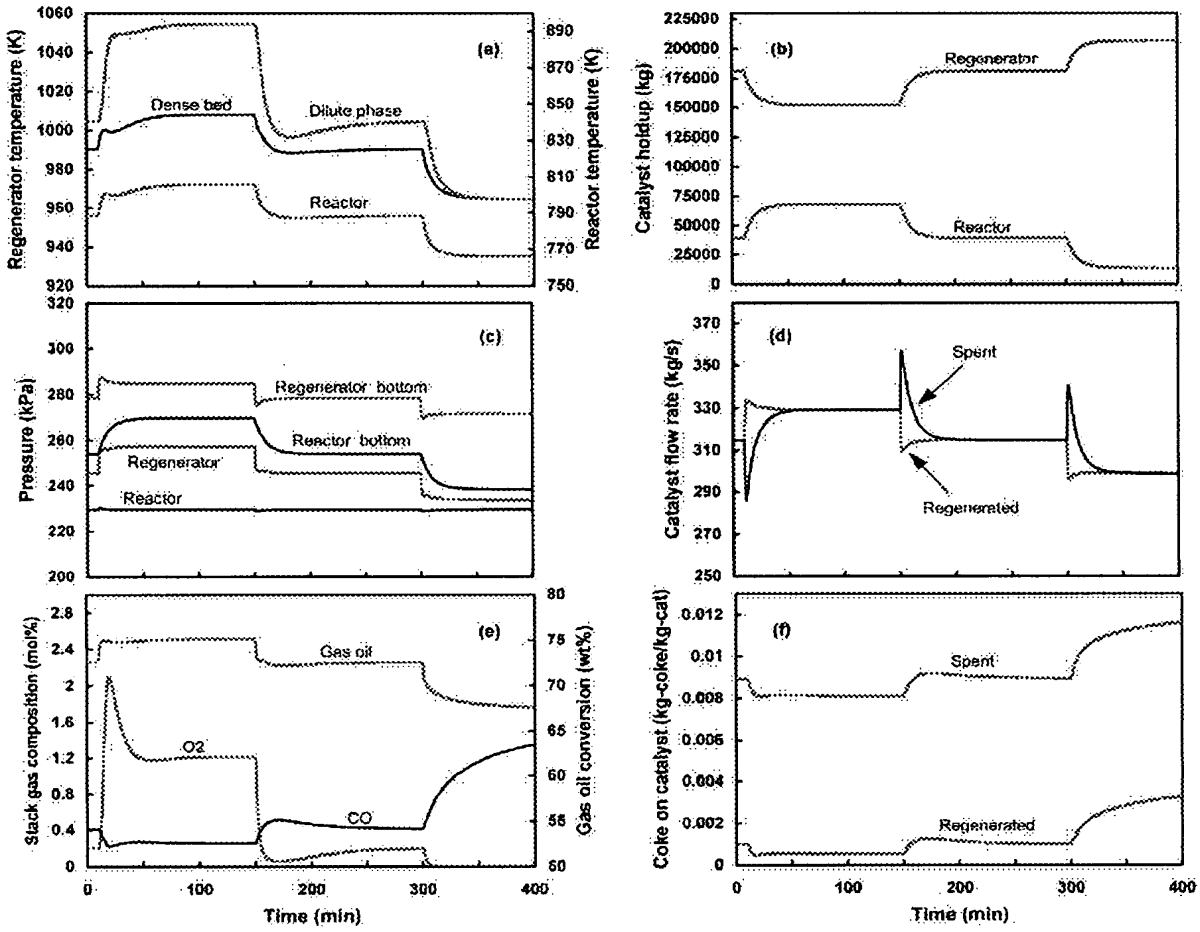

Fig. 9. Dynamic responses to step changes in air flow rate (case 2).

the CO concentration in the stack gas (Fig. 9e). It also causes the coke concentrations on both spent and regenerated catalyst to steadily drop to their respective steady state values (Fig. 9f). The conversion of gas oil is promoted by about 3.2 wt% by the elevated riser temperature and cleaner regenerated catalyst (Fig. 9e). When the air flow rate is decreased to its previous value, however, all the process variables are completely brought back to their original steady state.

A 5% step decrease in the air flow rate at time equal to 300 min brings about the state of oxygen deficiency in the regenerator. A large amount of coke cannot be burnt off, resulting in gradual accumulation on catalyst surfaces in both vessels over a long time (Fig. 9f, where the responses are partially shown). Such a long response time is characteristics of the composition dynamics in the regenerator that has large mass and thermal holdups and strong interactions with the reactor. CO concentration also shows a considerable increase because of poor after-burning reactions in both the dense bed and freeboard (Fig. 9e). This oxygen deficiency lowers the temperatures of both vessels by about 23–39 K (Fig. 9a) as well as the conversion of gas oil by 6.3 wt% (Fig. 9e). It was also found in our simulations that the process reaches a new stable state in the face of step changes in air flow rate of magnitude up to about $\pm$ 8%.

3.4.3. *Changes in the stem positions of slide valves*

Fig. 10 shows responses due to the changes in both the spent and regenerated catalyst flow rates as effected by slide valve manipulation. The stem positions of the slide valves on both the transport lines are adjusted upward by 5% at time equal to 10 min which corresponds to 8.5% increase in the catalyst circulation rate. Since both the spent and regenerated catalyst flow rates are raised by the approximately same amount, the catalyst holdup in each vessel is maintained constant (Fig. 10b). There is

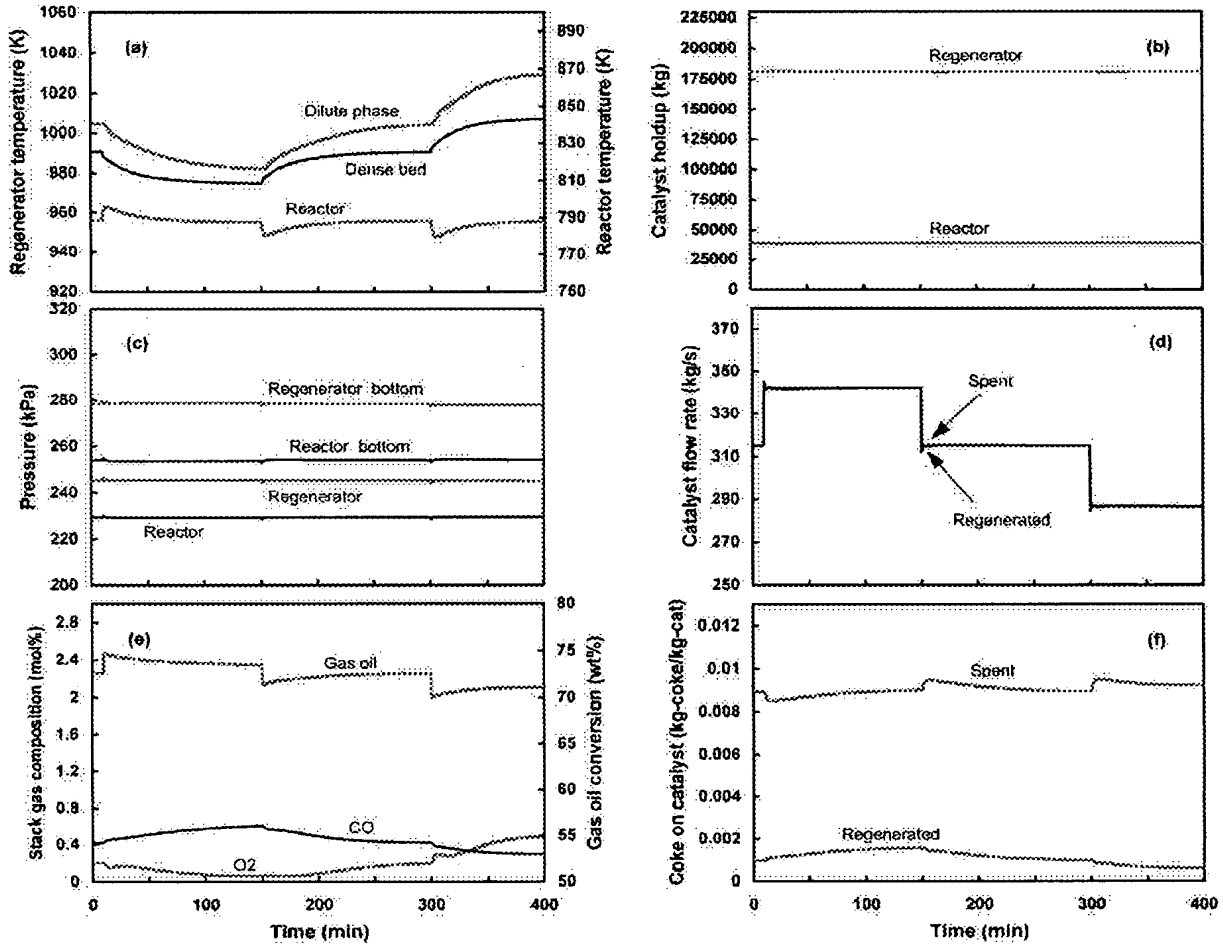

Fig. 10. Dynamic responses to step changes in stem positions of the slide valves (case 3).

also little variation in the pressures of the reactor and regenerator (Fig. 10c). However, the regenerator temperatures steadily drop both in the dense bed and freeboard because the increased flow of spent catalyst implies enhanced heat removal in energy balance for the regenerator. On the other hand, the reactor temperature initially rises due to increased catalyst flow from the regenerator but drops in a while as the dense bed temperature is lowered (Fig. 10a). The CO concentration slightly rises because after-burning reactions are suppressed by lowered freeboard temperature (Fig. 10e). Consequently, the cokes on both the regenerated and spent catalyst increase to new steady-state values (Fig. 10f). The gas oil conversion slightly increases by about 1.2 wt% due to an increased catalyst-to-oil ratio and elevated reactor temperature (Fig. 10e). If the stem positions of the slide valves are shifted back to their original positions, the process variables converge again to their previous values.

On the other hand, a 5% decrease in the stem positions at 300 min reduces the catalyst circulation rate by 9.6%. This reduction in the catalyst circulation rate decreases the gas oil conversion by 1.1% (Fig. 10e). The regenerator temperatures increase because the reduced spent catalyst flow provides not only a lowered heat removal rate but also a new oxygen-rich environment favorable to coke-burning reactions (Figs. 10a and e). Accordingly, there is a slight decrease in both the coke on regenerated catalyst and the CO concentration in the stack gas (Figs. 10e and f).

4. Conclusions

A dynamic simulator for fluid catalytic crackers called DSim-FCC was developed which implements the detailed dynamic model for an FCC process and the

model solver presented in Part I of this paper. The correlation equations were prepared for the thermodynamic properties and transport parameters contained in our model either by literature survey or by nonlinear regression of literature data.

The steady-state behavior was investigated as functions of the catalyst circulation rate and the air flow rate and the results showed good matches with those in the literature. For an industrial scale FCC unit of 30,000 BPD capacity, the base case steady-state profiles were obtained for velocity, pressure, temperature and composition in the reactor riser and the regenerator. Some steady-state predictions showed satisfactory agreement with the literature data. Then the issue of multiple steady states in FCC operations was addressed and confirmed by investigating the sensitivity of our model to initial conditions. Depending on initial conditions, the process was found to drift either toward an upper (ignited) steady state or toward a lower (quenched) steady state where normal operation of the unit is impossible. It was also found that the regenerator with exothermic reactions and back-mixed thermal dynamics is responsible for multiple steady states in FCC operation.

The dynamic step responses were obtained in an open-loop mode for gas oil feed rate, air flow rate, and stem positions of the slide valves on catalyst transport lines. The presented responses show typical inverse responses and nonlinear behavior which stem from complicated interaction between the reactor and regenerator dynamics.

Notation

A, B, C	coefficients of the Antoine equation
API	API gravity
C	mole concentration, kg mol/m^3
C_{ck}	coke on catalyst, kg-coke/kg-catalyst
C_{ckST0}	minimum coke content attainable by stripping, kg-coke/kg-catalyst
C_p	heat capacity, kJ/(kg K)
$\bar{C}_{pm}$	mean heat capacity, kJ/(kg K)
d	average diameter, m
D	diameter, m
D_f	effective diffusion coefficient, m^2/s
E	activation energy, kJ/kg mol
E_{ss}	exponent in the stripping function, s/kg
f	mole fraction
F	mass flow rate, kg/s
g	acceleration due to gravity, 9.8 m/s^2
h_p	interface heat transfer coefficient between catalyst and gas phases, kJ/(m^2 s K)
k	heat conductivity, kJ/(s m K)
k_v	valve flow rating factor, kg/(s kPa$^{0.5}$),
k_{vCY1}, k_{vCY2}	flow rating factors of the cyclone dip-legs, kg/(s m$^{2.5}$)
K_f	Watson characterization factor, K$^{1/3}$
K_I	interchange coefficients between bubble and emulsion phase, 1/s
M_w	molecular weight
N_{CY1}, N_{CY2}	numbers of cyclones in the reactor and regenerator, respectively
P	pressure, kPa
P_{pc}	pseudo-critical pressure, kPa
P_{pr}	pseudo-reduced pressure, kPa
R_{AN}	aromatics to naphthenes ratio in a liquid feedstock
S_g	specific gravity
T	Temperature, K
T_{10}, T_{30}, T_{50}, T_{70}, T_{90}	ASTM D86 distillation temperatures at distilled vol% equal to 10,30,50,70, and 90, respectively, K
T_{ASTM}	ASTM D86 distillation temperature, K
$T_D^{(0)}$	initial dense bed temperature, K
T_e	ambient temperature, K
T_{MABP}	molal average boiling temperature, K
T_{MeABP}	mean average boiling temperature, K
T_{pc}	pseudo-critical temperature, K
T_{pr}	pseudo-reduced temperature
T_{ref}	reference temperature, 298.15 K
T_{TBP}	TBP distillation temperature, K
T_v	normal boiling point, K
T_{VABP}	volume average boiling temperature, K
u	superficial velocity, m/s
U	overall heat transfer coefficient between a process unit and the surroundings, kJ/(m^2 s K)
v	interstitial velocity, m/s
v_{gm}	superficial gas velocity at a minimum fluidizing condition, m/s
w	holdup, kg
x_v	valve stem position, [0–1]
y	weight fraction
Y_{cc}	weight fraction of Conradson carbon residue in feedstock

Greek letters

α_c	catalyst deactivation coefficient
α_v	(valve head differential at maximum flow)/(valve head differential at zero flow), [0–1]
β_c	catalyst decay constant, 1/s
ΔH_f	heat of formation, kJ/kg mol
ΔH_{strip}	heat of stripping, kJ/kg
ΔH_v	heat of vaporization, kJ/kg
ε	volume fraction, [0–1]
ε_{gm}	void fraction at a minimum fluidizing condition
η_{CY1}, η_{CY2}	collection efficiencies of cyclones, [0–1]

μ	viscosity, kg/(m s)
μ_{pc}	pseudo-critical viscosity, kg/(m s)
μ_{pr}	pseudo-reduced viscosity
ρ	density, kg/m^3
σ	intrinsic CO_2/CO molar ratio in coke

Subscripts

a	air
b	bubble or catalyst bulk
B	bubble phase
c	catalyst
ck	coke
$CL1$	regenerated catalyst transport line (to reactor)
$CL2$	spent catalyst transport line (to regenerator)
CO	carbon monoxide
CO_2	carbon dioxide
CY1	reactor cyclone
CY2	regenerator cyclone
ds	dispersion steam
D	dense bed
E	emulsion phase
F	freeboard
g	gas
gl	gasoline
go	gas oil
gs	C_1–C_4 (lighter) gases
H_2O	water
lg	liquid feedstock (gas oil)
m	mixture
MF	main-fractionator
N_2	nitrogen
O_2	oxygen
RG	regenerator
RT	reactor
SG	stack gas valve
ss	stripping steam
ST	stripping section
$SV1$	regenerated catalyst slide valve
$SV2$	spent catalyst slide valve

Acknowledgements

The study was financially supported by Korea Science and Engineering Foundation under Grant No. 981-1104-013-2.

Appendix A. Correlation of physical properties and transport parameters

ASTM D86 and TBP distillation curves can be converted into each other by the following expressions (Riazi, 1988):

$$T_{TBP} = a(T_{ASTM})^b \quad (A.1)$$

$$T_{ASTM} = a^{-1/b}(T_{TBP})^{1/b}, \quad (A.2)$$

where the coefficients a and b vary with the percent of distilled volume as shown in Table 6. Then the ASTM D86 distillation curve can be used to estimate the volume, molal, and mean average boiling points, respectively (Technical Data Committee, 1988)

$$T_{VABP} = 0.2(T_{10} + T_{30} + T_{50} + T_{70} + T_{90}), \quad (A.3)$$

$$T_{MABP} = T_{VABP} - 0.5556\exp[-0.5638 - 0.0080(1.8T_{VABP} - 491.67)^{0.6667} + 3.0473(SI)^{0.3333}], \quad (A.4)$$

$$T_{MeABP} = T_{VABP} - 0.5556\exp[-0.9440 - 0.0087(1.8T_{VABP} - 491.67)^{0.6667} + 2.9972(SI)^{0.3333}], \quad (A.5)$$

where

$$(SI) = 0.0225(T_{90} - T_{10}). \quad (A.6)$$

The Watson characterization factor is calculated using specific gravity and mean average boiling point as follows:

$$S_g = \frac{141.5}{(API) + 131.5}, \quad (A.7)$$

$$K_f = \frac{(1.8T_{MeABP})^{1/3}}{S_g}. \quad (A.8)$$

The molecular weights of gas oil and gasoline lump can be estimated by Eq. (A.9) (Riazi, 1988), and the

Table 6
Coefficients in Eqs. (A.1) and (A.2)

Vol% distilled	a	b
0	0.9167	1.0019
10	0.5277	1.0900
30	0.7429	1.0425
50	0.8920	1.0176
70	0.8705	1.0226
90	0.9490	1.0110
95	0.8008	1.0355

average molecular weight of n component gas mixture is calculated by Eq. (A.10):

$$M_{wg} = 42.965[\exp(2.097\times10^{-4}T_{\mathrm{MeABP}} - 7.787S_g + 2.085\times10^{3}T_{\mathrm{MeABP}}S_g)] \times T_{\mathrm{MeABP}}^{1.26007}S_g^{4.98308}, \quad (A.9)$$

$$M_{wm} = 1\Big/\sum_{i=1}^{n}\left(\frac{y_i}{M_{wi}}\right). \quad (A.10)$$

The liquid- and gas-phase heat capacities of gas oil and gasoline lump are estimated using a modified Lee–Kesler correlation (Lee and Kesler, 1988) which neglects the pressure effect since typical FCC processes are operated under relatively low pressures ranging between 200 and 300 kPa:

$$C_{plg} = \alpha_1 + \alpha_2 T + \alpha_3 T^2, \quad (A.11)$$

$$C_{pg} = \beta_1 + \beta_2 T + \beta_3 T^2, \quad (A.12)$$

where

$$\alpha_1 = -4.90383 + (0.099319 + 0.104281S_g)K_f + \frac{(4.814066 - 0.194833K_f)}{S_g}, \quad (A.13)$$

$$\alpha_2 = (7.53624\times10^{-4})(1.0 + 0.82463K_f)\times\left(1.12172 - \frac{0.27634}{S_g}\right), \quad (A.14)$$

$$\alpha_3 = (-1.356523\times10^{-7})(1.0 + 0.82463K_f)\times\left(2.9027 - \frac{0.70958}{S_g}\right), \quad (A.15)$$

$$\beta_1 = -1.492343 + 0.124432K_f + \beta_4\times\left(1.23519 - \frac{1.04025}{S_g}\right), \quad (A.16)$$

$$\beta_2 = (-7.53624\times10^{-4})[2.9247 - (1.5524 - 0.05543K_f)K_f + \beta_4\left\{(6.0283 - \frac{5.0694}{S_g})\right\}], \quad (A.17)$$

$$\beta_3 = (1.356523\times10^{-6})(1.6946 + 0.0884\beta_4), \quad (A.18)$$

$$\beta_4 = \left[\left(\frac{12.8}{K_f} - 1.0\right)\left(1.0 - \frac{10.0}{K_f}\right)\times(S_g - 0.885)(S_g - 0.70)(10^4)\right]^2 \quad \text{for } 10.0 < K_f < 12.8,$$

$$\beta_4 = 0 \quad \text{for all other cases.} \quad (A.19)$$

The heat capacity of the light gas lump is calculated by Eq. (A.20) assuming the composition (H2 = 0.2%, C1 = 5.7%, C2 = 7.8%, C3 = 29.7%, and C4 = 56.6%) found in typical field operations (Mcketta and Cunningham, 1976):

$$C_{pgs} = 0.2457 + 5.3\times10^{-3}T - 2.1527\times10^{-6}T^2. \quad (A.20)$$

The heat capacities of carbon monoxide, carbon dioxide, nitrogen, oxygen, and steam are calculated by the following:

$$C_{p\mathrm{O_2}} = 1.081 + 0.000034T, \quad (A.21)$$

$$C_{p\mathrm{CO}} = 0.986 + 0.00018T, \quad (A.22)$$

$$C_{p\mathrm{CO_2}} = 0.983 + 0.00026T, \quad (A.23)$$

$$C_{p\mathrm{H_2O}} = 1.91 + 0.000035T, \quad (A.24)$$

$$C_{p\mathrm{N_2}} = 0.971 + 0.00015T. \quad (A.25)$$

Then the mean heat capacity of n component mixture can be calculated by

$$\bar{C}_{pm} = \frac{\int_{T_{ref}}^{T}\sum_{i=1}^{n} y_i C_{pi}(T)\,\mathrm{d}T}{T - T_{\mathrm{ref}}}. \quad (A.26)$$

The gas phase viscosities of hydrocarbon lumps are estimated by Eq. (A.27) which factorizes the viscosity into pseudo-reduced viscosity and pseudo-critical viscosity (Nelson, 1958)

$$\mu_g = \mu_{pr}\mu_{pc} = 3.515\times10^{-8}\mu_{pr}\frac{\sqrt{M_{wm}P_{pc}^{2/3}}}{T_{pc}^{1/6}}. \quad (A.27)$$

The correlation equation (A.28) for pseudo-reduced viscosity was obtained by nonlinear regression of literature data (Nelson, 1958) over the range of T_{pr} and P_{pr} given in Eq. (A.29)

$$\mu_{pr} = 0.435\exp[(1.3316 - T_{pr}^{0.6921})P_{pr}]T_{pr} + 0.0155, \quad (A.28)$$

$$0.75 < T_{pr} = \frac{T}{T_{pc}} < 3.0, \quad \text{and} \quad 0.01 < P_{pr} = \frac{P}{P_{pc}} < 0.2, \quad (A.29)$$

where the critical properties of hydrocarbons are estimated by the following equations:

$$T_{pc} = 17.1419[\exp(-9.3145\times10^{-4}T_{\mathrm{MeABP}} - 0.5444S_g + 6.4791\times10^{-4}T_{\mathrm{MeABP}}S_g)] \times T_{\mathrm{MeABP}}^{0.81067}S_g^{0.53691}, \quad (A.30)$$

$$P_{pc} = 4.6352\times10^{6}[\exp(-8.505\times10^{-3}T_{\mathrm{MeABP}} - 4.8014S_g + 5.749\times10^{-3}T_{\mathrm{MeABP}}S_g)] \times T_{\mathrm{MeABP}}^{-0.4844}S_g^{4.0846}. \quad (A.31)$$

On the other hand, the viscosities of the components in the coke burning reaction mixture are expressed as functions of temperature only as follows

$$\mu_{O_2} = 6.476\times10^{-6} + 4.818\times10^{-8}T, \quad (A.32)$$

$$\mu_{CO} = 5.38\times10^{-6} + 4.04\times10^{-8}T, \quad (A.33)$$

$$\mu_{CO_2} = 1.34\times10^{-6} + 4.5\times10^{-8}T, \quad (A.34)$$

$$\mu_{H_2O} = -1.90\times10^{-6} + 3.85\times10^{-8}T, \quad (A.35)$$

$$\mu_{N_2} = 1.101\times10^{-5} + 3.074\times10^{-8}T, \quad (A.36)$$

Finally, the mean viscosity of gaseous mixture is calculated by

$$\mu_m = \sum_{i=1}^{n}\mu_i\left\{1 + \sum_{\substack{j=1\\ j\neq i}}^{n}\frac{[1+(\mu_i/\mu_j)^{1/2}(M_{wj}/M_{wi})^{1/4}]^2 f_i}{\sqrt{8}[1+M_{wi}/M_{wj}]^{1/2}\ f_j}\right\}^{-1}. \quad (A.37)$$

The correlation equation for heat of vaporization of gas oil was obtained as Eq. (A.38) by nonlinear regression of literature data (Nelson, 1958). This equation is applicable when the molecular weight of gas oil ranges from 200 to 400.

$$\Delta H_{vlg} = 0.3843T_{\mathrm{MABP}} + 1.0878\times10^{3}\exp\left(\frac{-M_{wm}}{100}\right) - 98.153. \quad (A.38)$$

The vapor pressure of gas oil is calculated by solving for a trial-and-error solution of the following set of correlation equations adopted from literature (Technical Data Committee, 1988):

$$P_g = 0.133322\times10^{(3000.538\omega-6.761560)/(43\omega-0.987672)} \quad \text{for } \omega > 0.0022,$$

$$P_g = 0.133322\times10^{(2663.129\omega-5.994296)/(95.76\omega-0.972546)} \quad \text{for } 0.0013 \leqslant \omega \leqslant 0.0022,$$

$$P_g = 0.133322\times10^{(2770.085\omega-6.412631)/(36\omega-0.989679)} \quad \text{for } \omega < 0.0013, \quad (A.39)$$

where

$$\omega = \frac{T^*_{\mathrm{MeABP}}/T_v - 0.00051606T^*_{\mathrm{MeABP}}}{748.1 - 0.3861T^*_{\mathrm{MeABP}}}, \quad (A.40)$$

$$T^*_{\mathrm{MeABP}} = T_{\mathrm{MeABP}} - 1.3889\alpha \times (K_f - 12)\log(0.0098684P_g), \quad (A.41)$$

$$\alpha = 1 \quad \text{for } T_{\mathrm{MeABP}} > 477.8\ \mathrm{K},$$

$$\alpha = 0 \quad \text{for } T_{\mathrm{MeABP}} < 333.3\ \mathrm{K},$$

$$\alpha = (1.8T_{\mathrm{MeABP}} - 659.7)/200, \quad \text{for } 366.7\ K \leqslant T_{\mathrm{MeABP}} \leqslant 477.8\ \mathrm{K}. \quad (A.42)$$

To calculate the three coefficients in the Antoine equation for gas oil, vapor pressures are evaluated at three temperatures (T_{MeABP}, $T_{\mathrm{MeABP}} - 15$, and $T_{\mathrm{MeABP}} + 15$) using Eqs. (A.39)–(A.42) and are substituted into the following equations:

$$F_i(A_{lg}, B_{lg}, C_{lg}) = (T_{vi} + C_{lg})[A_{lg} - \log(P_{gi})] - B_{lg} = 0, \quad i = 1,2,3. \quad (A.43)$$

The resulting set of equations are solved using the Newton's method to get A_{lg}, B_{lg}, and C_{lg}.

The thermal conductivity of hydrocarbons is needed to calculate thermal diffusivity and heat transfer coefficient. The following equation was obtained by nonlinear regression of the data in API *technical data book* (Technical Data Committee, 1988):

$$k_g = 1\times10^{-6}(1.9469 - 0.374M_{wm} + 1.4815\times10^{-3}M_{wm}^2 + 0.1028T). \quad (A.44)$$

Then the interface heat transfer coefficient between solids and hydrocarbon gases can be estimated from the correlation between the Nusselt and Reynolds numbers (Kunii & Levenspiel, 1991):

$$h_p = 0.03\frac{k_g}{d_c^{2/3}}\left[\frac{|v_g - v_c|\rho_g\varepsilon_g}{\mu_g}\right]^{1/3}. \quad (A.45)$$

Then the overall interchange coefficient K_I for mass transfer between the emulsion and the bubble phases can be computed using the interchange coefficient K_1 between bubble and cloud and K_2 between cloud and emulsion (Kunii & Levenspiel, 1991)

$$K_I = \frac{\varepsilon_b}{1/K_1 + 1/K_2}, \quad (A.46)$$

$$K_1 = 4.5\frac{v_{gm}}{d_b} + 5.85\left[\frac{D_f^{1/2} g^{1/4}}{d_b^{5/4}}\right], \quad (A.47)$$

$$K_2 = 6.77\left[\frac{D_f \varepsilon_{gm} v_b}{d_b}\right]^{1/2}, \quad (A.48)$$

where the effective diffusion coefficient of gaseous mixture in the reactor and regenerator is calculated using the correlation equation proposed by Baird and Rice (1975):

$$D_f = 0.35(\mathrm{g}u_g)^{1/3} D^{4/3}. \quad (A.49)$$

Appendix B. Additional simulation data

The following is a list of additional data used in our simulation. These data together with those given in Tables 1–4 correspond to the base case simulation condition.

1. Initial conditions:

$C_{ckRT} = 0.009$, $w_{gRT} = 485.0$ kg,
$w_{cRT} = 38\,000.0$ kg, $y_{goRT} = 0.27$,
$y_{glRT} = 0.51$, $y_{gsRT} = 0.14$, $T_{RT} = 787.0$ K,
$w_{gRG} = 990$ kg, $w_{cRG} = 182\,000$ kg,
$C_{ckD} = 0.001$, $T_D = 991.0$ K,
$C_{O_2E} = 0.0005$ kg mol/m^3, $C_{COE} = 0.0003$ kg mol/m^3,
$C_{CO_2E} = 0.004$ kg mol/m^3, $C_{H_2OE} = 0.003$ kg mol/m^3,
$C_{N_2E} = 0.02$ kg mol/m^3, $C_{O_2B} = 0.0005$ kg mol/m^3,
$C_{COB} = 0.0003$ kg mol/m^3, $C_{CO_2B} = 0.004$ kg mol/m^3,
$C_{H_2OB} = 0.003$ kg mol/m^3, $C_{N_2B} = 0.02$ kg mol/m^3,
$C_{O_2F} = 0.0001$ kg mol/m^3, $C_{COF} = 0.0002$ kg mol/m^3,
$C_{CO_2F} = 0.004$ kg mol/m^3, $C_{H_2OF} = 0.003$ kg mol/m^3,
$C_{N_2F} = 0.02$ kg mol/m^3, $T_F = 1010.0$ K,
$C_{ckF} = 0.0008$.

2. Valve parameters:

$k_{vMF} = 4.35$ kg/(s kPa$^{0.5}$), $k_{vCY1} = 120.0$ kg/(s m$^{2.5}$),
$k_{vCY2} = 140.0$ kg/(s m$^{2.5}$), $k_{vSG} = 4.25$ kg/(s kPa$^{0.5}$),
$k_{vSV1} = 69.0$ kg/(s kPa$^{0.5}$), $k_{vSV2} = 69.0$ kg/(s kPa$^{0.5}$),
$\alpha_{vMF} = 1.0$, $\alpha_{vCY1} = 1.0$, $\alpha_{vCY2} = 1.0$, $\alpha_{vSG} = 0.8$,
$\alpha_{vSV1} = 0.9$, $\alpha_{vSV2} = 0.9$.

3. Heat transfer coefficients:

$U_{RT} = 0.035$ kJ/(m^2 s K), $U_D = 0.05$ kJ/(m^2 s K),
$U_F = 0.05$ kJ/(m^2 s K).

4. Miscellaneous parameters:

$C_{ckST0} = 0.0004$, $k_{ss0} = 0.0054$, $E_{ss} = 0.3311$ s/kg,
$\Delta H_{stripST} = 0$ kJ/kg, $\rho_{bCY1} = 350$ kg/s,
$\rho_{bCY2} = 350$ kg/s, $\rho_{bCL1} = 560$ kg/s,
$\rho_{bCL2} = 560$ kg/s, $c_T = 0K$, $\varepsilon_{gm} = 0.6$,
$\beta_c = 1.5\ \mathrm{s}^{-1}$, $\eta_{CY1} = 1$,
$\eta_{CY2} = 1$, $N_{tCY1} = 10$, $N_{tCY2} = 10$.

References

Ali, H., & Rohani, S. (1997). Dynamic modeling and simulation of a riser-type fluid catalytic cracking unit. *Chemical Engineering Technology, 20*, 118.

Ancheyta-Juarez, J., Lopez-Isunza, F., Aguila-Rodriguez, E., & Moreno-Mayorga, J. C. (1997). A strategy for kinetic parameter estimation in the fluid catalytic cracking process. *Industrial and Engineering Chemistry Research, 36*, 5170.

Arandes, J. M., & de Lasa, H. I. (1992). Simulation and multiplicity of steady states in fluidized FCCUs. *Chemical Engineering Science, 47*, 2535.

Arbel, A., Huang, Z., Rinard, I. R., Shinnar, R., & Sapre, A. V. (1995a). Dynamic and control of fluidized catalytic crackers-1. Modeling of the current generation of FCC's. *Industrial and Engineering Chemistry Research, 34*, 1228.

Arbel, A., Rinard, I. R., Shinnar, R., & Sapre, A. V. (1995b). Dynamic and control of fluidized catalytic crackers-2. Multiple steady states and instabilities. *Industrial and Engineering Chemistry Research, 34*, 3014.

ASTM (1991). Standard test method for distillation of petroleum product. In A. S. Roberta et al. (Eds.), *1991 annual book of ASTM standards: Petroleum products, lubricants, and fossil fuels*. Easton: ASTM.

Baird, H. M., & Rice, R. G. (1975). Axial dispersion in large unbaffled columns. *Chemical Engineering Journal, 9*, 171.

Callahan, K. P., & Ushiba, K. K. (1988). *Advances in fluid catalytic cracking part 2*. Mountain View: Catalytica.

Edwards, W. E., & Kim, H. N. (1988). Multiple stead states in FCC unit operations. *Chemical Engineering Science, 43*, 1825.

Elnashaie, S. S. E. H., & Elshishini, S. S. (1993). Digital simulation of industrial fluid catalytic cracking units-IV. Dynamic behavior. *Chemical Engineering Science, 48*, 567.

Elshishini, S. S., & Elnashaie, S. S. E. H. (1990). Digital simulation of industrial fluid catalytic cracking units-I. Bifurcation and its implications. *Chemical Engineering Science, 45*, 553.

Errazu, A. F., de Lasa, H. I., & Sarti, F. (1979). A fluidized bed catalytic cracking regenerator model: Grid effects. *Canadian Journal of Chemical Engineering, 57*, 191.

Faltsi-Saravelou, O., Vasalos, I. A., & Dimogiorgas, G. (1991). FBSim: A model for fluidized bed simulation-II. Simulation of an industrial fluidized catalytic cracking regenerator. *Computers & Chemical Engineering, 15*, 647.

Howard, J. B., Williams, G. C., & Fine, D. H. (1973). Kinetics of carbon monoxide oxidation in postflame gases. *Fourteenth symposium on international combustion* (p. 975).

Iscol, L. (1970). *The dynamics and stability of a fluid catalytic cracker*. Presented at 1970 JACC meeting, Atlanta, Ga, Paper 23-B (p. 602).

Kumar, S., Chadha, A., Gupta, R., & Sharma, R. (1995). CATCRACK: A process simulator for an integrated FCC-regenerator system. *Industrial and Engineering Chemistry Research, 34*, 3737.

Kunii, D., & Levenspiel, O. (1991). *Fluidization engineering*. Boston: Butterworth-Heinemann.

Lee, B. I., & Kesler, M. G. (1988). Isobaric heat capacity of petroleum fraction liquids/vapors. *Technical data book-Petroleum refining*. Tulsa, OK: American Petroleum Institute.

Lee, W., & Kugelman, A. M. (1973). Number of steady-state operating points and local stability of open-loop fluid catalytic cracker. *Industrial and Engineering Chemistry, Process, Design and Development, 12*, 197.

Maya-Yescas, R., & Lopez-Isunza, F. (1997). Comparison of two dynamic models for FCC units. *Catalysis Today, 38*, 137.

Mcketta, J. J., & Cunningham, W. A. (1976). *Encyclopedia of chemical processing and design*. New York: Marcel Dekker.

Meissner, L. P. (1995). *Fortran 90*. Boston: PWS Publishing Co.

Morley, K., & de Lasa, H. I. (1987). On the determination of kinetic parameters for the regeneration of cracking catalyst. *Canadian Journal of Chemistry and Engineering, 65*, 773.

Nelson, W. L. (1958). *Petroleum refinery engineering*. Tokyo: McGraw-Hill.

Riazi, M. R. (1988). Interconversion of ASTM D86-TBP distillation curves at atmospheric pressure. *Technical data book-Petroleum refining*. Tulsa, OK: American Petroleum Institute.

Technical Data Committee, X. (1988). *Technical data book-Petroleum refining*. Tulsa, OK: American Petroleum Institute.

Theologos, K. N., Nikou, I. D., Lygeros, A. I., & Markatos, N. C. (1997). Simulation and design of fluid catalytic-cracking riser-type reactors. *A.I.Ch.E. Journal, 43*, 486.

Zheng, Y. Y. (1994). Dynamic modeling and simulation of a catalytic cracking unit. *Computers & Chemical Engineering, 18*, 39.

ANNEX III

中国石化集团公司职工培训系列教材

催化裂化工艺计算与技术分析

曹汉昌　郝希仁　张 韩　主编

石 油 工 业 出 版 社

内 容 提 要

本书为继续工程教育培训教材，以广大中级技术人员为对象，在接受过系统学院教育的基础上，侧重理论联系实际，重点介绍与生产实际密切相关的实例和例题，以提高工程技术人员分析问题与解决问题的能力。

全书共分十三章及附录，每章后附有习题与思考题。

本书可供从事催化裂化工艺的工程技术人员、设计人员、研究人员阅读。

图书在版编目(CIP)数据

催化裂化工艺计算与技术分析/曹汉昌，郝希仁，张韩主编.
北京：石油工业出版社，2000.10
ISBN 7-5021-2933-2

Ⅰ.催…
Ⅱ.①曹… ②郝… ③张…
Ⅲ①石油炼制-催化裂化-工艺-计算
②石油炼制-催化裂化-技术-分析
Ⅳ.TE624.4

中国版本图书馆 CIP 数据核字(2000)第 13910 号

石油工业出版社出版
(100011 北京安定门外安华里二区一号楼)
北京市巨龙印刷厂排版
北京市迪鑫印刷厂印刷
新华书店北京发行所发行

787×1092 毫米 16 开本 37.5 印张 1 插页 960 千字 印 1-1200
2000 年 10 月北京第 1 版 2000 年 10 月北京第 1 次印刷
ISBN7-5021-2933-2/TE·2280
定价：80.00 元

(6)气体出口速度头 ΔP_{ga}

$$\Delta P_{ga} = \frac{1}{2} \cdot \rho_g \cdot u_f^2 \tag{7-68}$$

2. 水平稀相输送的压力降

水平稀相输送的压力降的计算公式较多，本书推荐

$$\Delta P = \frac{1}{2}\rho_g u_f^2 + G_s u_s + \frac{2 f_g \rho_g u_f^2 L}{d_T}\left[1 + \frac{f_s u_s G_s}{f_g u_f^2 \rho_g}\right] \tag{7-69}$$

$$f_s = \frac{3}{8} \times \frac{\rho_g}{\rho_p} C_D \times \frac{d_T}{d_P}\left(\frac{u_f - u_s}{u_s}\right)^2$$

$$u_s = u_f(1 - 0.0638 d_p^{0.3} \rho_P^{0.5})$$

$$C_D = 0.44$$

另外，当 $f_s u_s/(f_g u_f) > 1$ 时，取其值为 1 参与上述计算。

四、提升管反应器的操作参数核算

[例 7-12] 以某提升管为例，计算操作参数。

原始数据

1.反应条件：	
提升管出口温度	537℃
再生催化剂温度	686℃
新鲜原料预热温度	256℃
回炼油浆温度	360℃
回炼油温度	325℃
沉降器顶压力	0.234MPa(绝)
提升管总用汽量	4900kg/h
馏分油流量	33370kg/h,94.265kmol/h
重油流量	11870kg/h,23.98kmol/h
回炼油浆流量	6220kg/h,18.4kmol/h
回炼油流量	0
催化剂循环量	344300kg/h
再生剂夹带烟气量	412kg/h,14.207kmol/h
2.产品流量：	
干气和损失	2090kg/h,104.657kmol/h
液化石油气	8960kg/h,182.22kmol/h
汽油	19040kg/h,184.854kmol/h
轻柴油	10350kg/h,50.735kmol/h
油浆	1730kg/h
焦炭	3070kg/h
3.原料，产品性质(略)：	
4.提升管结构尺寸：	
内径	0.85m
预提升段长	4.0m
水平段长	5.0m
垂直段长	30m
5.提升管压降等参数：	
总压降(实测)	41.4kPa
实测水平段及快分压降	5.7kPa
预提升段密度	560kg/m^3
反吹风密度	2.5kg/m^3
沉降器顶至提升管出口的稀相静压	0.5kPa

解：1.提升管物料平衡及气速、密度计算

1)物料平衡。

提升管进口物料：

名称	质量流量,kg/h	摩尔流量,kmol/h
馏分油	33370	94.265
重油	11870	23.98
回炼油,回炼油浆	6220	18.40
蒸汽	4900	272.22
再生剂夹带烟气	412	14.207
催化剂	344300	
合计	401072	423.072
油气合计	56772	423.072

提升管出口物料：

名称	质量流量,kg/h	摩尔流量,kmol/h
干气和损失	2090	104.657
液化石油气	8960	182.22
汽油	19040	184.854
轻柴油	10350	50.735
油浆	7950 = 6220 + 1730	23.521
蒸汽	4900	272.22
再生剂夹带烟气	412	14.207
焦炭,催化剂	347370 = 344300 + 3070	
合计	401072	832.414
油气合计	53702	832.414

2)提升管入口处的压力、温度。

①压力：

提升管入口处操作压力 = 沉降器压力 + 沉降器顶至提升管出口的稀相静压 + 提升管总压降(不含预提升段)

提升管总压降的实测值为 41.4kPa,校正后为

$\Delta P = 41.4 + 2.5 \times 30 \times 10^{-2} = 42.15\text{kPa}$

扣除预提升段的静压为 $4 \times 560/100 = 22.40\text{kPa}$

则不含预提升段的提升管总压降为 19.75kPa,从而提升管进口处的操作压力为：

$0.234 \times 1000 + 19.75 = 253.75\text{kPa} = 0.254\text{MPa}$

②温度：

由热平衡可得到剂油接触原料气化后的混合温度为 579℃(计算过程略)。

3)提升管入口线速。

提升管入口油气体积流量为：

$$V_{油} = 423.072 \times 22.4 \times [(579 + 273)/273] \times [1.033/(0.254 \times 10.19)]$$
$$= 11804.07\text{m}^3/\text{h} = 3.28\text{m}^3/\text{s}$$

提升管入口线速为 $u_{gi}=V_{gi}/A=3.28/0.567=5.78\text{m/s}$。

4)提升管出口线速。

提升管出口油气体积流量 V_{ge} 为：

$$V_{ge}=832.414\times22.4\times[(537+273)/273]\times[1.033/0.24\times10.19]$$
$$=23368.17\text{m}^3/\text{h}=6.49\text{m}^3/\text{s}$$

所以，提升管出口线速 u_{ge} 为：

$$u_{ge}=V_{ge}/A=6.49/0.567=11.45\text{m/s}$$

5)提升管平均线速。

按对数平均值计算：

$$u_g=\frac{u_{ge}-u_{gi}}{\ln\frac{u_{ge}}{u_{gi}}}=\frac{11.45-5.78}{\ln\frac{11.45}{5.78}}=8.29\text{m/s}$$

6)油气密度。

油气重量流量与油气体积流量的比值就是油气密度。

对进口，$\rho_{gi}=56772/11804.07=4.81\text{kg/m}^3$，

对出口，$\rho_{ge}=53702/23368.117=2.30\text{kg/m}^3$，

提升管对数平均密度为 $\rho_g=3.4\text{kg/m}^3$。

2.提升管藏量计算

(1)估算固体颗粒速度

参考有关资料及提升管气速，估计进口、出口的滑落系数，从而求得颗粒速度：

	进口处	出口处	平均
油气速度，m/s	5.78	11.45	8.29
估计的 K_{sl}	2.5	1.5	1.86
催化剂速度，m/s	2.31	7.63	4.45

这一步只是用于计算催化剂加速压降，其结果还需进一步校正。

(2)计算除催化剂静压头的各项压降

$$\Delta P_{gf}=1.3\times10^{-2}(L/d_T)\rho_g\times u_t^2$$
$$=1.3\times10^{-2}(30/0.85)\times3.4\times8.29^2$$
$$=107.21\text{Pa}$$

$$\Delta P_{gh}=\rho_g\times L\times g=3.4\times30\times9.81=1000.6\text{Pa}$$

$$\Delta P_{ga}=0.5\times\rho_g\times u_t^2=0.5\times3.4\times8.29^2=146.4\text{Pa}$$

$$\Delta P_{sa}=G_s u_{se}$$

$$G_s=344300/(0.567\times3600)=168.7\text{kg/(m}^2\cdot\text{s)}$$

$$\Delta P_{sa}=168.7\times7.63=1286.99\text{Pa}$$

$$\Delta P_{sf}=5.7\times10^{-2}\times G_s L\times g\times(gd_T)^{-0.5}$$
$$=5.7\times10^{-2}\times168.7\times30\times9.81\times(9.81\times0.85)^{-0.5}$$
$$=980.02\text{Pa}$$

则 $\Delta P_{gf}+\Delta P_{gh}+\Delta P_{ga}+\Delta P_{sa}+\Delta P_{sf}=3521.24\text{Pa}$

ANNEX IV

Process Calculation and Technical Analysis of Catalytic Cracking

Editor-in-chief: Cao Hanchang Hao Xiren Zhang Han

Petroleum Industry Press

(6) Gas velocity head at the outlet is represented by ΔP_{ga} and calculated according to the following equation:

$$\Delta P_{ga} = \frac{1}{2} \cdot \rho_g \cdot u_f^2 \qquad (7\text{-}68)$$

2. Pressure drop of horizontally transported dilute phase

There are a lot of equations for calculating pressure drop of horizontally transported dilute phase, of which the one available hereinbelow is recommended:

$$\Delta P = \frac{1}{2}\rho_g u_f^2 + G_s u_s + \frac{2 f_g \rho_g u_f^2 L}{d_T}\left[1 + \frac{f_s u_s G_s}{f_g u_f^2 \rho_g}\right] \qquad (7\text{-}69)$$

$$f_s = \frac{3}{8} \times \frac{\rho_g}{\rho_p} C_D \times \frac{d_T}{d_P}\left(\frac{u_f - u_s}{u_s}\right)^2$$

$$u_s = u_f(1 - 0.0638 d_p^{0.3} \rho_P^{0.5})$$

$$C_D = 0.44$$

In addition, when $f_s u_s/(f_g u_f) > 1$, the value of 1 is taken for use in the above equation.

IV. Accounting of the Operational Parameters of Riser reactors

[Example 7-12] The operational parameters are calculated based on a sample riser.

Original Data

1. Reaction Conditions	
Temperature at the outlet of the riser	537 °C
Temperature of the regenerated catalyst	686 °C
Preheating temperature of the fresh feedstock	256 °C
Temperature of the recycle slurry	360 °C
Temperature of the heavy cycle oil(HCO)	325 °C
Pressure at the top of the disengager	0.234 MPa (absolute pressure)

Total flow rate of steam in the riser	4900 kg/h
Flow rate of the distillate oil	33370 kg/h, 94.265 kmol/h
Flow rate of the heavy oil	11870 kg/h, 23.98 kmol/h
Flow rate of the recycle slurry	6220 kg/h, 18.4 kmol/h
Flow rate of the heavy cycle oil(HCO)	0
Circulation rate of the catalyst	344300 kg/h
Flow rate of the flue gas carried by the regenerated catalyst	412 kg/h, 14.207 kmol/h
2. Flow Rates of the Products	
Dry gas and loss	2090 kg/h, 104.657 kmol/h
LPG	8960 kg/h, 182.22 kmol/h
Gasoline	19040 kg/h, 184.854 kmol/h
Light cycle oil	10350 kg/h, 50.735 kmol/h
Slurry	1730 kg/h
Coke	3070 kg/h
3. Properties of the Feedstock and Products (omitted)	
4. Dimensions of the Riser Structure	
Inner diameter	0.85 m
Length of the prelift zone	4.0 m
Length of the horizontal zone	5.0 m
Length of the vertical zone	30 m
5. Parameters of the Riser such as Pressure Drop	
Total pressure drop (as actually measured)	41.4 kPa
Pressure drop of Horizontal Section and cyclone as actually measured	5.7 kPa
Density of the prelift zone	560 kg/m^3
Density of the counter draught	2.5 kg/m^3
Dilute-phase static pressure from the top of the disengager to the outlet of the riser	0.5 kPa

1. Material Balance in the Riser and Calculation of Velocity and Density

1) Material Balance

Materials at the Inlet of the Riser

Name	Mass Flow (kg/h)	Molar Flow (kmol/h)
Distillate oil	33370	94.265
Heavy oil	11870	23.98
Heavy cycle oil/ recycle slurry	6220	18.40
steam	4900	272.22
Flue gas carried by the regenerated catalyst	412	14.207
Catalyst	344300	
Total	401072	423.072
Total of vapor	56772	423.072

Materials at the outlet of the riser

Name	Mass Flow (kg/h)	Molar Flow (kmol/h)
Dry gas and loss	2090	104.657
LPG	8960	182.22
Gasoline	19040	184.854
Light cycle oil	10350	50.735
Slurry	7950	23.521
Steam	4900	272.22
Flue gas carried by the regenerated catalyst	412	14.207
Coke/Catalyst	347370	
Total	401072	832.414
Total of vapor	53702	832.414

2) Pressure and Temperature at the Inlet of the Riser

(1) Pressure

Operational pressure at the inlet of the riser = Pressure in the disengager + Dilute-phase static pressure from the top of the disengager to the outlet of the riser + Total pressure drop in the riser (excluding the prelift zone)

The measured value of the total pressure drop in the riser is 41.4 kPa, which is revised as:
$\Delta P = 41.4 + 2.5 \times 30 \times 10^{-2} = 42.15$ kPa.

The static pressure in the prelift zone that should be deducted is 4 x 560/100 = 22.40 kPa.

Then, the total pressure drop in the riser excluding the prelift zone is 19.75 kPa. Consequently, the operational pressure at the inlet of the riser is:
0.234 x 1000 + 19.75 = 253.75 kPa = 0.254 MPa.

(2) Temperature

Owing to heat balance, the mixed temperature obtained after gasification of the feedstock resulting from the catalyst-oil contact is 597 °C (the calculation procedure is omitted here).

3) Linear Velocity at the Inlet of the Riser

The volume flow rate of the vapor at the inlet of the riser is calculated as follows:
V_{gi} = 423.072 x 22.4 x [(597 + 273) / 273] x [1.033 / (0.254 x 10.19)] = 11804.07 m^3/h = 3.28 m^3/s.

The linear velocity at the inlet of the riser is: $u_{gi} = V_{gi} / A = 3.28/0.567 =$ 5.78 m/s.

4) Linear Velocity at the Outlet of the Riser

The volume flow rate of the vapor at the outlet of the riser is calculated as follows:
V_{ge} = 832.414 x 22.4 x [(537 + 273) / 273] x [1.033 / 0.24 x 10.19] = 23368.17 m^3/h = 6.49 m^3/s.

Thus, the linear velocity at the outlet of the riser, u_{ge}, is calculated as:
$u_{ge} = V_{ge} / A = 6.49/0.567 = 11.45$ m/s.

5) Mean Linear Velocity in the Riser

It is calculated based on the logarithmic mean value:

$$u_g = \frac{u_{ge} - u_{gi}}{\ln \frac{u_{ge}}{u_{gi}}} = \frac{11.45 - 5.78}{\ln \frac{11.45}{5.78}} = 8.29 \text{m/s}$$

6) Density of the Vapor

The ratio of the weight flow rate of the vapor to the volume flow rate of the vapor is the density of the vapor.

With respect to the inlet: $\rho_{gi} = 56772/11804.07 = 4.81$ kg/m^3;
With respect to the outlet: $\rho_{ge} = 53702/23368.117 = 2.30$ kg/m^3.

The logarithmic mean density in the riser is: $\rho_g = 3.4$ kg/m^3.

2. Calculation of the Inventory of the Riser

(1) Estimation of the Velocity of Solid Particles

The velocity of the particles is obtained by estimating the sliding coefficients at the inlet and outlet in light of relevant information and the gas velocity in the riser.

	Inlet	Outlet	Average
Velocity of the vapor, m/s	5.78	11.45	8.29
Estimated K_{sl}	2.5	1.5	1.86
Velocity of the catalyst, m/s	2.31	7.63	4.45

In this step, only the catalyst-accelerated pressure drop is calculated, and the results need to be revised further.

(2) Calculation of Pressure Drops Excluding the Catalyst Static Head

$\Delta P_{gf} = 1.3 \times 10^{-2} (L/d_T)\ \rho_g \times u_f^2$

$= 1.3 \times 10^{-2} (30/0.85) \times 3.4 \times 8.29^2$

$= 107.21$ Pa

$\Delta P_{gh} = \rho_g \times L \times g = 3.4 \times 30 \times 9.81 = 1000.6$ Pa

$\Delta P_{ga} = 0.5 \times \rho_g \times u_f^2 = 0.5 \times 3.4 \times 8.29^2 = 146.4$ Pa

$\Delta P_{sa} = G_s u_{se}$

$G_s = 344300/(0.567 \times 3600) = 168.7$ kg/(m^2.s)

$\Delta P_{sa} = 168.7 \times 7.63 = 1286.99$ Pa

$\Delta P_{sf} = 5.7 \times 10^{-2} \times G_s L \times g \times (g d_T)^{-0.5}$

$= 5.7 \times 10^{-2} \times 168.7 \times 30 \times 9.81 \times (9.81 \times 0.85)^{-0.5}$

$= 980.02$ Pa

Thus, $\Delta P_{gf} + \Delta P_{gh} + \Delta P_{ga} + \Delta P_{sa} + \Delta P_{sf} = 3521.24$ Pa